The Institute of Immunology

Director: Prof. Dr. Hans-Jürgen Thiesen

Phosphoproteome analysis of the near-haploid cell line HAP1 reveals phosphorylation events originating from PDZ-binding kinase/T-LAK cell-originated protein kinase (PBK/TOPK)

DISSERTATION

zur

Erlangung des akademischen Grades

doctor rerum humanum (Dr. rer. hum)

der Universitätsmedizin Rostock

der Universität Rostock

Vorgelegt von

Hasan Albony, geboren am 27.12.1981 in Damas Suburb, Syrien,

Rostock, 29.04.2021

https://doi.org/10.18453/rosdok_id00004478

Gutachter

Erster Gutachter: Prof. Dr. med. Hans-Jürgen Thiesen
Institut für Immunologie
Universität Rostock

Zweiter Gutachter: Univ.-Prof. Dr. Christopher Gerner
Fakultät für Chemie
Universität Wien

Dritter Gutachter: PD Dr. rer. nat. habil. Hugo Murua Escobar
Medizinische Klinik III
Universität Rostock

Eingereicht am: 29.04.2021

Datum der Verteidigung: 20.09.2022

Table of Contents

Table of contents

Table of contents

1. Summary

PDZ-binding kinase/T-LAK cell-originated protein kinase (PBK/TOPK) is a serine/threonine kinase, phylogenetically related to mitogen-activated protein kinase kinase (MAPKK). PBK has a low abundance on the protein level in differentiated cells, while its abundance and activity increase in fetal cells and various malignant cells. During the G2/M transition, PBK has been reported to phosphorylate the inter-zinc finger linker sequence (TGEKP) of hundreds of C2H2 zinc finger proteins implicated in liberating these transcription factors from the condensing chromatin.

This study aimed to interrogate PBK-regulated proteome and investigate PBK-dependent phosphorylation events by analyzing the proteome and the phosphoproteome of both wild and PBK knockout HAP1 cells.

The near-haploid human cell line HAP1 was adopted as a model to identify PBK-dependent phosphorylation events due to the availability of wild type and PBK knockout cell lines. The wild type and PBK knockout HAP1 cells were either arrested in the mitotic phase or allowed to proliferate exponentially, representing four conditions. PBK activity was then evaluated by examining PBK phosphorylation of its specific substrate (TGEKP) using monoclonal antibodies. Flow cytometry was used to characterize the cell cycle phases. Liquid chromatography with tandem mass spectrometry (LC-MS/MS) was used to acquire the proteome and phosphoproteome of the analyzed conditions.

The proteome analysis showed 20 proteins being downregulated and one protein (GPC4) upregulated during the mitotic phase. A total of 39 proteins had significantly different abundances among the four analyzed conditions. Besides PBK kinase, only three proteins displayed different expression levels between mitotic wild type and PBK knockout cells. Western blot validation of three differentially regulated proteins (ANXAI, G6PD, and EMD) revealed that protein abundances vary among different HAP1 clones, which have the same genotype. Due to the variability of protein abundances among clones with the same genotype, several individual clones have to be analyzed.

Phosphoproteome analysis of mitotic and non-mitotic HAP1 cells revealed 299 upregulated and 45 downregulated phosphosites during mitosis. Motif analysis of the

mitotic upregulated phosphosites showed seven consensus phosphorylation motifs (RXXpS, pSL, pS/T, pSA, pSV, and GpS). Comparing the phosphoproteomes of mitotic wild type and PBK knockout HAP1 cells showed five candidate PBK-dependent phosphosites. The identified candidates belong to DNA- and RNA binding proteins (ADNP and FUBP1) or dynamic regulators of cell organelles (MARCKS and PGRMC1). Interestingly, one of these candidates is derived from FUBP1 and has the amino acid sequence (TGADKP) that resembles a specific substrate of PBK (TGEKP).

These results suggest that PBK is responsible for these phosphorylation events on ADNP, FUBP1, MARKS, and PGRMC1, either by the direct phosphorylation (direct substrates) or by phosphorylation and activation of their upstream kinases (indirect substrates). These phosphorylation events may modulate the activities of these proteins and have a vital role in cell division. Further inspection of the PBK`s impact on the identified candidate PBK-dependent phosphosites is requested to differentiate between direct and indirect PBK substrates. Besides, the investigation of these phosphosites in regulating protein functions is essential to understand the impact of PBK on modulating the involved biological processes.

2- Introduction

2.1- Protein phosphorylation

Protein phosphorylation is one of the most ubiquitous and vital post-translational modifications (PTMs). In eukaryotes, protein phosphorylation events typically occur at the side-chain hydroxyl groups of serine, threonine, and tyrosine residues, adding a negative charge to the amino acid chain. Phosphorylation is described as an evolutionary process that reversibly modifies and changes the polarities of these amino acids that lead to conformational changes in the phosphorylated proteins. These events activate or inactivate protein functions and modulate signal transduction pathways that control various biological functions (Manning et al., 2002; Pearlman et al., 2011). For example, Zhou et al., 2000 elucidated that the phosphorylation of Bcl2-associated agonist of cell death (BAD) abolishes its affinity to Bcl-2-like protein 1 (BCL2L1). In some instances, protein phosphorylation induces conformational changes in the proteins' tertiary structures, which convert them into an active form or at least increases their activity. The phosphorylation-dependent activation of mitogen-activated protein kinase (MAPK) is an example of this kind (Zhou and Zhang, 2002). Furthermore, protein phosphorylation can have a decisive role in the regulation of protein degradation. The phosphorylation of mitogen-activated protein kinase phosphatase 1 (MAPK1) decreases its ubiquitination and increases its stability (Li et al., 2011a).

Kinases form one of the largest protein families. The human genome encodes 539 kinase genes (Brognard and Hunter, 2011). Kinases catalyze the transfer of the phosphoryl group from adenosine triphosphate (ATP) to its target motif. The kinase recognizes its specific substrates through the physical interaction between the kinase's catalytic domain with few residues flanking the phosphosite (Miller and Turk, 2018).

Phosphatases are responsible for removing the phosphoryl groups from their target phosphorylated sequences and diminish protein phosphorylation levels. The phosphatase family comprises 199 proteins of the human proteome (Sacco et al., 2012). Phosphatases regulate many molecular functions by reversing protein kinase functionalities by dephosphorylating target substrates.

Altogether, the concerted activities of kinases and phosphatases modulate protein phosphorylation, which decisively regulates numerous cell functions. The therapeutical application of small molecules that inhibit phosphatase activity can break this phosphorylation/dephosphorylation balance and modify involved biological processes (Meraldi and Nigg, 2001).

2.2- Protein phosphorylation as a mitotic regulator

Once cells enter the mitotic phase, the chromatin condenses, and the packaged DNA becomes much less accessible to transcription factors in general (Spellman et al., 1998). This phenomenon is associated with global transcriptional reduction. Moreover, the mitotic cells show an apparent reduction in translation efficiency compared with the interphase cells (Tanenbaum et al., 2015). Unlike protein regulation, the transition from interphase to mitotic phase is marked by a notable increase in overall protein phosphorylation. The upregulation of protein phosphorylation during the mitotic phase is attributed to enhanced kinase activity and diminished phosphatase activity (Gowdy et al., 1998).

Cyclin-dependent kinase 1 (CDK1) is the primary driving force for mitotic entry through the phosphorylation of its mitotic substrates. Other mitotic kinases, in particular Aurora kinase A/B (AURKA/B) and serine/threonine-protein kinase PLK1 (Plk1), are concurrently activated to support G2/M transition (Salaun et al., 2008). CDK1 activation requires CDK1 association with cyclin B (Fig. 1), the phosphorylation of Thr161, and the dephosphorylation of Thr14 as well as Tyr15 in CDK1 molecule (Hunter T., 1989; Draetta, 1993; Gould and Nurse, 1989).

The increased activity of the CDK1-cyclin B complex is responsible for the phosphorylation of many mitotic substrates. Among these substrates, protein phosphatase 1 (PP1) which is phosphorylated at Thr320 and deactivated (Dohadwala et al., 1994). CDK1-cyclin B can also inactivate protein phosphatase 2A (PP2A) through the activation of its inhibitor α-endosulfine (Ensa). CDK1-cyclin B phosphorylates Ensa directly or

indirectly (mediated by activation of Greatwall kinase: Gwl), leading to PP2A deactivation (Okumura et al., 2014).

At the end of the mitotic phase, cyclin B is ubiquitinated by anaphase-promoting complex/cyclosome (APC/C) and degraded, leading to reduced cellular CDK1 activity (Hershko, 1999).

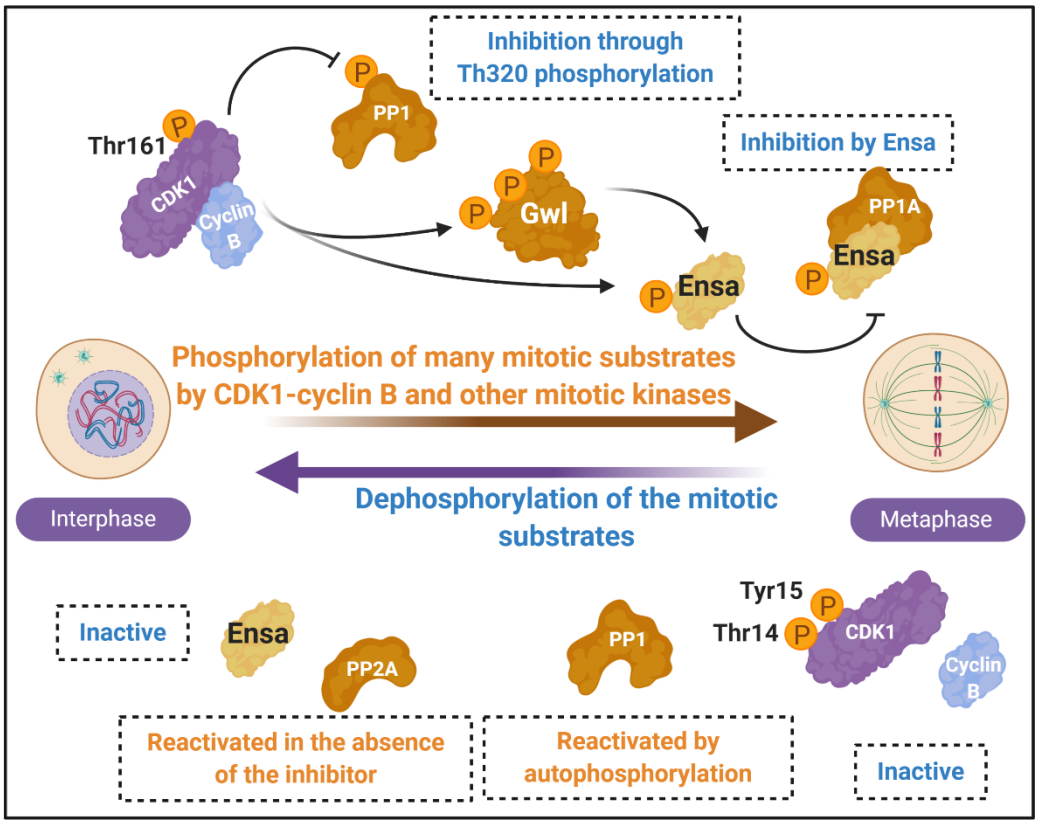

Figure 1: *The model shows the counteracting roles of CDK1 and protein phosphatases in regulating mitotic entry and exit. Upon the mitotic entry, CDK1 forms the complex CDK1-cyclin B. It is phosphorylated at Thr161 and dephosphorylated at both Thr14 and Tyr15. The active complex CDK1-cyclin B phosphorylates PP1 at Thr320 and deactivates it. Gwl is also phosphorylated and activated by CDK1-cyclin B. Gwl activates Ensa, which is a PP2A inhibitor. The active CDK1-cyclin B phosphorylates Ensa directly and activates it. As mitosis is ending, CDK1 activity reduces. On the other side, protein phosphatases are activated due to the reduction of the inhibitory effect of CDK1. Numerous mitotic motifs are dephosphorylated, and the cells enter interphase. Once CDK1 is phosphorylated at Thr14 and Tyr15 by MYT1 and Wee1, CDK is inactivated during interphase.*

The reduction in CDK1 activity enables the reactivation of PP1 by auto-dephosphorylation. Additionally, CDK1 deactivation deprives Ensa (PP2A inhibitor) of the activation, which means that PP2A will regain its activity.

Myelin transcription factor 1 (MYT1) and wee1-like protein kinase (Wee1) phosphorylate CDK1 at Tyr14 and 15 to ensure CDK1 inhibition during interphase and to prevent the cells from going back into mitosis (Booher et al., 1997; Parker et al., 1992).

The active PP1, PP2A, and other phosphatases are responsible for dephosphorylating the mitotic substrates and driving the mitotic phase's exit (Wu et al., 2009; Williams et al., 2014).

Okadaic acid (OA) is a polyether fatty acid toxin. It is naturally produced by the marine dinoflagellates *Dinophysis* and *Prorocentrum* (Cembella, 1989; Dickey et al., 1990). OA is a potent serine/threonine protein phosphatase inhibitor. It inhibits PP1 and PP2A with a higher affinity to the latter and can also inhibit other protein phosphatases such as PP4 and PP5 (Swingle et al., 2007). As discussed previously, protein phosphatase activities are crucial for mitotic exit. OA acid treatment restrains the reactivation of these phosphatases upon CDK1 inactivation and prevents the cells from passing the mitotic phase (Holder et al., 2019).

Anti-mitotic agents such as nocodazole are used to arrest cells in the mitotic phase. Unlike OA, nocodazole does not affect the activity of protein phosphatases. It induces disassembling of the microtubules by interfering with α/β-tubulin dimers (Chen and Horwitz, 2002).

2.3- PDZ-binding kinase/T-LAK activated killer cell-originated protein kinase (PBK/TOPK)

According to the HUGO Gene Nomenclature Committee (HGNC), PBK is the gene name of PDZ-binding kinas. It has a PDZ binding domain, which interacts with the human homolog of the Drosophila Discs-large tumor suppressor protein (*hDlg*). It is also called T-lymphokine-activated killer cell-originated protein kinase (TOPK) (Gray et al., 2016).

PBK is a 322-amino-acid serine/threonine kinase. It was cloned by screening the upregulated genes during the activation of lymphokine-activated killer T cells (T-LAK). PBK belongs to the mitogen-activated protein kinase kinase (MAPKK) family and locates phylogenetically between MAP2K1 and MAP2K7 branches according to sequence homology analyses (Abe et al., 2000). PBK expression can be detected on the mRNA level in normally proliferating cells. However, it is barely detectable on the protein level in such cells. Elevated PBK protein levels are found in rapidly proliferating cells such as testicular tissues, embryonic tissues, proliferating brain neural stem cells, and malignancies like lymphoma, leukemia, melanoma, breast cancer, cholangiocarcinoma, lung cancer, and renal cell carcinoma. (He et al., 2010; Park et al., 2010; Simons-Evelyn et al., 2001)

2.3.1- The overall structure and activity regulation of PBK

The overall structure of PBK has been described by Dong et al. in 2016 and deposited in the protein data bank with the accession code 5j0A. It consists of 6 β-strands and 14 α-helices. In alkaline conditions, PBK forms an inactive homodimer in which the N-terminus of one molecule joins the other molecule at its C-terminal region. Crystal structure analysis of PBK showed that the regions between α10 to α11 and β2 to α2 are the most flexible. It is thought that the interaction of two PBK monomers takes place between the loop region located among α10-α11 of one monomer and the groove region located among β2-α2 form another monomer (Fig. 2A). It should be noted that the PBK dimer was identified solely in an alkaline buffer in vitro, whereas the active and inactive monomers were identified in in vivo (Dong et al., 2016).

The human PBK C- terminus has a PDZ binding domain (Fig. 2B), which contains the short amino acid motif T/SXV (X is any amino acid). T/SXV motif binds to the human homolog of the Drosophila Discs-large tumor suppressor protein (*hDlg*).

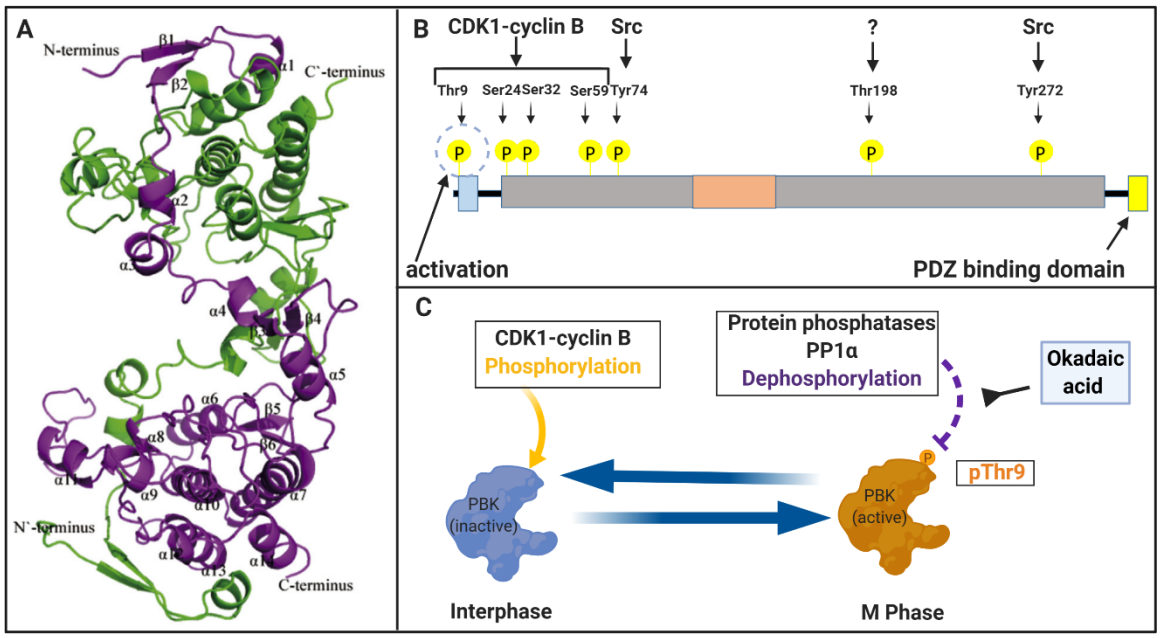

Figure 2: *PBK dimerization, phosphosites, and activation. (A) Ribbon representation of a PBK dimer (taken from PDB file 5j0A; Dong et al., 2016) (B)The phosphosites in PBK molecule and their relevant kinases. (C) The transition between the active (blue color) and inactive (orange color) states of the PBK monomer.*

The interaction between *hDlg* and tumor suppressor protein APC or the human papillomavirus E6 transforming protein blocks the cell cycle progression and inhibits cancer development. Mutating Thr220 and Val223 to Ala220 and Ala 223 ablates PBK's ability to bind to *hDlg* (Ishidate et al., 2000; Kiyono et al., 1997). Protein sequence alignment of PBK among Homo sapiens, Mus musculus, Rattus norvegicus, Xenopus laevis, and Danio rerio shows roughly 55% amino acid sequence identity (Dong et al., 2016).

According to the PhosphoSitePlus database (Hornbeck et al., 2012a), 25 phosphosites have been identified on PBK kinase. The functional impact and the upstream kinase of seven of these phosphosites were investigated in the literature. CDK1–cyclin-B1 mediates mitotic phosphorylation of four residues on PBK to convert the kinase from an inactive to an active form. Thr9 was firstly identified by Matsumoto et al., 2004. They described the association between PBK phosphorylation at Thr9 by CDK1–cyclin-B1 and the mitotic entry. Thr9 phosphorylation starts at prophase and lasts till the end of metaphase, while the dephosphorylation takes place at the end of mitosis (anaphase)

(Rizkallah et al., 2015) (Fig. 2C). Protein phosphatase 1 alpha (PP1α) is responsible for PBK deactivation at the end of the mitotic phase by removing the phosphate group from Thr9. The treatment with PP1α inhibitors such as OA will perpetuate Thr9 phosphorylation and arrest the cells at a prometaphase-like state (Vandre and Wills, 1992; Park et al., 2010). Fujibuchi et al., 2005 described Thr198 phosphorylation. In contrast to Thr9 phosphorylation, Thr198 phosphorylation is also observed in interphase, but it is mildly upregulated during mitosis. The responsible kinase is not identified yet. Additionally, three other mitotic PBK phosphosites were recently identified. CDK1–cyclin-B1 phosphorylates Ser24, Ser32, and Ser59 from prophase to metaphase. The phosphorylation at these sites diminishes in anaphase and abates in telophase and the following cytokinesis. Proto-oncogene tyrosine-protein kinase Src (Src) was identified as another PBK upstream modulator that can phosphorylate PBK at Tyr74 and Tyr272 (Fig. 2B). Ex vivo and in vivo experiments showed that the phosphorylation of these two tyrosine residues enhances PBK activity and promotes the tumorigenesis of the colon cancer cells (Xiao et al., 2016).

2.3.2- PBK regulation on protein level

PBK activity is primarily regulated by phosphorylation, but gene expression modulators and protein degradation regulators have been shown to play a role in controlling the cellular protein abundance of PBK. Five players have been mentioned in the literature to be responsible for this role.

Myc proto-oncogene protein (c-MYC) and Transcription factor E2F1 (E2F1): c-MYC is an oncogenic transcription factor, regulates the transcription of its target genes through the formation of an active heterodimeric complex with MAX protein, and binds to well-conserved enhancer sequences within regulatory regions of target genes (García-Gutiérrez et al., 2019). E2F1 is also an oncogenic transcription factor, targets the promoter region of several genes that regulate cell growth, proliferation, and DNA replication. It is upregulated on the transcriptional level by c-MYC. The miR-17-92 cluster is another target of c-MYC, which transactivates its expression. Increased levels of this microRNA decrease the stability of the mRNA of E2F1 and inhibit its translation

(Zhang et al., 2012). In silico analysis of the interaction between the promoter and transcription factor showed that the PBK promoter has a possible E2F1 DNA binding site on the sequence stretches from 103 to 96 relative to the PBK gene (sequence: TTTGGCGC). This interaction was validated by knocking down E2F1 in the prostate cancer cell lines (LNCaP, DU145), which was combined by the down-regulation of PBK on mRNA and protein levels. A positive correlation between E2F1 and PBK on mRNA and protein levels was observed in prostate cancer. These high levels were also associated with adverse outcomes in the patients, such as tumor aggressiveness, advanced pathological phase, metastasis (Chen et al., 2015).

Forkhead box protein M1 (FoxM1): FoxM1 is a transcription factor. It plays an essential role in regulating DNA replication and mitosis (Wang et al., 2002). The correlation between the upregulation of PBK and FoxM1 was observed by analysis of transcriptional data recorded in The Cancer Genome Atlas (TCGA) for hepatocellular carcinoma (HCC), thus demonstrating FoxM1 to be a potential vital transcriptional regulator of PBK. Immunohistochemistry using tissue microarrays (TMA) validated this observation. Note, tumorous tissues had five times higher PBK positive staining than non-tumorous regions in hepatocellular carcinoma tissues. Luciferase receptor assays verified that FoxM1 modulates the PBK promoter and enhances its expression. Additionally, FoxM1 depletion attenuates PBK expression. In view of these observations, FoxM1 is an upstream regulator of PBK in hepatocellular carcinoma cells. (Yang et al., 2017).

Checkpoint with forkhead-associated and RING finger domains (CHFR): CHFR is a mitotic checkpoint protein. It is implicated in promoting the delayed entry into metaphase upon exposure to microtubule poisoning agents such as colcemid but not required for normal cell cycle. CHFR possesses an E3 ligase activity. (Sanbhnani and Yeong, 2012). Several mitosis regulatory proteins like AURKA and PLK1 have been mentioned in the literature as CHFR substrates. They are ubiquitinated and negatively regulated by CHFR, leading to suppression of cell cycle progression. (Kang et al., 2002; Oh et al., 2009). Shinde et al., 2013 , revealed that PBK is co-immunoprecipitated with CHFR in the HEK 293T cell line. This interaction does not require any post-translational modifications or

additional molecules that enable CHFR-PBK complex formation, as it was confirmed in CHFR and PBK expressing bacteria. Besides the full-length protein, only deletion mutants that comprise the C-terminal cysteine-rich domain of CHFR and the C-terminal region of PBK were able to form this type of complex. Thus, the interaction domain of PBK is located in the C-terminal region. Although the interaction only required C-terminal fragments, the ubiquitination process was exclusively seen in the presence of two full-length proteins. The ubiquitination of PBK mediates its negative regulation via proteasomal recognition and degradation. The impact of CHFR on PBK degradation was ascertained by determining PBK half-life in CHFR knockout Hela cells, which was higher than its value in wild type Hela cells. The half-life of PBK was remarkably reduced in CHFR transfected Hela cells and could be rescued by treatment with proteasome inhibitor MG132 (Shinde et al., 2013).

2.3.3- PBK substrates

The intensive screening of PBK substrates and analysis of their biological functions are essential to understand the PBK-mediated biological process. The literature review shows manifold proteins that can be phosphorylated and regulated by PBK (Table 1). The functional diversity of these substrates reflects the variety of the biological processes in which PBK is involved.

PBK is a mitotic kinase and responsible for phosphorylation of several mitotic substrates. On entry into the prophase, the active PBK contributes to chromatin condensation through the phosphorylation of Histone H3 and consensus TGEKP linkers between C2H2 zinc fingers (Park et al., 2006; Rizkallah et al., 2015).

In addition to the role of PBK on chromatin regulation, it modulates other cell organelles during the mitotic phase. PBK activates Valosin Containing Protein (VCP/p97) that participates in spindle disassembly. LGN/GPSM2 is another PBK mitotic substrate. It recruits dynein motor protein complex and regulates mitotic spindle positioning. (Park et al., 2010; Fukukawa et al., 2010). PBK phosphorylates and negatively regulates the

mitotic checkpoint protein PTEN, which enhances Akt signaling pathway during mitosis (Shinde et al., 2013).

PBK also has a key role in promoting apoptosis-resistance after cellular response to DNA damage. Upon cellular exposure to arsenic(3+) ions, or UV radiation, or oxidative stress, PBK activates proteins that enhance DNA repair (histone H2A), promote cell survival (JNK1/3), and reduce the derivatives of hydrogen peroxide by activating Periaxin (PRX) to enhance cell survival (Zykova et al., 2006; Oh et al., 2007; Zykova et al., 2010).

Table 1: *List of PBK substrates mentioned in the literature.*

Substrate_Accession number	Substrate_Gene name	11 amino acids*	literature
P16104	H2AX	KATQA**S**QEY--	Zykova et al., 2006
P68431	H3C1	QTARK**S**TGGKA	Park et al., 2006
P25963	NFKBIA	DDRHD**S**GLDSM	Park et al., 2013
P45983	MAPK8	TSFMM**T**PYVVT	Oh et al., 2007
P05412	JUN	SDLLT**S**PDVGL	Li et al., 2016
P05412	JUN	LLKLA**S**PELER	Li et al., 2016
P28482	ERK2	EIMLN**S**KGYTK	Abe et al., 2000; Zhu et al., 2007
P81274	GPSM2	GKKYK**T**NSSTK	Fukukawa et al., 2010
P28562	DUSP1	LSYLQ**S**PITTS	Li et al., 2011; Win et al., 2018
Q96S44	PRPK	RGRKR**S**MVG--	Zykova et al., 2018
P60484	PTEN	DHYRY**S**DTTDS	Shinde et al., 2013
P55072	VCP	unknown residue	Park et al., 2010
Q06830	PRDX1	KDISL**S**DYKGK	Zykova et al., 2010
conserved linker in C2H2 zinc finger proteins	An example YY1	HQLVH**T**GEKPF	Rizkallah et al., 2015
O75385	ULK1	RSGST**S**PLGFA	Lu H et al., 2019
O75385	ULK1	LARKM**S**LGGGR	Lu H et al., 2019
O75385	ULK1	MRGGR**S**PRPGS	Lu H et al., 2019

***The phosphorylated residue is highlighted in red.**

PBK is also a regulator of several transcription factors. It regulates their activity by direct (c-Jun) or indirect phosphorylation (JNK1/3, ERK2, and PRPK/TP53RK). Moreover, PBK phosphorylates the interactors of some transcription factors (IκBα), which modulates the activity and the localization of the target transcription factor (Li et al., 2016; Oh et al., 2007; Abe et al., 2000; Zykova et al., 2018; Park et al., 2013).

The response to UV radiation can be mediated by indirect inhibition of the inflammatory signal transduction of MAPK. Upon UV radiation, PBK phosphorylates MAPK inhibitory dual-specificity phosphatase 1 (DUSP1). This modification increases the stability of DUSP1. Thus, PBK has a protective effect against UV radiation-induced-inflammation in the PBK knockout mouse model (Li et al., 2011a).

Finally, PBK plays a crucial role in autophagy inhibition and promotes drug resistance in cancer therapy. PBK phosphorylates serine/threonine-protein kinase ULK1 (ULK1). The phosphorylation of ULK1 reduces its activity and stability. Thus, this modification reduces autophagy and enhances cell proliferation (Lu et al., 2019).

2.3.4- PBK as a regulator for C2H2 zinc finger proteins

C2H2-ZNF proteins are characterized by having C2H2 zinc finger DNA-binding domains (Thiesen and Bach, 1990);. These zinc finger proteins form one of the largest families of mammalian transcription factors (Vaquerizas et al., 2009). They modulate gene expression to regulate several biological processes such as cellular differentiation, genome integrity, and tumor suppression (Sa et al., 2018). The three-dimensional structure of the C2H2 zinc finger domain comprises one α-helix and two adjacent β-sheets (Fig. 3), which coordinate a zinc atom using two cysteines and two histidine residues (Dovat et al., 2002; Vilas et al., 2018).

A single C2H2-ZNF domain recognizes its target DNA sequence by reaching into the DNA major groove. Typically 3-4 bases (three successive nucleotides of one DNA strand plus one nucleotide on the opposite strand) contact with the residues −1, +2, +3, and +6 of its α-helix. The amino acids that participate in this interaction are called the fingerprint amino acids (Wolfe et al., 2000).

The occurrence of C2H2-ZNF domains is not the same in all C2H2-ZNF proteins. It varies from 3 to 40 domains per C2H2-ZNF protein that form arrays within the protein (Vilas et al., 2018; Bruno et al., 2019).

Several factors control the binding specificity between C2H2-ZNFs and the DNA. They include the epigenetic modification of the target sequences, the number of the C2H2-ZNF

domains, and the adjacent amino acid sequences. The conserved linker peptides modify the binding affinity of C2H2-ZNF protein (Bruno et al., 2019). A few conserved linker motifs have been reported as targets of this regulatory phosphorylation. PBK and CK2 Protein Kinase CK2 are involved in this mechanism. (Sekiya et al., 2017).

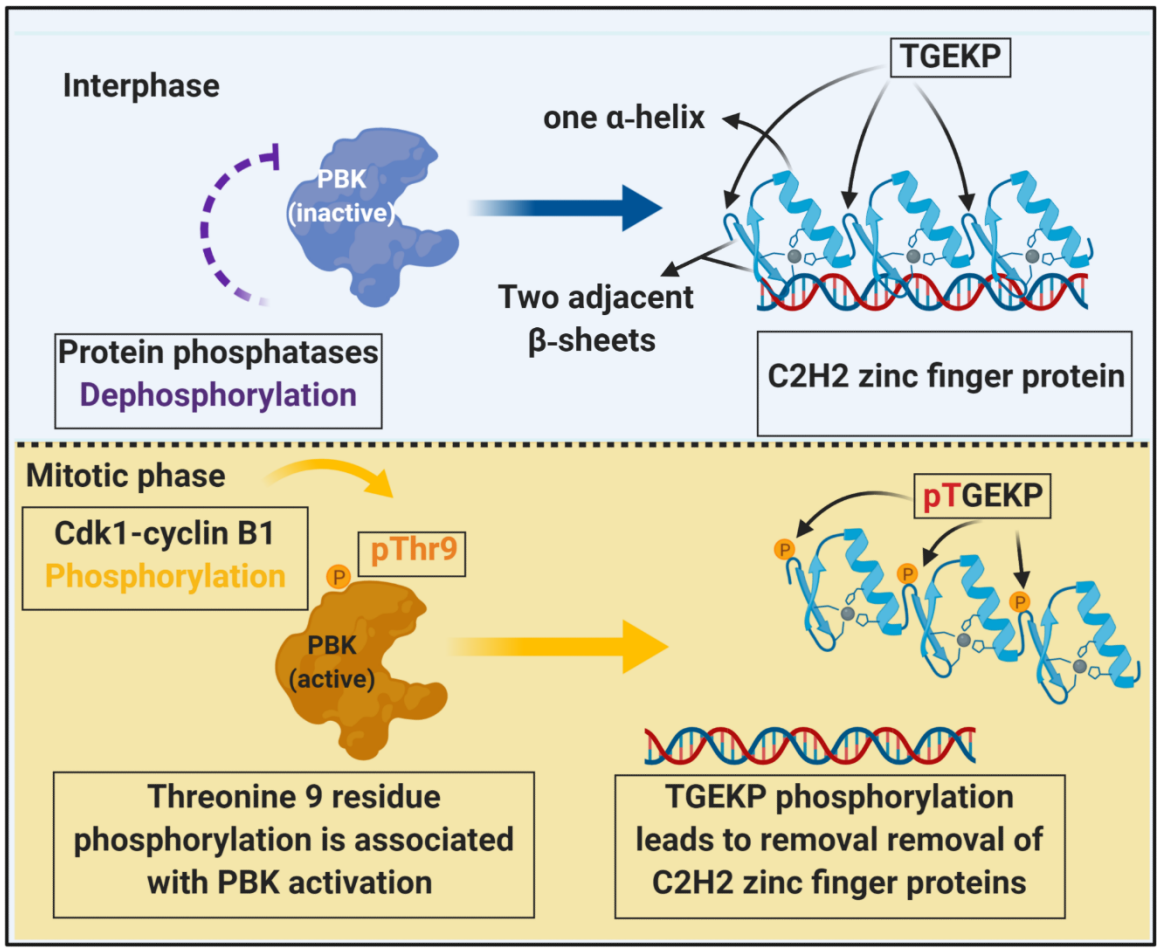

Figure 3: *The role of PBK in the regulation of C2H2-ZNF proteins binding activity. C2H2-ZNF proteins bind to DNA during the interphase. This binding is associated with both TGEKP dephosphorylation and PBK deactivation. When cells enter the mitotic phase, PBK is activated by its upstream kinase (CDK1). Active PBK phosphorylates the motif TGEKP. The phosphorylation of conserved linker sequence TGEKP in hundreds of C2H2-ZNF protein linker sequences leads to removing these proteins from the condensing chromatin.*

The highly conserved linker sequence TGEKP encompasses roughly half of the linkers of ZNF proteins. It separates neighboring C2H2-ZNF domains that are arranged in a multi-finger array. The consensus sequence mutation reduces the DNA binding affinity of

C2H2-ZNF proteins 10-100 fold (Wolfe et al., 2000; Jantz and Berg, 2004), indicating that this linker phosphorylation might significantly reduce the DNA binding ability of C2H2-ZNF proteins regardless of the sequence specificity of the bound DNA. This functionality was proposed to be a global mechanism for how C2H2 transcription factors are inactivated (Fig. 3) (Dovat et al., 2002). Rizkallah et al., 2011 evinced this global phosphorylation event during mitosis using a specific antibody against the phosphorylated motif (HpTGEKP). Later, Rizkallah et al., 2015 found that the inhibition of PBK by a kinase inhibitor or by gene knockdown technique reduces the phosphorylation of TGEKP significantly. They also showed that activated recombinant PBK phosphorylates TGEKP in vitro. These observations ascertained that PBK is the specific mitotic kinase of conserved linker sequence TGEKP. It is responsible for this global phosphorylation event that removes hundreds of proteins from the condensing chromatin (Rizkallah et al., 2015). Additional conserved linker motifs encompassing similar sequences have been reported as well as targets of phosphorylation (Sekiya et al., 2017).

2.3.5- The impact of PBK in tumor cells

PBK shows elevated expression levels in many tumors compared to differentiated cells (He et al., 2010). The correlation between tumor aggressiveness and the increased activity of PBK has been reported frequently in the literature (Herbert et al., 2018). This correlation was studied in several types of tumors, such as lung, cervix, and colorectal cancer. Tumor cells overexpressing PBK are significantly associated with low survival rates and high metastases rates (Lei et al., 2015; Luo et al., 2014). The aberrant activation of PBK in malignant cells activates several cellular mediators such as extracellular signal-related protein kinase 2 (ERK2) that promotes tumor growth (Abe et al., 2000; Zhu et al., 2007), and p53-related protein kinase (PRPK) that increases the migration and invasion of the cancer cells (Zykova et al., 2018). Furthermore, in vivo studies showed that PBK inhibition using small molecules or gene knockdown enhances the sensitivity of tumor cells to radiation and increases apoptotic cell death (Pirovano et al., 2017). This observation is attributed to transcription factors that are activated by PBK and boost the

expression of survival mediators. An example of this function is the phosphorylation of nuclear factor of NF-ϰB inhibitor alpha (IκBα) by PBK upon doxorubicin treatment, which releases the active NF-ϰB from the complex IκBα-NF-ϰB. The active NF-ϰB promotes the transcription of some survival mediators such as B-cell lymphoma 2 (Bcl-2), an inhibitor of apoptosis (IAP) proteins, and Survivin (Gyrd-Hansen and Meier, 2010).

Remarkably, PBK seems not to be an essential kinase for cell function and development since PBK knockout cells grow and proliferate in vitro, as demonstrated in the HAP1 PBK knockout model herein. PBK knockout mice are viable (Li et al., 2011b). However, PBK inhibition delays malignant progression, prevents cancer metastasis, and overcomes the therapeutic resistance with less toxicity to normal cells (Herbert et al., 2018).

2.4- Mass spectrometric analysis of phosphoproteome

Mass spectrometric phosphoproteome analysis enables the identification of phosphorylation events that occur on serine, threonine, and tyrosine residues after enrichment of phosphoproteins or phosphopeptides. This enrichment step is indispensable to overcome the following inherent limitations:

- Functionally important phosphorylation events commonly take place on low abundant proteins. In contrast, the phosphorylation events of limited or no function that result from off-target kinase activity are frequently seen on high abundant proteins (Levy et al., 2012).
- Phosphorylation often happens in substoichiometric ratios; thus, only small portions of the target proteins exist in a phosphorylated state (Steen et al., 2006).
- High abundant non-phosphorylated peptides sequences do suppress the phosphorylated ones due to ionizations that occur during mass spectrometric measures (Steen et al., 2006).

2.4.1- Immobilized metal affinity chromatography (IMAC)

In IMAC methods, the chelating metal is attached non-covalently to a matrix such as an iminodiacetate agar. Upon the exposure of peptides and phosphopeptides to mildly acidic conditions, the metal captures the phosphomonoester groups of the phosphopeptides preferentially. If the pH gets basic, the metal releases the captured phosphopeptides (Porath J., 1986). Zhou et al., 2008 have introduced immobilized titanium ion affinity chromatography ($Ti4^{+}$-IMAC) as a new method to enrich the phosphopeptides from a standard digest mixture of phosphorylated and non-phosphorylated bovine serum albumin (BSA) in a low ratio (1:500). $Ti4^{+}$-IMAC also provides higher efficiency and specificity than other IMAC methods such as $Fe3^{+}$-IMAC, $Zr4^{+}$-IMAC, TiO2, and ZrO2 (Zhou et al., 2008).

2.4.2-. Metal oxide affinity chromatography (MOAC)

The mechanism of the interaction between the phosphopeptides and MOAC is not elucidated and understood in detail. However, it is thought that this interaction depends on ion exchange mechanisms and Lewis acid/base interactions. Likewise, the enrichment of phosphopeptides by IMAC, MOAC particles bind to the phosphopeptides in low pH buffers and set them free in high pH. However, MOAC is less specific than IMAC and can capture more non-phosphopeptides rich with aspartic and glutamic acid residues. The presence of a strong organic acid in the loading buffer like trifluoroacetic acid (TFA) or glycolic acid reduces the nonspecific binding of the non-phosphopeptides and increases the enrichment specificity. MOAC can be produced from the oxides of different metals such as titanium, iron, zirconium, and aluminum, but titanium and zirconium oxides are the most used MOACs owing to their commercial availability (Jensen and Larsen, 2007; Kurylo et al., 2017).

2.5- Mass spectrometry instrumentation

Although the immense and fast progress in mass spectrometric technology, its essential function is to determine the mass-to-charge ratio (*m/z*) of the ionized analytes. Thus, mass spectrometry devices are made up of three fundamental parts: the ion source, the

analyzer, and the detector. Other parts, such as liquid chromatography unite (LC), and ion mobility separation unit can be coupled to mass spectrometry to add more separation dimensions.

2.5.1- Electrospray ionization (ESI)

ESI is one of the most prominent soft ionization methods. It is often online coupled to a liquid chromatography that separates the analytes in the liquid phase to be ionized and later analyzed by the mass analyzer (Ho et al., 2003). The ionization process consists of three steps: In the first step, the analyte solution pass through the top of the electrospray needle, which sustains a high voltage (e.g., 2.5 – 6.0 kV). The diffused solution containing the analyte undergoes two competing forces; the surface tension of the solvent prevents it from scattering and the electrostatic coulomb attraction that pulls the liquid to the counter electrode (Hogan et al., 2009; Wilm, 2011). The balance between these two contrary forces forms the Taylor cone. The potential difference between the capillary needle and the counter electrode brings the positive ions to the solvent cone's surface (Fig. 4). In the second step, the electrostatic force overcomes the surface tension, and charged droplets are generated at the collapsed Taylor cone's end. The charged droplets surrounding the solvent evaporates, leading to an increase in the charge density on the droplets' surface.

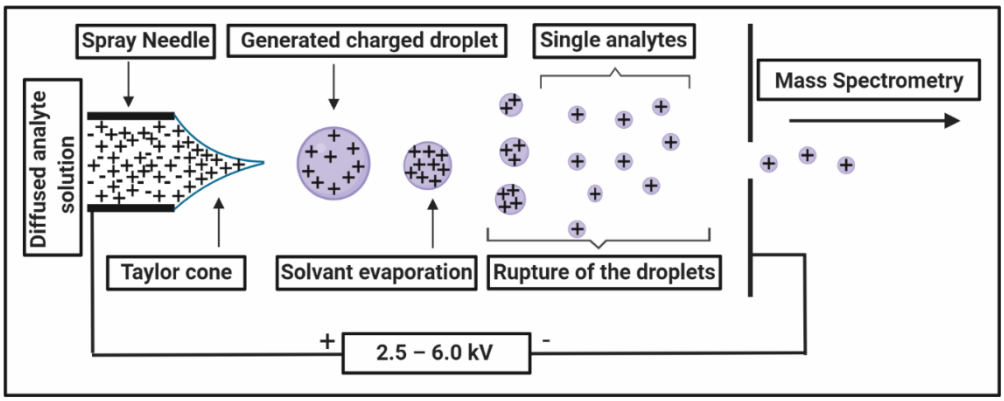

Figure 4: *The electrospray ionization principle. The Taylor cone is formed upon pumping the dissolved analytes through the needle under an electric field. The droplets are generated and then deformed with the repeated solvent evaporation to generate finely single charged analytes.*

In the third step, the increased charge density increases the coulombic repulsion force to reach the Rayleigh limit, at which the droplets are ruptured into smaller droplets. This fission event is called the coulombic explosion; it fractures the droplets to produce single analytes. This explanation is called the charge residue model (CRM).

There are two additional possible explanations for this event; the ion emission model (IEM) and the chain ejection model (CEM). According to IEM theory, a nano-droplet formed of an ion with a solvation shell is ejected repeatedly from the droplets when the forces resulting from the excessed droplet charge overcomes the surface tension. The residual solvent evaporates, and the gaseous ion is generated. According to CEM theory, steady evaporation of the solvent leads to secondary Taylor cone formation. The top of the new cone is collapsed again, and highly charged nano-droplets are ejected. The process is repeated, producing ions in the gaseous phase (Konermann et al., 2013).

2.5.2- Quadrupole mass analyzer

A quadrupole is a type of mass analyzer. It is composed of four cylindrical metallic rods arranged around a central axis. A static direct current (DC) and a radio frequency (RF) alternating current (AC) voltage are applied on rods in a manner that one pair of rods have the opposite polarity of the other pair. The superposition of the applied voltages generates a fluctuating electrical field between the rods, making the ions move in a spiral trajectory.

An ion's ability to pass through the electric field depends on its *m/z* value and the applied voltage. For a defined voltage, solely the ions that follow specific spiral trajectories stably reach the detector (Fig. 5). The other ions will deflect and collide with the rods or be ejected due to their high oscillating movement. DC and RF can be adjusted to transmit ions with specific *m/z* or broad *m/z* range values and eject the rest (Haag, 2016).

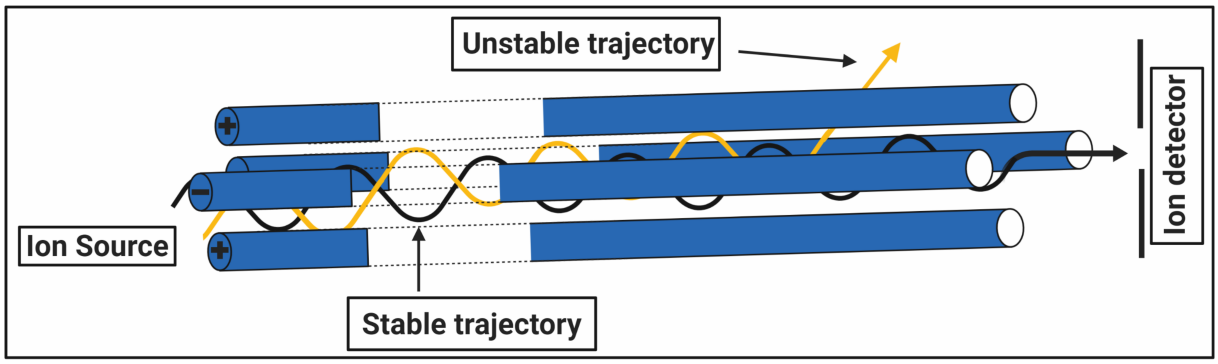

Figure 5: *A schematic illustration of the quadrupole mass analyzer. The four rodes are assembled around a central axis. The superposition of the applied static direct current (DC) and the radio frequency alternating (AC) voltage generates the fluctuating electrical field. The passing ions will follow a spiral trajectory. The radius of moving ions depends on the generated electrical field and m/z values of these ions.*

2.5.3- Ion mobility separation (IMS)

IMS is a gas-phase separation technique, separates the gaseous ions depending on the essential characteristics, such as the mass (m), the charge (z), and the mobility of the ion in the supplied gas phase (K). Ion mobility separator consists basically of a tube situated in a vacuum system, refilled with an inert gas buffer until defined pressure. The gas buffer is subjected to a weak electric field. As the gaseous ions are injected into IMS tube, they are exposed to two contrary forces; the electric field leads the inserted ion to travel through the gaseous buffer and the hindrance force, which results from the collisions between the ions and the gas buffer molecules (Jurneczko and Barran, 2011). The mobility of an ion (K) and the applied electric field (E) determine the ion velocity (v_d) of a given ion and can be calculated from the formula:

$$v_d = KE$$

The physical shape of the ion in the gas buffer affects the analyte ion mobility, so it can be used to distinguish between phosphorylated and non-phosphorylated sequences (Ruotolo et al., 2002).

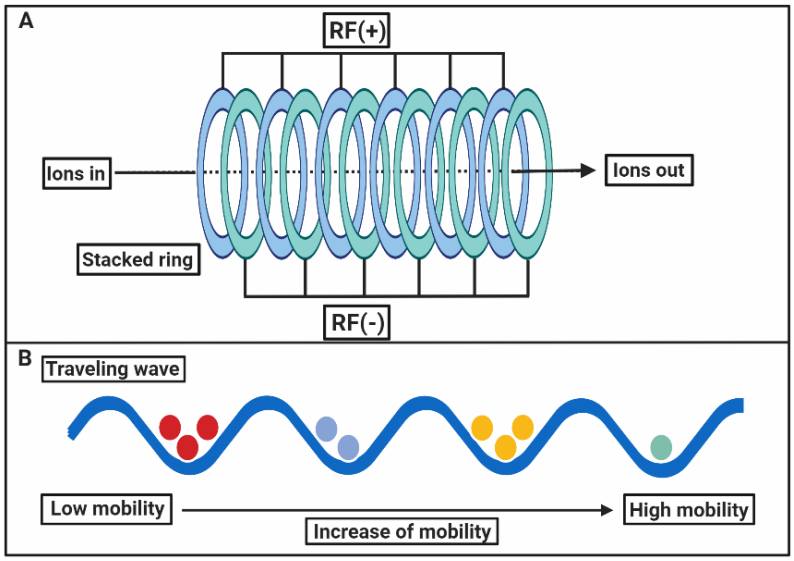

Figure 6: *Traveling wave ion mobility separator (A) A schematic illustration of the device. (B) The separation of the analyzed ions depending on the mobility of the ion in the traveling waves.*

The traveling wave ion mobility spectrometry (TWIMS) is one of the most used ion mobility separators in proteomics. The basic structure of the traveling wave ion mobility separator is an assembly of stacked rings ion guide (SRIG). The rings are subjected to radiofrequency (RF) voltage in a manner that each two adjacent rings have an opposite RF (Fig. 6). The applied opposite voltages confine or slow the ions that arrive at the axial tarp. A transient direct current (DC) is superimposed with the radiofrequency (RF) voltage, leading to generating a potential hill that drives the ions forward. This process is repeated subsequentially at regular time intervals along the stacked rings' length to generate continuous waves. The ions move under the propelling traveling waves, which overcome the gas retardance, so the ions are separated depending on their mobility (Giles et al., 2004; Giles et al., 2011)

High mobility ions keep up with the traveling wave path to precede the low mobility ions that need a longer time to pass the separator. Traveling wave ion mobility separation is used by Waters to produce a hybrid Q-IM separator-TOF instrument, which is called the Synapt HDMS system (Pringle et al., 2007).

2.5.4- Time of flight analyzer (TOF)

TOF analyzer identifies the ions depending on *m/z* values, which are calculated from their flight velocities. The ions of interest are accelerated under an electric field *P*. Then, they enter a vacuum tube (field-free drift) to fly with the same velocity until they reach the detector after they pass the distance *d*. If the electron charge is *e*, the kinetic energy can be calculated from the equation:

$$zeP = \frac{mv^2}{2}$$

Each ion needs the time *t* to reach the detector

$t = d/v$

$$t^2 = \frac{d^2}{v^2} = \frac{m}{z}\frac{d^2}{2eP}$$

$$t = \frac{d}{\sqrt{2ep}}\sqrt{\frac{m}{z}} = c\sqrt{\frac{m}{z}}$$

Since *c* is a constant, the time of flight *t* can be converted to *m/z* value.

When the ions fly longer distances, the differences between arriving times will be longer, and the resolution will be higher. An electrostatic mirror, called a reflection, is set at the end of the flight path to achieve this goal. The ions strike the reflectron to fly back in a new path that makes a small angle with the original path (Fig. 7). Besides the increased flight distance and the higher resolution, the reflectron focuses the ions with the same *m/z* value, but they acquired slightly different velocities. Ions with lower kinetic energy reflect easier than those with higher kinetic energy since the last ones cross further in the reflectron before they reflect again. The reflectron corrects the accelerated ion initial kinetic energy representing identical *m/z* values (Haag, 2016).

4.6- Synapt G2S Mass Spectrometer instrument

Synapt G2 S is a Q-TOF mass spectrometer is provided by ion mobility separation cell and coupled with nanoAcquity UPLC liquid chromatography unit (Fig. 7). UPLC unit

separates the peptide precursors of high complex protein samples to reduce their complexity. The eluted precursors are ionized by ESI, transferred to the quadrupole analyzer to be filtered or pass freely to the ion mobility separation unit, and then later to the collision cell. The ions are accelerated then and separated in the TOF analyzer according to their m/z values. When the ion mobility separation unit is activated, an additional separation dimension is appended, as explained before. Collision cell can also be operated on high or low energy mode to measure *m/z* values, to analyze the precursors or the fragmented peptides. The instrument enables measuring the peptides in two different acquisition modes: data independent acquisition mode (DIA) and data dependent acquisition mode (DDA)

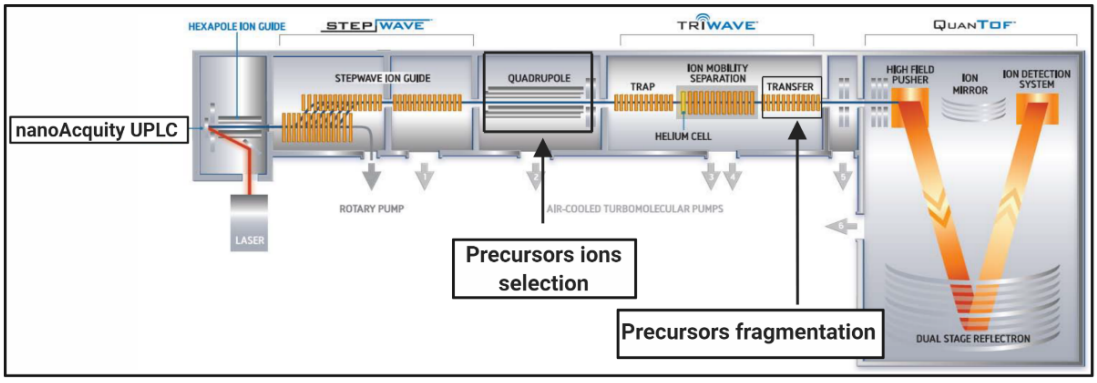

Figure 7: *Schematic of Synapt G2S mass spectrometer (www.waters.com; modified figure).*

4.6.1- Data independent acquisition mode (DIA)

Hoaglund-Hyzer et al. 2000 developed a data independent LC-IMS/MS acquisition (DIA). The approach depends on parallel fragmentation of the precursor across the entire *m/z* range and consists of two steps: MS and MSMS step. In the first step (MS), the precursor ions are acquired without fragmentation (Fig. 8). In the second step (MSMS), the energy of the collision cell is elevated, the precursors are fragmented and acquired. The collision cell is alternated between the low and high energy states. Since there is no selection during the acquisition, all fragments and precursors are matched retrospectively, depending on their retention time (Hoaglund-Hyzer et al., 2000).

.

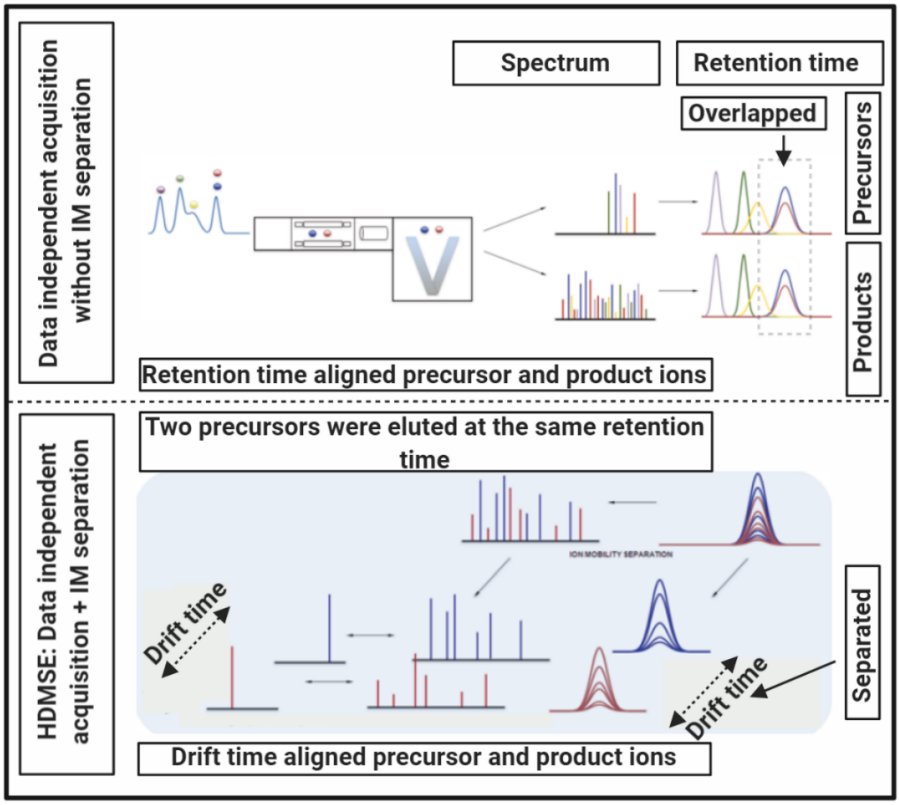

Figure 8: *The principle of DIA and the benefit of integrating IM separation into the system. During the DIA approach, the spectra of the precursors and products are acquired with their retention times. IM separates the precursors that have different motilities in the traveling waves. The acquired spectra, retention times, drift times aligned (www.waters.com; modified figure).*

Waters Corporation incorporated traveling wave ion mobility spectrometry (TWIMS) to develop a variant of the DIA approach called HDMS^E. HD refers to the high definition that results from coupling ion mobility separator as a new separation dimension and E to the elevated energy. HDMS^E provides three subsequent separation dimensions with appropriate decreasing time scales: LC, IM, and TOF analyzer. In HDMS^E acquisition, the precursors are separated on the LC system, ionized by ESI, and the separated in IM unite depending on their motilities in the traveling wave. Finely the ions reach the TOF analyzer to be separated depending on *m/z* values. After the measurement, the proteinLynx Global SERVER (PLGS) matches a precursor ion with its fragments based on a retention time alignment. In HDMS^E, the additional drift time is also aligned. (Shliaha et al., 2013, Li et al., 2009).

4.6.2- Data dependent acquisition mode (DDA)

DDA was introduced by Stahl et al. .1996. It is now the most widely used approach in proteomic research. To decrease sample complexity and to increase the identification, DDA foregrounds the ionized precursors depending on their intensities (Fig. 9). During the acquisition, the ionized precursors are screened by the MS scan survey. Then, the most intense precursors (n) are selected (n=5 precursors in this work), fragmented, and analyzed by MSMS. For a precisely defined time, precursors that have the same *m/z* values of the selected precursors in the MS step will be excluded to avoid redundant selection of the same precursors. The problematic disadvantage of DDA is that that a portion of the analyzed tryptic peptides have low intensity, so they will never be fragmented and measured (Stahl et al., 1996; Fenaille et al., 2017).

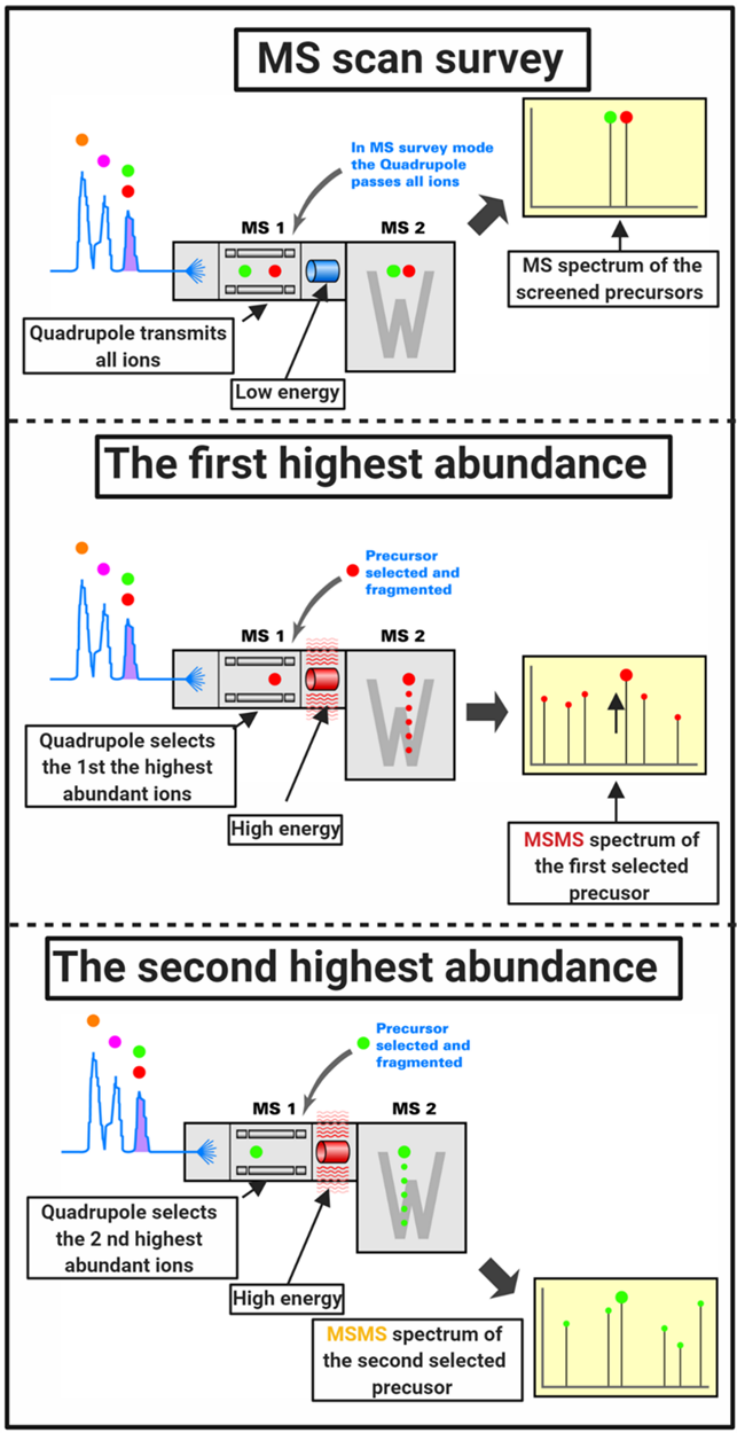

Figure 9: *A schematic illustration of data dependent acquisition (DDA): the ions are selected depending on their abundances (www.waters.com; modified figure).*

3- Aim

Several studies reported the upregulation and the phosphoregulatory activation of PBK in various tumors and suggested it as a promising therapeutic target (Ishikawa et al., 2018). The focal point of this work is to determine novel PBK-dependent phosphorylation events.

- Novel PBK-dependent phosphorylation events shall be identified to understand the role of PBK in normal and cancer cells.
- HAP1 cells (wild type and PBK knock out) are suspected to provide a convenient model to study PBK-dependent phosphorylation events-
- Appropriate treatment will be investigated to arrest the HAP1 cells in the mitotic phase (PBK is active during mitosis).
- Regulation of proteins will be monitored by studying mitotic and PBK-dependent phosphorylation events.

Assorted approaches are deployed to achieve these goals: cell culture, flow cytometry, western blot, phosphopeptides enrichment, mass spectrometry, and bioinformatics tools.

4- Materials and methods

4.1- Cell culture

4.1.1- Cell lines

HAP1 wild type cells (WT.1 and WT.2) and PBK knockout cells (K.1 and K.2) were generated by Horizon Genomics (Vienna) in response to recommendations of Thiesen's lab (Table 2). The cells were grown at 37 ºC, 5 % CO2 in Iscove's Modified Dulbecco's Medium (IMDM) (Gibco®,12440-053) supplemented with 45 units/ml penicillin, 45 µg/ml streptomycin (Gibco® #15070-063) and 10 % FBS (Biochrom Superior S 0615).

Table 2: *Product information of the used cell lines.*

Cell Line	Catalog Number	Description
WT.1	C631	Human HAP1 parental control cell line
WT.2	C665	Human HAP1 control cell line
K.1	HZGHC000098c016	Human PBK knockout cell line 2bp deletion
K.2	HZGHC000098c014	Human PBK knockout cell line 8bp deletion

4.1.2- Cell passaging

HAP1 cells were grown as mentioned above until ~75 % confluence, and then the medium was discarded. The cells were washed with 1x DPBS (Gibco, #14/90-094) and then treated with pre-warmed 0.05 % Trypsin-EDTA solution (Gibco, # 25300-054) for approximately 5 minutes at 37 °C. When the treated cells detached, trypsin was deactivated with an appropriate volume of pre-warmed IMDM medium. The cells were counted, and the required number of cells was seeded for the next experiments in a 6-well plate or flask using the pre-warmed medium.

4.1.3- Cell counting

After cell-detachment and trypsin deactivation, a small portion of the cells was transferred to a new centrifuge tube. The cells were diluted ten times, and ~12µl of the diluted cells were loaded at hemacytometer (Neubauer Improved counting chamber, Art.

No.T729.1). The cell's content of the four large squares in the corners of the frame was counted, and the average was calculated.

$$Cell\ count\ (cell/ml) = The\ average\ cell\ count\ \times\ Dilution\ factor\ \times\ 10^4$$

4.1.4- Cell thawing

The cells were transferred from liquid nitrogen to the cell culture laboratory in dry ice. The cells were then incubated in a water bath until they were thawed (around 3 minutes), diluted in 5 ml medium, and centrifuged for 5 min at 210 x g (1100 rpm; Heraeus, Megafuge® 1.0) at room temperature. The medium was discarded, and the cells were resuspended in the medium again to remove DMSO. The cells were seeded and passaged at least once before they were used in the experiments.

4.1.5- Cryogenic storage

At least six cryo-vials were stored of each cell line to be used later in case of need. After trypsinization, the cells were counted, and the desired number of cells was transferred to a new 15 ml tube. The cells were centrifuged for 5 min at 210 x g (1100 rpm; Heraeus, Megafuge® 1.0) at room temperature, resuspended in an appropriate volume of freezing medium. This medium consists of growth medium supplemented with fetal calf serum (FCS) (Biochrom FBS Superior, #S 0615) and DMSO (50 % IMDM growth medium + 40 % FBS + 10 % DMSO). The cells were distributed into cryo-vials. Each cryo-vial contains between 1-2 million cells per vial. The cryo-vials were put in a CoolCell® cell freezing container (Biocision®, BCS-172), transferred immediately to -80°C for two weeks before permanent storage in liquid nitrogen.

4.1.6- Cell viability test with trypan blue exclusion method

Trypan blue exclusion test was used to determine the cell viability. The cells were diluted according to the cell density after harvesting in pre-cooled PBS. Equal volumes of the diluted cell suspension and pre-cooled 5 % trypan blue in PBS were mixed and

homogenized by pipetting up and down and gentle use of a vortex mixer. Roughly, 12 µl of cell suspension/trypan blue was applied to the hemacytometer. The cells were visually examined by microscope (Nikon TMS) within 3 minutes to count and differentiate the viable cells that exclude trypan blue dye by their intact cell membranes from nonviable cells that were stained with blue. The count of the viable, nonviable, and total cells was determined, and then the cell viability was calculated using the equation:

$$\text{Cell viability (\%)} = \frac{The\ number\ of\ viable\ cells}{The\ total\ number\ of\ cells}$$

4.1.7- Cell harvesting and total protein extract preparation for western blot analysis

The floating mitotic cells were collected by gentle up and down pipetting, transferred to 2 ml centrifuge tube, and centrifuged at 381 ×g (2000 rpm; Heraeus biofuge fresco) for 5 min at 4 °C. Vehicle treated cells (ethanol treated) were trypsinized with 200 µl of trypsin EDTA solution and incubated at 37 °C, 5 % CO2 for 5 min to be detached. After that, trypsin was deactivated by adding fetal calf serum containing cell culture medium. The cells were collected, as mentioned before. The cells were washed three times with pre-cooled PBS and pelleted. Finally, the cell pellets were dissolved in an appropriate volume of 1× SDS sample buffer, vortexed, and homogenized in a QIA shredder spin column (Qiagen Cat No. 79656). The homogenized lysates were transferred to new 1.5 ml tubes and stored at -20 °C.

4.2- Cell cycle synchronization

Two methods were used to arrest the cells at the G2/M phase. The cells were treated with double thymidine and nocodazole (DTB-Noc) or with okadaic acid (OA) (Table 3).

Table 3: *The used chemicals for cell cycle synchronization*

Chemical	Catalog Number
Thymidine	Sigma-Aldrich®, T1895-5G
Nocodazole	Cayman Chemical, 13857
Okadaic acid	Cayman Chemical, 10011490

4.2.1- Double thymidine block and nocodazole (DTB-Noc)

The cells were seeded in a 6-well plate, allowed to grow spontaneously in the growth medium until they achieved approximately 40 % confluence. After that, the medium was replaced by a fresh medium containing 2 mM thymidine, and then the cells were incubated at standard conditions for 12 hours to arrest cells at the G1/S phase. The cells were washed in pre-warmed sterile 1x DPBS three times and then fed with a pre-warmed growth medium. After 12 hours, the cells were subjected to the second thymidine block treatment and release as described before. Upon releasing the cells from G1/S block- the time point "0 hours"- the cells were fed with a fresh medium containing one of the following concentrations of nocodazole: 0, 40, 60, 80, 100 ng/ml, for 10 hours, to arrest cells at the G2/M phase.

4.2.2- Treatment with okadaic acid (OA)

The cells were seeded in a 6-well plate, allowed to grow spontaneously in the growth medium until they achieved approximately 75 % confluence. Thence, the medium was replaced by a medium containing an appropriate concentration of okadaic acid for 6 hours. Different OA-concentrations were tested (0, 40, 60, 80, 100 nM, and 1 µM) to identify the appropriate concentration. Thereafter, 1 µM was adopted to synchronize the cells at the G2/M phase in the later experiments.

4.3- Protein quantification

Protein concentration was determined using either the Qubit® Protein Assay (Thermofisher Scientific, Waltham, MA, Q33212) for digested peptide sample or RC DC Protein Assay (Bio-Rad; 500-0119) for total protein extract prepared in SDS sample buffer or the Bio-Rad protein assay (Bio-Rad, Hercules, 500-00006) for total protein extract.

4.3.1- Qubit™ Protein Assay

For the Qubit® Protein Assay, an appropriate volume of working solution was prepared by diluting Qubit™ protein reagent (Component A) in Qubit™ protein buffer (Component B) 200 times. The final assay volume was 200 µl. The standards were prepared by transferring 190 µl of working solutions to three 500 µl tubes and 10 µl of each Qubit™ protein standard (Component C, D, and E). The samples were prepared by transferring appropriate volumes of working solution (between 197 and 195 µl) to new tubes and the fitting volumes of each digested peptide sample (between 3 and 5 µl). The standards and samples were incubated at room temperature for 15 minutes (the fluorescence is stable for 2 hours at room temperature according to the manufacturer's instructions). The standards and samples were measured consecutively in less than 10 minutes, and the readouts (QF value) were used to calculate the peptide concentration using the following equation:

$$Concentration\ of\ the\ sample\ (\mu g/mL) = \frac{QF\ value\ \times 200}{x}$$

QF value = the given value by the Qubit® 2.0 Fluorometer.

x = the number of microliters of the sample that were used in the assay.

4.3.2- RC DC Protein Assay

The assay is based on protein precipitation and discarding the solvent to remove the reducing agent (reducing agent compatible RC) as well as the detergent (detergent

compatible DC), which can interfere in the assay. The precipitated proteins were later re-dissolved and quantified by Lowry assay. The assay was performed as follows:

Five dilutions of a protein standard (from 0.2 mg/ml to 1.5 mg/ml protein) were prepared in 1X SDS sample buffer from 25 mg/ml stock solution of Bovine Serum Albumin (BSA). 25 µl of sample and standards were transferred to new centrifuge tubes in triplicate. 125 µl of RC reagent I was mixed with each sample and standard replicate. The tubes were vortexed and incubated at room temperature for 1 minute.

125 µl of RC reagent II was added into each sample and standard tube. The tubes were vortexed and centrifuged at 15,000 × g for 5 minutes. The supernatant was discarded, the rest of the solvent was drawn off using new clean loading tips without disturbing the protein pellet. Later on, the tubes were inverted on clean absorbent tissue to allow the remaining solvent to drain. The tubes were put back in the rack and left open to allow the residual solvent to evaporate.

While the tubes were let to dry, an appropriate amount of A' reagent was prepared by mixing 1 volume of the reagent S to 50 volume of the reagent A. 127 µl of reagent A' was added to each sample and reagent tube. The tubes were vortexed well and incubated for 5 min or till the complete dissolving of the protein pellet at room temperature.

1 ml of DC reagent B was added to each sample and standard tubes. The tubes were vortexed well and incubated for 15 minutes at room temperature. After that, the standards and samples' absorbance values were determined at 750 nm, using SmartSpec™3000 spectrophotometer (Bio-Rad). The absorbance is known to be stable for 1 hour. The standard curve was drawn using Excel, and protein amounts were calculated.

4.3.3- Bio-Rad protein assay

Bio-Rad protein assay was used unless the samples were dissolved in SDS sample buffer. The assay depends on the Bradford protein assay to determine the concentration of the soluble proteins. The assay was performed as follows:

Appropriate volumes of distilled water were dispensed into the tubes of standards, blanks, and samples to make the final volume of 800 µl after adding the proteins and the lysing buffer. BSA stock solution (25 mg/ml) was diluted to 0.1 mg/ml, and appropriate volumes contain 3, 6, 9, 12, 15 µg BSA were transferred to centrifuge tubs to prepare a set of protein standards in triplicates. 10 µl of lysing buffer was added to each tube of the standards and the blank, whereas 10 µl of protein lysates were transferred to sample tubs in triplicates. Finally, 200 µl of dye assay reagent was added to each tube (the final volume 1 ml). The tubes were closed inverted a few times to mix protein solution with the reagent, vortexed, and incubated for 5 minutes at room temperature. The absorbance values were determined using SmartSpec™3000 spectrophotometer (Bio-Rad) at 595 nm. The standard curve was drawn using Excel, and protein amounts were calculated.

4.4- Measuring the mitotic index by flow cytometry

The cells were stained with antibody against the phosphoserine 28 of histone H3, according to the intracellular flow cytometry staining protocol (BioLegend). BD FACSVerse™ (BD Biosciences) flow cytometry was used to distinguish the mitotic from non-mitotic cells.

The fixation step: The cells were collected, washed three times with PBS, and 1 million cells were resuspended in 0.5 ml of the fixation buffer (BioLegend Cat. No. 420801) and incubated in the dark for 20 min at room temperature. The cells were centrifuged at 350 x g for 5 minutes, and the supernatant was discarded.

The Permeabilization step: The cells were resuspended in 1× intracellular Staining Perm Wash Buffer (BioLegend Cat. No. 421002) and then spun down by centrifugation at 350 x g for 5 minutes. This step was conducted three times in total.

The staining step: The fixed-permeabilized cells were resuspended in Intracellular Staining Perm Wash Buffer. An appropriate amount of both PerCP/Cy5.5 anti-Histone H3-phosphoserine 28 (BioLegend Cat. No.641014), PerCP/Cy5.5 Rat IgG2a, k Isotype Ctr (BioLegend Cat. No. 400532) were calculated (5 µl antibody per 1 million cells)

depending on cells count of the stained cells. Each sample was split into three equal portions. These potions were incubated with anti-H3-phosphoserine 28 antibody (stained with anti-H3-phosphoserine 28), or control antibody (stained with control antibodies), or Wash Buffer (unstained) for 20 minutes in the dark at room temperature.

The washing step: The cells were washed twice in Intracellular Staining Perm Wash Buffer and centrifuged at 350 x g for 5 minutes. Each sample was resuspended in 0.5 ml of Cell Staining Buffer.

The measurement: The cells were analyzed by BD FACSVerse™ flow cytometer for 10,000 gated events, Filter: 700/54 Mirror: 665 LP, Laser: Blau (488 nm), and BD FACSuiteTM software.

4.5- Western blot

Western blotting was deployed to detect the proteins of interest (phosphorylated and non-phosphorylated). The proteins were denaturated, separated by sodium dodecyl sulfate-polyacrylamide gel electrophoresis (SDS-PAGE), transferred to a membrane, and finally, the antigens of interest were detected using appropriate antibodies.

4.5.1- Sodium dodecyl sulfate-polyacrylamide gel electrophoresis (SDS-PAGE)

The samples that contain the analyzed proteins were dissolved in SDS sample buffer (Table. 4) and cooked at 95 °C in 1×SDS for 5 min to convert the proteins into denatured polypeptides carrying negative charges with equal densities per unit length. Appropriate volumes of protein lysates that contain 40 µg protein were loaded into sodium dodecyl sulfate-polyacrylamide gel. PageRuler prestained and unstained protein ladders (Thermo scientific, #26616, #26614) were also loaded, whereas the empty wells were filled with sample buffer.

Table 4: *5x Laemmli SDS Sample buffer composition*

Chemical	Molarity or percentage
TRIS/HCL pH=6,8	312.5 mM
SDS	10 %
Dithiothreitol	325 mM
Bromophenol blue	0.4 %
Glycerol	50 %

The denaturated proteins were separated using one-dimensional electrophoreses in the presence of 0.1 % SDS. The handcast gel is composed of two parts; 4.5 % staking sodium dodecyl sulfate-polyacrylamide gel and separating denaturing sodium dodecyl sulfate-polyacrylamide gel (10 %). The samples were loaded into the stacking gel, and electrophoresis was performed at a constant 30 mA. Protein migration was monitored using a prestained protein ladder, which was loaded in a separate well. The electrophoresis was stopped just as the dye front was released from the gel to the running buffer. Tables 5, 6, and 7 show the composition of the used buffers and materials.

Table 5: *The buffer and solutions that were used for SDS PAGE gels casting*

Solution	Composition
Tris/HCl buffer pH=8.9	1 M Tris/HCl
Tris/HCl buffer pH=6.8	1 M Tris/HCl
Acrylamide (AA) / Methylenbisacrylamide (BisAA) (Roth Rotiphorese Gel 30, Cat. No. 3029.1)	30 %/0.8 % (v/v)
Tetramethylethylendiamine (TEMED) (Serva Cat.No.: 35930)	99.0 %
Ammonium persulfate (APS) (Serva Cat. No.: 13375.03)	99.0 %

Table 6: *10x Running Buffer for SDS-PAGE*

Chemical	Molarity or percentage
TRIS Base	0.25 M
SDS	1 %
Glycine	1.92 M

Table 7: *The composition of SDS- polyacrylamide gel*

Solution	10 % separation gel	4,5 % stacking gel
AA/BisAA	7 ml	1.5 ml
Tris/HCl buffer pH=8,9	8 ml	---
Tris/HCl buffer pH=6,8	---	1.25 ml
H_2O	5 ml	7 ml
10 % SDS	216 µl	100 µl
10 % APS	160µl	100 µl
TEMED	20 µl	10 l

4.5.2- Protein transfer

The semi-dry transfer was used to move the separated proteins out of the gel and onto the inert membrane made of polyvinylidene difluoride (PVDF) (Immobilon®-FL, cat.no. IPFL00010), according to Kyhse-Anderson protocol (Kyhse-Andersen, 1984). Protein transfer was performed using the Bio-Rad Trans-Blot SD Semi-Dry blotter, appropriate buffers (Tables 8, 9, 10, and 11), and wetted filter papers as following:

- PVDF membrane and filter paper were cut in appropriate sizes to fit the separation gel.
- The gel was equilibrated in an ε-aminocaproic acid buffer.
- The membrane was pre-wetted in isopropanol and water before it was equilibrated in LT buffer.

- The anode was wetted with HT buffer. Three filter papers were pre-wetted in HT buffer and placed on the anode, followed by six filter papers pre-wetted in LT buffer.
- The pre-wetted PVDF membrane was mounted on the filter papers.
- The gel was placed on the membrane.
- Nine filter papers were pre-wetted in an ε-aminocaproic acid buffer and placed onto the gel.
- The anode was wetted with HT buffer.
- The transfer device was assembled, the voltage was adjusted at 25 Volt, and the transfer was run for 2 hours.

Afterward, the membrane was dried, immersed in Ponceau S with shaking, washed three times with distilled water, let dry out, and then scanned or photographed.

After scanning, the membrane was wetted in isopropanol and water, after that equilibrated in PBS and incubated overnight at 4°C in Odyssey® Blocking buffer (LI-COR; #927-40000) in PBS.

Table 8*: HT buffer, pH = 10.4*

Chemical	Molarity or percentage
TRIS base	0.3M
Methanol	20 %

Table 9: *LT buffer, pH = 10.4*

Chemical	Molarity or percentage
TRIS base	0.025M
Methanol	20 %

Table 10: *ε-aminocaproic acid buffer*

Chemical	Molarity or percentage
ε-Aminocaproic acid buffer	0.04 M
TRIS base	0.025 M
20 % Methanol	0.1 M

Table 11: *10×PBS, pH = 7.44*

Chemical	Molarity
NaCl	1.37 M
KCl	0.027 M
Na2HPO4	0.1 M
KH2PO4	0.018 M

4.5.3- Antibody staining

The antibodies were diluted in antibody buffer (Odyssey® Blocking buffer 1:2 diluted with filtrated 1x PBS supplemented with 0.1 % Tween) according to the manufacturer's recommendations (Tables 12 and 13). The blocked membrane was incubated with primary antibodies at room temperature with mild shaking for 2 hours. The membrane was washed four times for 5 minutes with a washing buffer on the shaker at room temperature. After the fourth wash step, the membrane was incubated with diluted secondary antibodies for one hour at room temperature with mild shaking. Afterward, the membrane was washed four times as described before and rinsed once in PBS. The stained membrane was kept in PBS protected from light at 4 C to be imaged later using LI-COR Odyssey® CLx imager.

Table 12: *List of the primary antibodies*

Antibody	Producer	Catalog number	dilution (antibody working concentration)
pTGEKP	BioLegend	678902	1:1000 (0.5 µg/m)l
PBK/TOPK	Cell signaling	4942	1:1000
Annexin I	Santa Cruz Biotechnology	sc-12740	1:1000 (0.2 µg/ml)
G6PD	Santa Cruz Biotechnology	sc-373886	1:1000 (0.2 µg/ml)
EMD	Santa Cruz Biotechnology	sc-25284	1:1000 (0.2 µg/ml)
Phospho-p38 alpha(Thr180/Tyr182)	ThermoFisher	36-8500	1:1000
GAPDH	Millipore	MAB374	1:5000 (0.4 µg/ml)
β-actin	BioLegend	622102	1:1000

Table 13: *List of the secondary antibodies*

Antibody	Producer	Catalog number	dilution
IRDye 800CW	Licor	926-32211	1:10000 (0.1 µg/ml)
IRDye 680CW	Licor	926-32220	1:10000 (0.1 µg/ml)

4.6- Total protein extract, trypsin digestion of proteins, and desalting of peptides

The frozen pellets were thawed quickly (pellet weight was about 50 µg), and the total protein was extracted according to Fulda et al., 2006. The cells were resuspended in sodium deoxycholate (SDC) based buffer (Table 14). The suspended cells were heated at 95°C for 5 min and then sonicated twice at level 2 for 15 s to shear the DNA (Laborrette 17, Fritsch, Berlin). After that, the samples were incubated at room temperature for 10 min.

Table 14: *SDC based extraction buffer*

Chemicals	Concentration
Sodium deoxycholate (SDC)	1.5 %
Dithiothreitol (DTT)	20 mM
Ammonium bicarbonate (ABC)	50 mM
Halt-Phosphatase Inhibitor (Thermo Scientific; 78420)	3 times working concentration

A total of 800 µl of the cell extract was transferred to a new centrifuge tube, and the protein content was determined using a Bio-Rad protein assay kit as described previously. The sulfhydryl groups on the proteins were carbamidomethylated by addition iodoacetamide (IAA) to a final concentration of 15 mM. They were incubated for 20 min at room temperature in the dark, and then the samples were diluted twice with 50 mM ammonium bicarbonate (ABC).

Afterward, 1 mg of protein was digested using a 1:100 ratio of sequencing grade modified trypsin (Promega; # V511A) at 37°C overnight.

The ionic detergent (SDC) was removed, according to Masuda et al., 2008. The digest was mixed with the selfsame volume of ethyl acetate, acidified with 1/50 volume of 25 % trifluoroacetic acid, mixed well for 2 min, and centrifuged at 16060 x g for 10 min. The water phase was transferred to a new centrifuge tube and then concentrated to 100 µl using the SpeedDry vacuum concentrator (Martin Christ, Germany). The peptides' content was measured by Qubit™ Protein Assay Kit, as described previously (4.3.1).

The peptides were desalted using Oasis HLB 1 cc Vac cartridge (Waters; #WAT094225) according to the following steps:

- The cartridge was conditioned with acetonitrile and centrifuged at 100 × g for 1 min.
- The cartridge was equilibrated with 0.1 % trifluoroacetic acid and centrifuged 100 × g 1 min.
- The peptides solution was acidified with 0.1 % trifluoroacetic acid, loaded on the cartridge, and centrifuged 75 × g for 2 min.
- The cartridge was washed with 0.1 % trifluoroacetic acid and centrifuged at 100 × g for 1 min.
- The cartridge was washed with H2O and centrifuged 100 × g for 1 min.
- The cartridge was eluted with 70 % acetonitrile, 0.05 % trifluoroacetic acid 75 x g for 1 min.
- The elution step was repeated with 70 % acetonitrile, 0.05 % trifluoroacetic acid 100 x g for 1 min.

The eluates were concentrated in the SpeedDry vacuum concentrator; the peptide content was determined by Qubit™ Protein Assay Kit, and then stored at -20 °C. Later on, the desalted peptides were used for proteome measurement and the enrichment of the phosphorylated peptides.

4.7- Phosphopeptide enrichment and desalting

The enrichment of phosphopeptides using Ti-IMAC and TiO2 microparticles (ReSyn Biosciences; MR-TIM002 and MR-TID002) was conducted in two steps (Tape et al., 2014). In the first step, the microparticles were activated and equilibrated. In the second step, the phosphorylated peptides were enriched (Fig. 10).

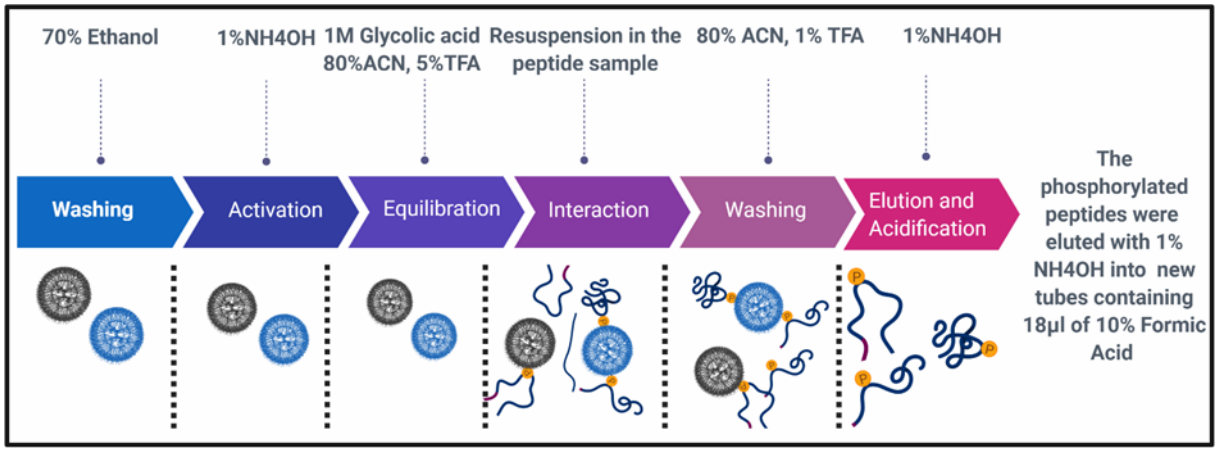

Figure 10: *Phosphopeptides enrichment by MagReSyn® Ti-IMAC and TiO2*

4.7.1- Activation and equilibration of MagReSyn® Ti-IMAC and TiO2 microparticles

- MagReSyn® Ti-IMAC and TiO2 microparticles were resuspended by vortex mixing.
- An appropriate and sufficient volume of MagReSyn® Ti-IMAC and TiO2 microparticles were transferred to a new centrifuge tube to prepare a master mix comprising 75 % Ti-IMAC and 25 % TiO2. Each enrichment round needs 1 mg of the microparticles master mix.
- The microparticles were separated from the shipping buffer by placing the tube on a magnetic separator for 10 seconds.
- The clear shipping buffer was discarded.

- The microparticles were washed twice with 70 % ethanol by resuspending them in ethanol and vortex mixing for 5 min. Thereafter, the tube was placed on a magnetic separator for 10 seconds. The ethanol was removed and discarded by pipette aspiration
- The microparticles were resuspended in activation buffer (1 % NH4OH) and gently agitated for 10 min.
- The activation buffer was removed and discarded by pipette aspiration after placing the tube on a magnetic separator for 10 seconds.
- The microparticles were resuspended in the loading buffer (1 M glycolic acid in 80 % acetonitrile, 5 % trifluoroacetic acid) for equilibration (50 µl for each enrichment) and left for 60 seconds to be equilibrated. Thereafter the tube was placed on a magnetic separator for 10 seconds.
- The microparticles were cleared, the loading buffer was removed, and discarded by pipette aspiration.
- The equilibration step was repeated twice, as well. The equilibration step was done three times in total.
- After removing the loading buffer, the microparticles were ready to be used for phosphopeptide enrichment.

4.7.2- Phosphopeptides enrichment

- An appropriate volume of tryptic digest, containing 50 µg of peptides, was dried in the SpeedDry vacuum and then resuspend in loading buffer.
- The peptides were transferred to the equilibrated microparticles and gently vortexed.
- The peptides were allowed to interact with the microparticles by agitating the tube for 20 minutes at room temperature.
- The microparticles and bound phosphopeptides were separated from the supernatant that contains non-phosphopeptides and unbound phosphopeptides by placing the tube on a magnetic separator for 10 seconds.

- The supernatant was aspirated and transferred to new tubes to be used later in the second enrichment round.
- The microparticles were washed three times by dispensing them in the wash buffer (80 % acetonitrile, 1 % trifluoroacetic acid) and vortexing them gently for 2 m.
- The bound phosphopeptides were separated from the supernatant by placing the tube on a magnetic separator for 10 seconds.
- After accomplishing the three washing steps, the bound peptides were eluted from the microparticles with elution buffer (1 % NH4OH) and mixed gently by vortex for 15 minutes. The supernatant was transferred to a new tube containing 10 % formic acid to acidify the eluates. The pH was controlled using pH-Fix 0-14 strips (ROTH; 0549).
- The last elution step was repeated three times, and the acidified eluates were pooled in a new tube.

The pooled eluates were concentrated in the SpeedDry vacuum to few microliters. Phosphopeptides enrichment was done in three rounds. In other words, the acquired supernatant underwent a second enrichment round. A third enrichment round was applied on the second round supernatant to make three enrichment rounds in total. The phosphopeptides were concentrated in the SpeedDry vacuum and desalted.

4.7.3- Phosphopeptides desalting

The desalting was performed using homemade StageTip that contains two layers of reversed-phase C18 (Rappsilber et al., 2007):

- The two StageTips were prepared by cutting two mini-discs of C18 and then plugging them into a 200 µl pipette tip for each StageTip.
- The StageTips were conditioned with 100 % methanol and then centrifuged at 450 × g for around 2 min. The centrifuge speed was increased in case of need or decreased to avert over centrifuge.
- The StageTips were conditioned by adding conditioning buffer (80 % acetonitrile, 0.5 % acetic acid) and centrifuged at 450 × g for around 2 minutes.

- The StageTips were equilibrated with 0.5 % acetic acid and centrifuged at 450 × g for around 2 minutes.
- The concentrated phosphopeptides were diluted in 150 µl of 0.5 % acetic acid loaded on an equilibrated tip and centrifuged at 450 × g for around 2 min.
- The bound phosphopeptides were washed with 0.5 % acetic acid and centrifuged at 450 × g for around 2 minutes.
- The bound phosphopeptides were eluted with elution buffer (80 % acetonitrile, 0.5 % acetic acid) and centrifuge 225-450 × g for around 2 minutes.
- The eluates were concentrated in the SpeedDry vacuum concentrator to less than 4 µl and then mixed with 20 µl of 2 % acetonitrile in 0.1 % formic acid.

4.8- Mass spectrometric acquisition

4.8.1- The measurement of phosphopeptides by HDMS^E and DDA acquisition modes

The phosphopeptides of the first enrichment round were measured separately. In contrast, the second and third enrichment rounds were pooled before the measurement, to have in total two samples for each condition in three replicates. The phosphopeptides were separated on a nanoAcquity UPLC system (Waters), using a mobile phase consists of two eluents, eluent (A) 0.1 % formic acid in LC grade water and eluent (B) acetonitrile in 0.1 % formic acid. The samples were loaded and trapped on a trap column (nanoAcquity UPLC Symmetry C18, 5 µm, 180 µm × 20 mm, Waters) for desalting. The desalting step was followed by a separation step, which was performed on an analytical column (ACQUITY UPLC HSS T3, 1.8 µm, 75 µm × 250 mm, Waters), using a linear gradient of 3 % B, which was increased over 20 min to 7 % and then to 32 % over 120 min. After 125 min, B reached 85 %, and 5 min later, the column was washed with 90 % B. At the end of the separation step, the column was re-equilibrated with 3 % mobile phase B for 25 min. During the separation, the column temperature was maintained at 35° C. For lock mass correction, 100 fmol/µL Glu-fibrinopeptide B (785.8427 *m/z*) was acquired once every 30 s for 1 s. The solution was delivered from the auxiliary pump of the

nanoAcquity UPLC at a flow rate of 0.5 µL/min to the reference sprayer of the NanoLockSpray source, measured, registered, and applied during data processing. Synapt G2-S mass spectrometer (Waters) was used to analyze the separated phosphopeptides in two modes. In HDMS^E acquisition mode, the collision energy cell was cycled between high and low collision energy statuses in equal durations of 0.6 s. The precursor ions were scanned at low collision energy, and then the energy was elevated, the precursors were fragmented and measured. Both precursors and fragments were analyzed over the *m/z*-range of 50-2000 by the time of flight analyzer (TOF), recorded, and stored as raw data files for each sample. In DDA acquisition mode, the precursor ions were scanned for 0.2 s. The most abundant precursors (5 in this work) were selected, and the instrument was switched automatically between MS and MSMS. The ions were fragmented and analyzed by the TOF analyzer.

The raw data files of these measurements were aligned, normalized, and processed using Progenesis QI for Proteomics, version 2.0 (Nonlinear Dynamic).

For HDMS^E acquisition mode, ProteinLynx Global Server (PLGS) version3.0.2 (Waters) was used to search the peaks against a SwissProt database downloaded from (https://www.uniprot.org) and adjoined sequence of porcine trypsin.

In DDA acquisition mode, the data were exported as MGF files and then imported in Mascot (Matrix Science) to be searched against a SwissProt database. The following parameters were used to identify tryptic peptides for protein identification: 13 ppm precursor ion mass tolerance; 0.2 Da product-ion mass tolerance; up to two missed trypsin cleavage sites; peptides charges +2, +3, and +4; carbamidomethylation of cysteine was set as a fixed modification; oxidation of methionine and phosphorylation of serin, threonine, and tyrosine were set as variable modifications. The identified peptides were exported as pepXML files and imported again in Progenesis QI to perform the analysis.

4.8.2- The measurement of peptides by nanoLC-HDMS^E acquisition mode

Before the acquisition, the peptides of each sample were mixed with Hi3 Ecoli standard (Waters; #186006012) to reach a concentration of 60 ng/µl for the peptides, and 20 fmol/µl of Hi3 Ecoli standard, which is composed of 6 synthetically prepared peptides, derived from E. coli chaperone protein ClpB. Similarly to the previously described HDMS^E acquisition, the samples were desalted and separated on a nanoAcquity UPLC system (Waters) using a linear gradient of 3 % B, which was increased over 150 min to 35 % then to 85 % in 5 min. After 160 min, the column was washed with 90 % B. At the end of the separation step, the column was re-equilibrated with 3 % mobile phase B for 25 min.

The raw data files of these measurements were aligned processed using Progenesis QI for Proteomics, version 2.0 (Nonlinear Dynamics). Peak lists were searched against a database containing 20205 reviewed protein sequences of the human proteome (UniProt release 2017_06) appended with Hi3 Ecoli standard and porcine trypsin (https://www.uniprot.org). The following parameters were used to identify tryptic peptides for protein identification: 13 ppm precursor ion mass tolerance; up to two missed trypsin cleavage sites; a peptide score higher than 5.5; the shortest considered .peptide should be composed of 6 amino acids; charges +2, +3 and +4; carbamidomethylation of cysteine was set as a fixed modification; oxidation of methionine was set as variable modification. The label-free Hi-3 quantification method was used to quantify the acquired proteins.

4.9- Data analysis of the acquired phosphopeptides

The analysis of the acquired phosphopeptides by one or several database search engines is a complicated process since each phosphosite could be identified on several phosphopeptides that differ in their lengths. Two methods were applied to overcome this limitation. In the first one, the identified phosphosites were converted into identifiers. In

the second method, the phosphopeptides were transformed into unique phosphosites. The two methods were compared to find an optimal way to analyze the data.

4.9.1- Converting the phosphosites into identifiers

All the acquired sequences were searched in the Protein Information Resource (https://proteininformationresource.org) (Wu et al., 2003) to find the start (S) and the end (E) of each identified sequence.

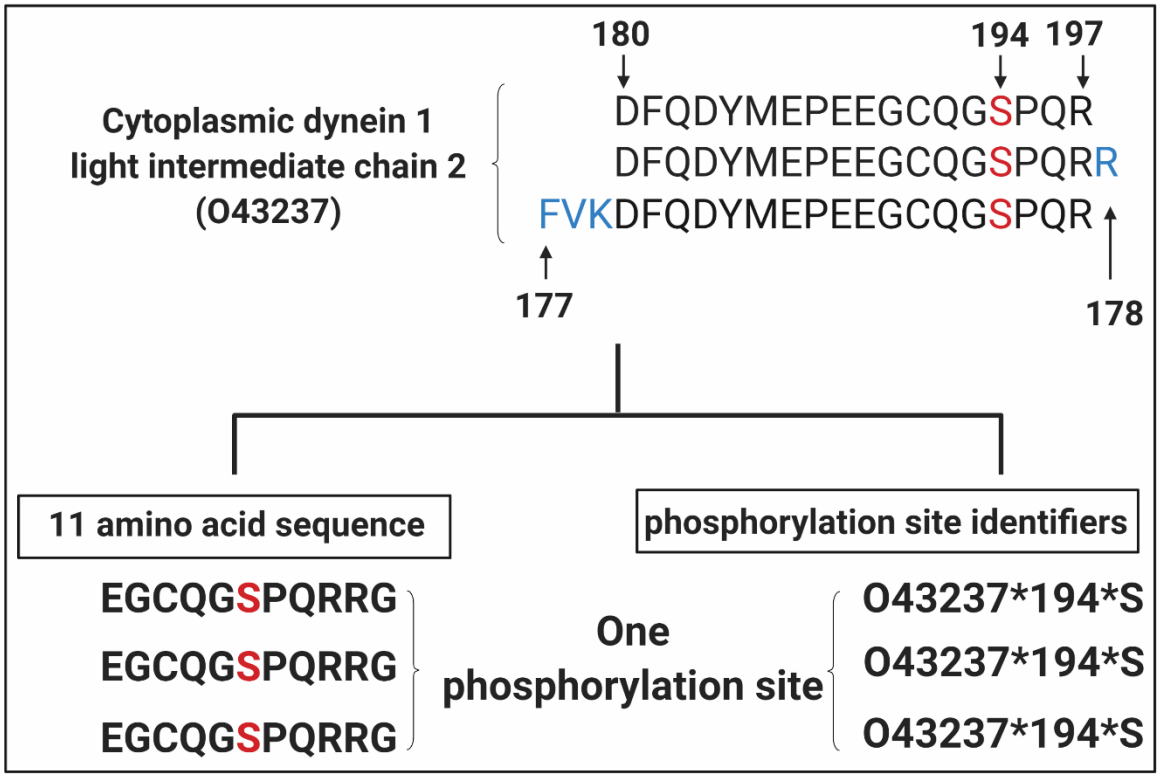

Figure 11: *A diagram shows the workflow of converting the identified phosphosites into identifiers. The phosphosite (EGQGSPQRRG) is shared among the three identified phosphopeptides. The second phosphopeptide has additional amino acid at C-terminus (R) - comparing with the first one. The third phosphopeptide has additional three amino acids at - N-terminus (FVK) - comparing with the first one. The shared amino acids were written in black, except the phosphoserine, which was written in red. The identified phosphopeptides can vary in length but carry the same phosphosite (bold). The unshared amino acids were written in blue. The generated identifier O43237*194*S codes this phosphosite (EGQGSPQRRG).*

The phosphosite (Phos.Site) on the protein from which the sequences originate was calculated using the equation:

$$Phos.Site = S + E - 1$$

The generated codes consist of UniProt accession of the phosphoprotein, phosphorylated residue (S or T or Y), and the phosphosite, respectively. Asterisks separate the code components (Figure 11).

4.9.2- Transformation of the identified phosphopeptides into unique phosphosites

The identified phosphopeptides were marked by # after the phosphorylated residue using Excel 2016. The hashed sequences were transformed into monophosphorylated sequences by duplicating the doubly phosphorylated sequences and triplicating the triply phosphorylated ones (Fig. 12).

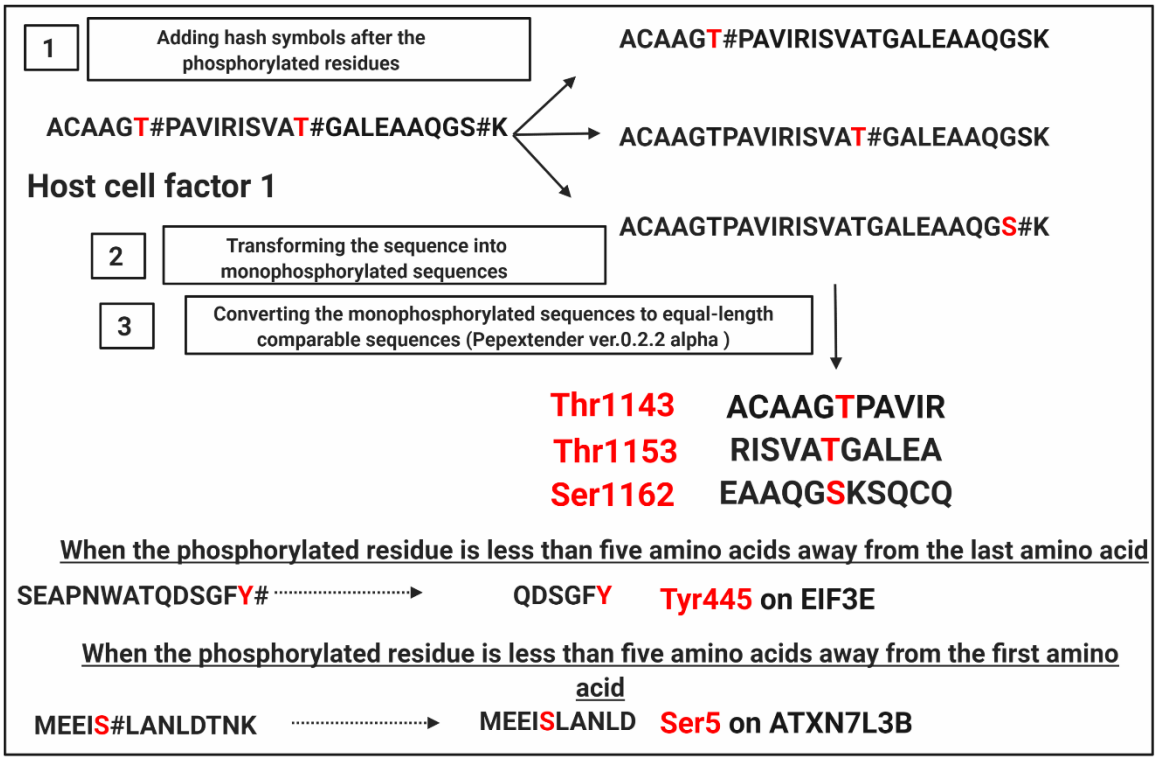

Figure 12: *A diagram shows the workflow of transforming the identified phosphopeptides into unique phosphosites (11-amino acid phosphopeptides).*

The first sequence holds only the first phosphosite as a monophosphorylated sequence, the second sequence holds only the second phosphosite as a monophosphorylated sequence, and so on. The transformed monophosphorylated sequences were uploaded on Pepextender ver.0.2.2 alpha (https://schwartzlab.uconn.edu/pepextend/) and extended to 11-amino acid sequences, in which the phosphorylated residue is located in the middle of the sequence and has five amino acids on each side (Fig. 12). The phosphosite that locates less than five amino acids away from the first or the last amino acid was uploaded on Protein Information Resource (Wu et al., 2003) and searched again. The phosphorylated residue, the five adjacent amino acids of one side, and the rest amino acids of the other side formed the sequences that represent the phosphosite.

4.10- The statistical and computational analysis

Gene ontology (GO) function analyses were performed for the acquired genes with an online tool FunRich (Pathan et al., 2015). The enriched biological functions, processes, and cellular compartment were considered statistically significant when p-value < 0.05.

PhosphoSitePlus database (Hornbeck et al., 2012b) was used to search the upstream kinases of the identified phosphosites. Motif analysis was conducted using the tools of PhosphoSitePlus. The significance threshold was set to 10^{-6} (default setting), and the occurrence threshold of the analyzed motifs was set to 20. The regulated motifs were visualized by plogo http://plogo.uconn.edu/ (O'Shea et al., 2013).

An unpaired two-sided Student's t-test (for comparing two groups) or ANOVA test (for comparing multiple groups) was used to measure the significance of the observations.

4.11- The workflow of phosphoproteome and proteome analysis

This dissertation focused on the proteome and phosphoproteome analysis of exponentially growing cells compared to cells arrested in mitosis using the phosphatase inhibitor okadaic acid (OA). Particular emphasis was placed on phosphorylation events

dependent on PBK by analyzing wild type and PBK knockout cells side by side. The used workflow is depicted in Figure 13.

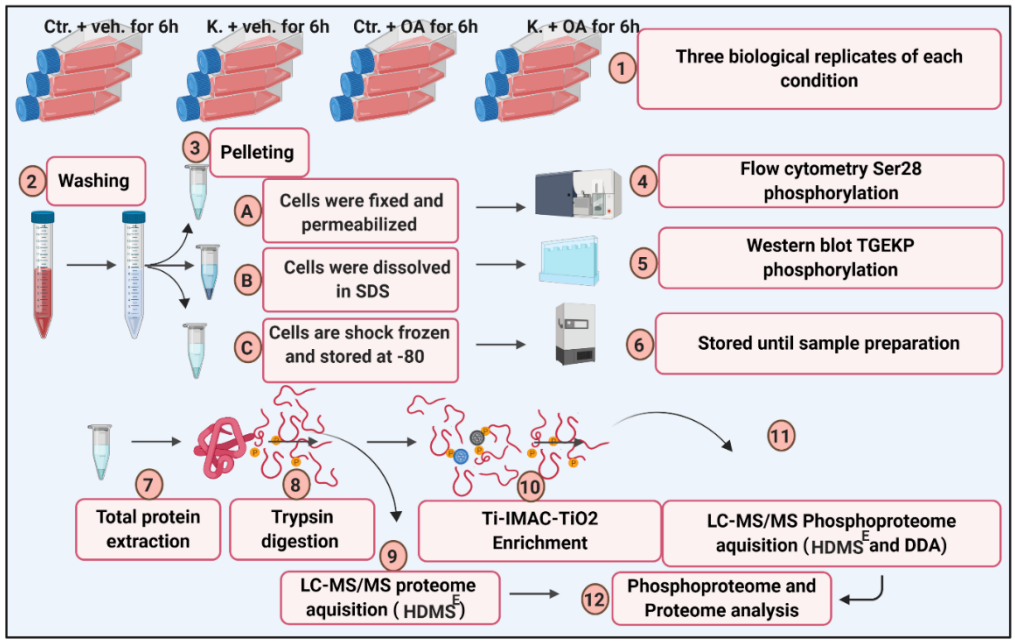

Figure 13: *The workflow of proteome and phosphoproteome analysis: (1) Cell culture and treatment in three replicates. (2 and 3) Cells' harvesting and splitting into three tubes: A, B, and C. (4) Measuring the mitotic index: The cells were fixed, permeabilized, stained, and measured by flow cytometry. (5) TGEKP phosphorylation screening by western blot analysis: The cell pellet was dissolved in 1×SDS sample buffer, protein content was determined for each sample, and 40 µg was analyzed by western blot. (6,7,8 and 9) Pellet storage, total protein extract preparation, protein digestion, and proteome acquisition: The pellet was shock frozen in liquid nitrogen and stored in the fridge at -80°C until sample preparation. Thereafter, the pellets were thawed, dissolved, and total proteins were extracted. After protein content determination, 1 mg of protein was digested with trypsin. The digest was desalted; the content of peptides was determined. (10) Phosphopeptides enrichment: 50 µg of the digested peptides were used for enrichment by Ti-IMAC and TiO2 microparticles. (11) Phosphopeptides acquisition: The phosphopeptides were measured by mass spectrometer Synapt G2-S using HDMS^E and DDA acquisition modes. (12) Proteome and phosphoproteome analysis: Progenesis QI was used for proteome analysis, the differently regulated proteins were obtained, and three of them were selected for verification by western blot. The acquired phosphosites were converted into identifiers and unique phosphosites. The acquired phosphosites were used for further analysis.*

5- Results

5.1- Mitotic synchronization of HAP1 cells

5.1.1- Determining an appropriate treatment to activate PBK in HAP1 cells

Since PBK is a mitotic kinase, the investigation of PBK-dependent phosphorylation events requires synchronization of HAP1 cells at the G2/M phase. Two different treatments were compared to achieve a suitable synchronization. The treatment had to fulfill two essential requirements: a proper activation of PBK, which associates the phosphorylation of C2H2 linker (TGEKP), and adequate viability of HAP1 cells. A double-thymidine block followed by nocodazole (DTB-Noc) was applied as the first treatment (Figure 14A). Alternatively, the cells were treated with okadaic acid (OA). Respectively, control cultures received medium (ethanol: EtOH) without any compounds.

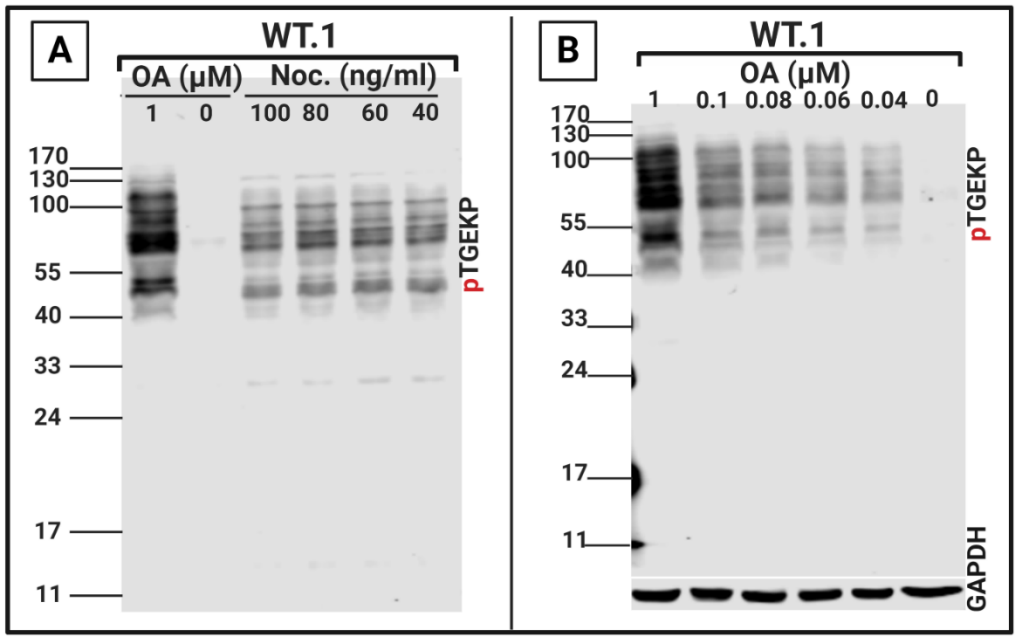

Figure 14: *Western blot screening of phosphorylated linker sequence (pTGEKP). (A) Wild type cells (C631: WT.1) were treated with OA, EtOH, or DTB-Noc. (B) Wild type cells were treated with decreasing concentrations of OA or EtOH.*

Western blot was deployed to visualize the extent of PBK-related phosphorylation of C2H2 linker (TGEKP), which occurs during the mitotic entry.

Unlike EtOH-treated cells that did not show phosphorylation of the TGEKP linker sequence, DTB-Noc treatment induced remarkable phosphorylation, regardless of the applied nocodazole concentration (Fig. 14 A). Signal intensities did not vary, i.e., lowest (40 ng/ml) and highest (100 ng/ml) concentrations led to similar PBK activities. This treatment was accompanied by relatively bad cell viability, as judged by the trypan blue exclusion assay. The highest viability rate (72.6%) was seen in the cells treated with 40 ng/ml nocodazole. Using higher concentrations of nocodazole: 60, 80, 100 ng/ml decreased the viability rates considerably to 71.9, 50.96%, and 47.14%, respectively.

The intensities of signals that reflect TGEKP phosphorylation were much higher when the wild type cells were treated with OA instead of nocodazole. The viability rate of OA-treated cells was 95%, which is close to the viability rate of EtOH-treated cells (96.38%).

5.1.2- Measuring the mitotic index with flow cytometry

The phosphorylated Ser28 of H3 (pSer28) was used as a mitotic marker. Flow cytometry was deployed to screen the phosphorylation of H3 at Ser28 by an anti-H3-phosphorylated Ser28 antibody (anti-H3 pSer28) in HAP1 wild type cells. The mitotic marker, pSer28, indicates the mitotic cells.

HAP1 wild type cells were treated with OA or with EtOH for 6 hours and stained with anti-H3 pSer28 or with a control antibody (anti-KLH). The control antibody detects the carrier protein, keyhole limpet hemocyanin (KLH). OA-treated cells showed a double-peak when they were stained with an anti-H3 pSer28 antibody and one peak when they were stained with anti-KLH. Merging the two histograms in one manifested an unambiguous shift to the right side in the histogram of the double-peak histogram (Fig. 15A). The double-peaked histogram shows the detected pSer28 in contrast to the other histogram. The observed double-peak is attributed to the haploid and diploid HAP1 cells

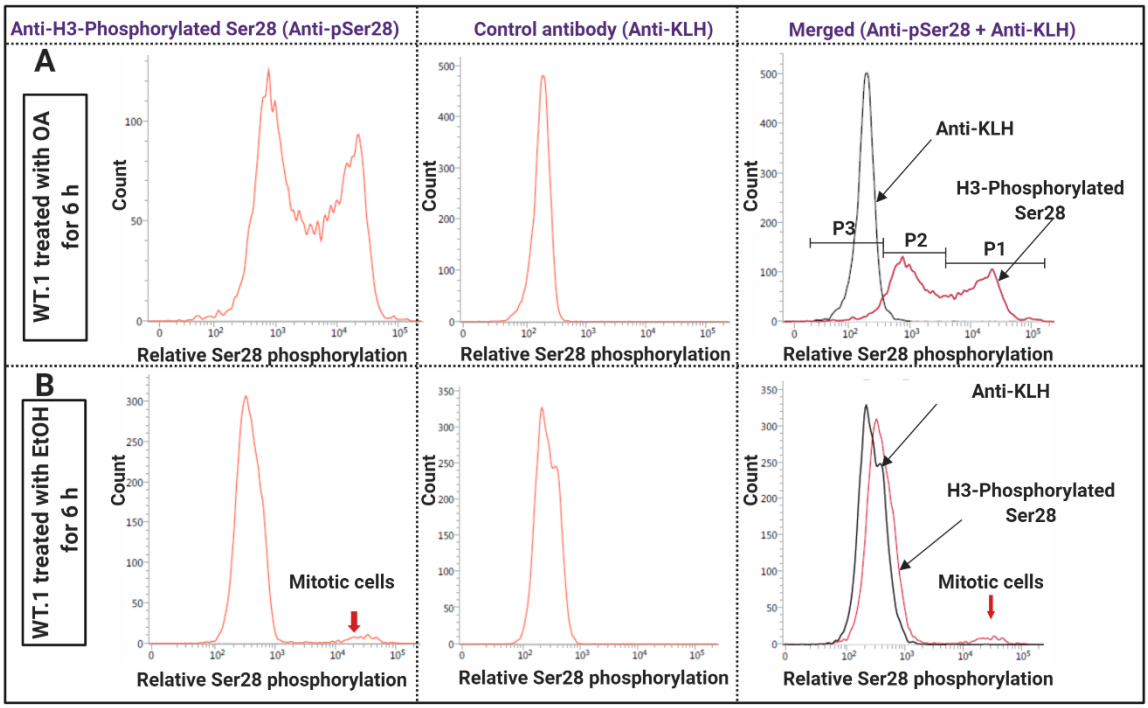

Figure 15: *The flow cytometry histogram plot of wild type HAP1 cell line (WT.1). The histogram of the cells that were stained with anti-pSer28 (left side) or anti-KLH antibody (middle), and the merged histograms (right side). (A) The cells were treated with OA for 6 hours. The merged histograms show the recognized phosphorylated Ser28 of the diploid cells (P1), the haploid cells (P2), and the background signal (P3), which was recognized by the control antibody. (B) The cells were treated with EtOH for 6 hours. Anti-pSer28 and anti-KLH histograms show almost a complete overlap with a minimal shift of anti-pSer28 to the right side (Figure 15B). The mitotic cells were marked with a red arrow.*

EtOH-treated cells showed a prominent peak and a tiny one upon staining with an anti-H3 pSer28 (Fig. 15B). The tiny peak was shifted to the right side (marked with a red arrow). Staining with the control antibody resulted in one peak. Merging the two histograms in one reveals a substantial overlap between the two histograms. The shifted tiny peak is explained by the fact that just a tiny portion of the asynchronized cells is in the mitotic phase.

This method was deployed to measure OA-treated cell mitotic indexes (WT.1 and KO.1), see Figure 16. After fixation and permeabilization, three different stainings were applied to each cell line. The cells were stained with antibody buffer, or control antibody, or anti-

H3 pSer28 antibody (Fig. 16). The identified events phosphorylation events (pSer28) were used to calculate the mitotic index. This experiment was repeated in three biological replicates.

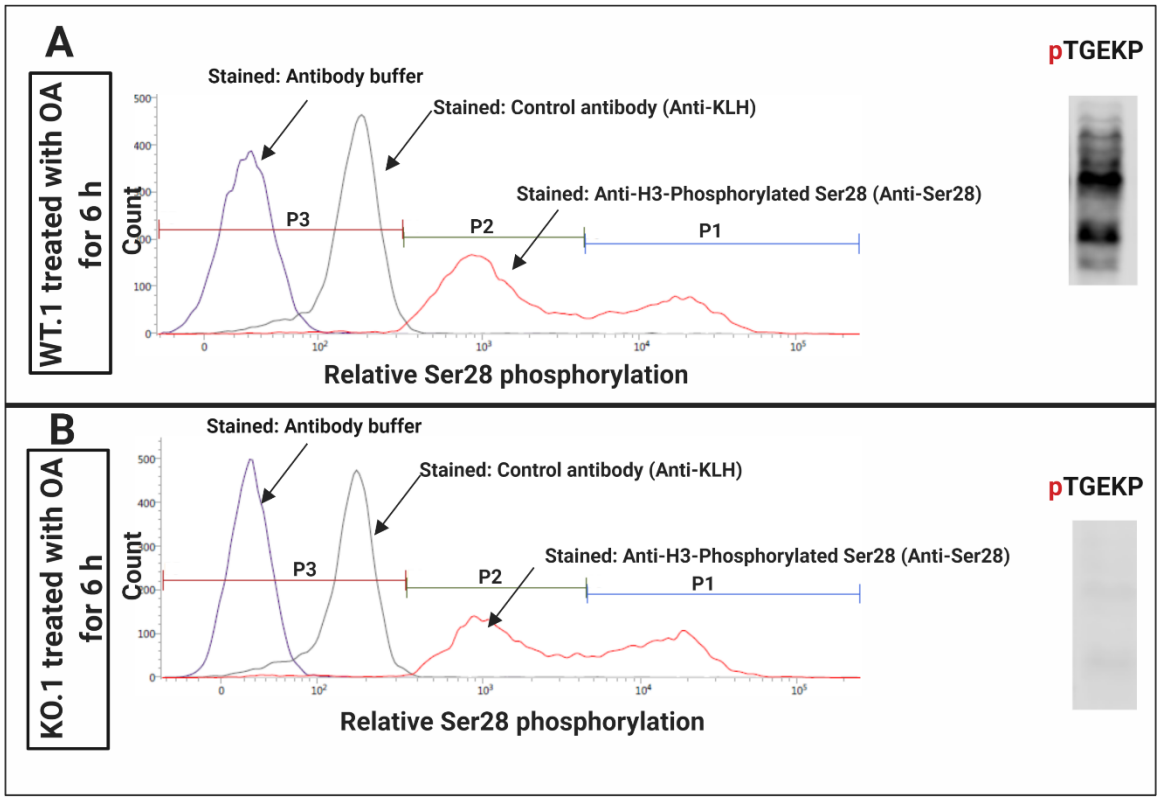

Figure 16: *Comparing the wild type and PBK knockout HAP1 cells regarding the histogram of pSer28 and PBK activation after okadaic acid treatment. (A) Wild type cells (WT.1). (B) PBK knockout cells (KO.1). The cells were stained with antibody buffer or with the anti-KLH control antibody, or anti-H3 pSer28. P1 and P2 indicate the relative phosphorylation of Ser28 that results from diploid cells and haploid cells after the staining with anti-H3 pSer28, respectively. P3 indicates the background signal resulted from staining with the control antibody and the antibody buffer, respectively. (right) Western blot screening of TGEKP phosphorylation.*

Wild type HAP1 cells showed a mitotic index of 95.04±2.33% and viability of 93.74±0.94%. Similarly, PBK knockout HAP1 cells had a mitotic index of 98,44±0.76% and viability of 93,23±1.8%. The phosphorylation of TGEKP, which reflects PBK activity in the wild type mitotic cells, was manifestly high compared with no detected phosphorylation in PBK knockout mitotic cells.

5.1.3- p38 phosphorylation in HAP1 knock out cells

According to the scientific literature, PBK has two contradicting effects on p38 phosphorylation. On the one hand, PBK phosphorylates p38 at Thr180 and activates it (Abe et al., 2000b). On the other hand, PBK promotes MKP1 stability, which dephosphorylates Thr180 of p38 (Ayllón and O'Connor, 2007). If there is no other alternative kinase, the balance between these two effects determines the phosphorylation state of Thr180 and p38 activity.

The HAP1 cell line provides an appropriate system to screen p38 phosphorylation levels in the presence and absence of PBK. Wild type and PBK knockout cell lines were treated with OA or EtOH to evaluate PBK's role in p38 activation. Thr180 phosphorylation levels in these four conditions were checked by western blot using an antibody against the phosphorylated p38 (active p38) (Fig. 17A). As a control, the phosphorylation of TGEKP was also investigated in the four conditions (Fig. 17B).

The phosphorylation levels of p38 were hardly detectable in exponentially growing cells (EtOH-treated cells) in wild type as well as PBK knockout cells. These levels increased dramatically during the mitotic phase (OA-treated cells). The differences in the phosphorylation levels between the mitotic and spontaneously growing cells were significant regardless of the cell line genotype. After OA treatment, the phosphorylation level of p38 in PBK knockout cells was slightly higher than its level in the wild type cells, but this difference was not significant.

On the other hand, neither okadaic acid nor EtOH could induce TGEKP phosphorylation in knockout cells. Therefore, pTGEKP signals could not result from another kinase activity besides PBK, unlike p38 phosphorylation (Fig. 17).

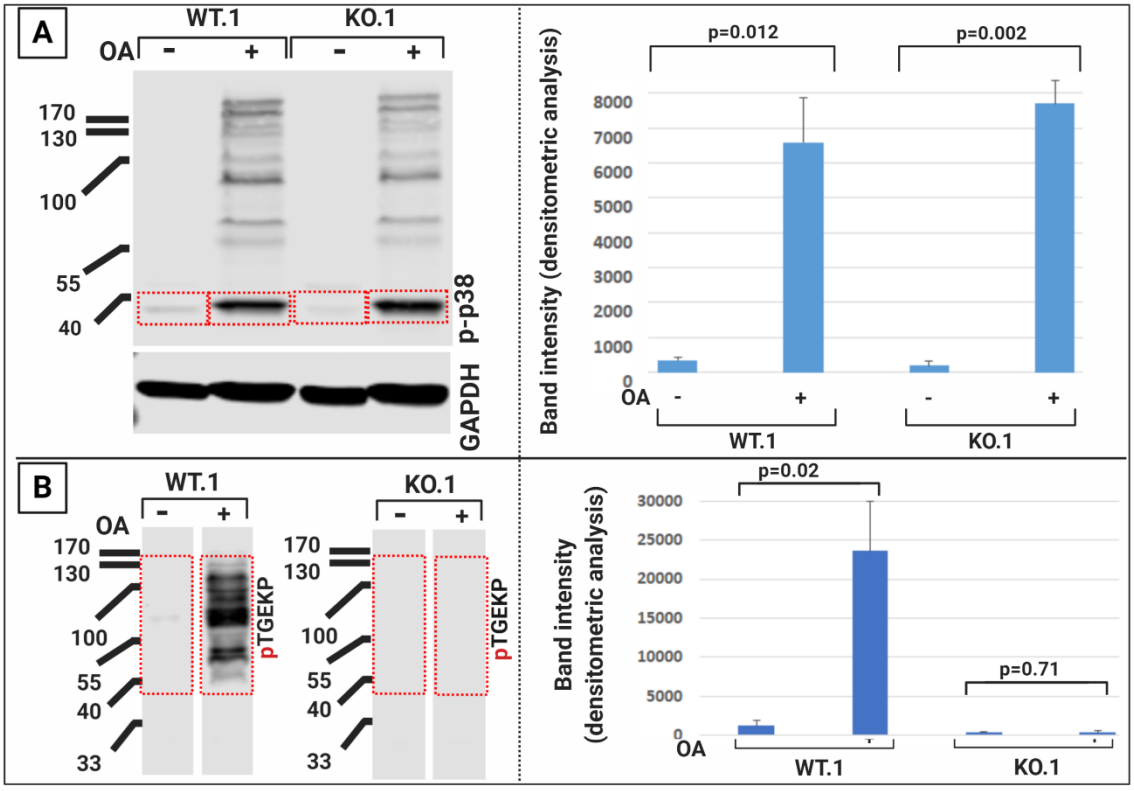

Figure 17: *Western blot analysis of p38 phosphorylation (A) and TGEKP phosphorylation (B) in wild type (WT.1) and PBK knockout (KO.1) cells. The cells were treated with EtOH or with OA. The phosphorylation levels were screened using an antibody against the phosphorylated p38/TGEKP. The experiment was done in three biological replicates. One replicate is presented in this figure on the left side. Dotted red lines surround the quantified bands/smears. On the right side, the quantified intensities were presented as mean values and standard deviations. GAPDH was screened just to verify the equal loading of the protein. p38 showed increased phosphorylation levels after OA treatment regardless of the cell line genotype.*

5.2- Proteomic analysis of HAP1 cells

Global proteome analysis of the wild type and PBK knockout HAP1 was performed. Four conditions were prepared by treating the cells with OA or EtOH in three replicates to make 12 runs. LC-HDMS^{E} mass spectrometry was deployed to measure the peptide digests. Of 12 runs, one run representing the second replicate of the EtOH-treated wild type HAP1 cells showed an impaired chromatogram. It was therefore excluded.

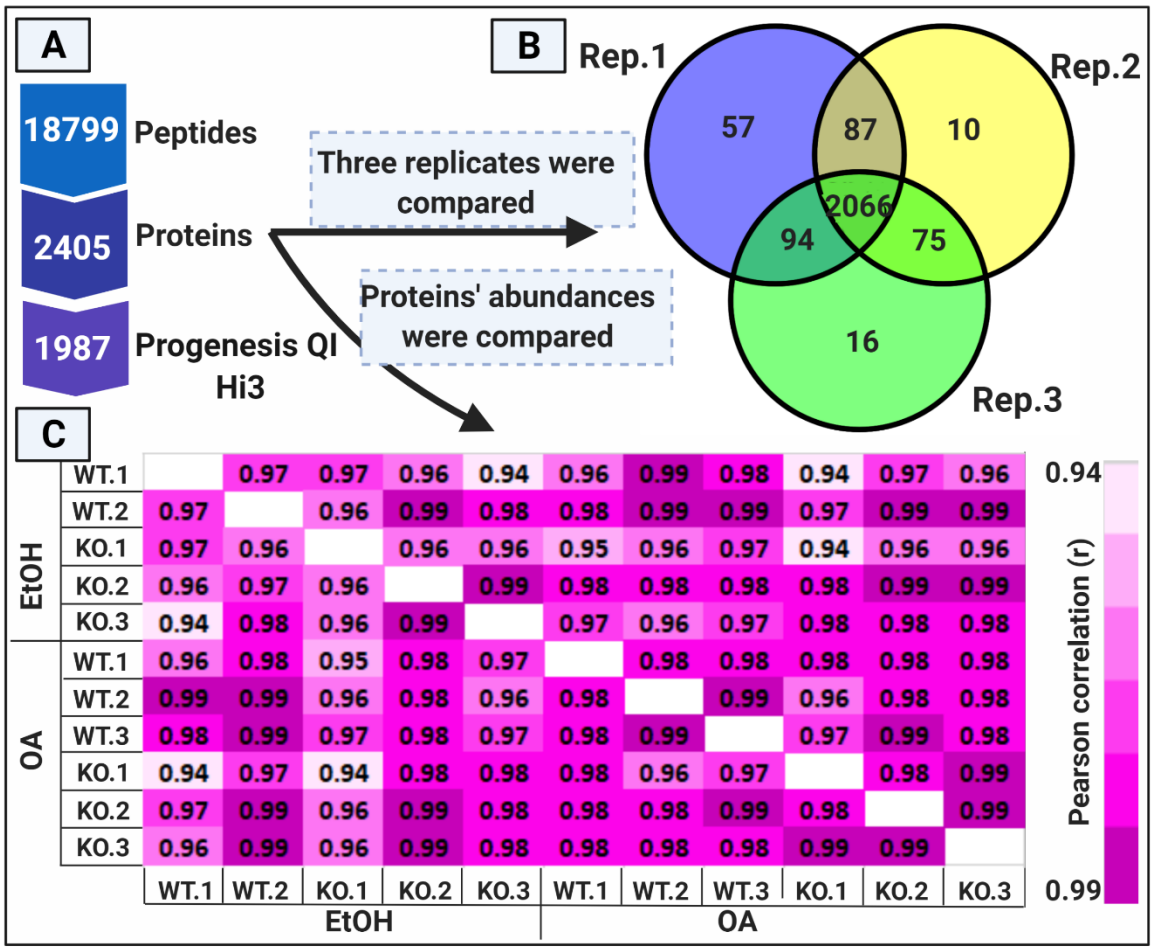

Figure 18: *Protein identification summary and the correlation between the biological replicates. (A) The total number of identified peptides and proteins. (B) Venn diagram represents the identified proteins in three biological replicates. (C) Pearson correlation of the normalized protein abundance in eleven analyzed runs. The color intensity refers to the correlation r-value.*

A total of 18799 unique peptides were identified in eleven runs representing the four conditions. The identified peptides were assigned to 2405 unique proteins (Table.1 of the appendices). The overlap between the biological replicates was high; around 97% of the acquired proteins were identified in two replicates at least (Fig. 18A and B).

The abundances of the identified proteins were calculated by Progenesis QI for Proteomics, using the Hi3 method. Comparing the abundances between the eleven samples showed a strong correlation. Pearson correlation's lowest value was equal to or higher than 0.94 (Fig. 18C), which indicates that the mass spectrometry runs were very reproducible.

Before doing the quantitative analysis, proteins that were only identified by one peptide were removed to avoid false quantification, so a total of 1987 proteins were kept for later analysis.

Protein abundances were evaluated concerning the analyzed conditions in order to identify differentially regulated proteins. The fold change values were considered significant when they were greater than or equal to 2, and p-values were less than 0.05. These criteria were used to nominate differentially regulated proteins.

5.2.1- Screening PBK regulated proteins

The OA-treated cells were used for the analysis (six runs). They were divided into two groups: the mitotic wild type cells (three runs) and the mitotic PBK knockout cells (three runs). Besides PBK, only three proteins were upregulated in mitotic PBK knockout cells (Table 18): annexin A1 (ANXA1), 55 kDa erythrocyte membrane protein (MPP1), and renin receptor (ATP6AP2) showed differential expression levels.

Table 18: *The proteins that showed different expression levels between mitotic WT and PBK-KO cells.*

Accession	Gene name	ANOVA (p)	Max fold change	Highest mean	Lowest mean
Q96KB5	PBK	0.000	5.69	WT.1+OA	KO.1+OA
P04083	ANXA1	0.004	3.26	WT.1+OA	KO.1+OA
Q00013	MPP1	0.001	2.61	KO.1+OA	WT.1+OA
O75787	ATP6AP2	0.007	2.27	KO.1+OA	WT.1+OA

5.2.2- Screening the mitotic regulated proteins

The panel was divided into two groups: the first group comprises the mitotic cells (six runs). The second group comprises the spontaneously growing cells (five runs), irrespective of the genotype.

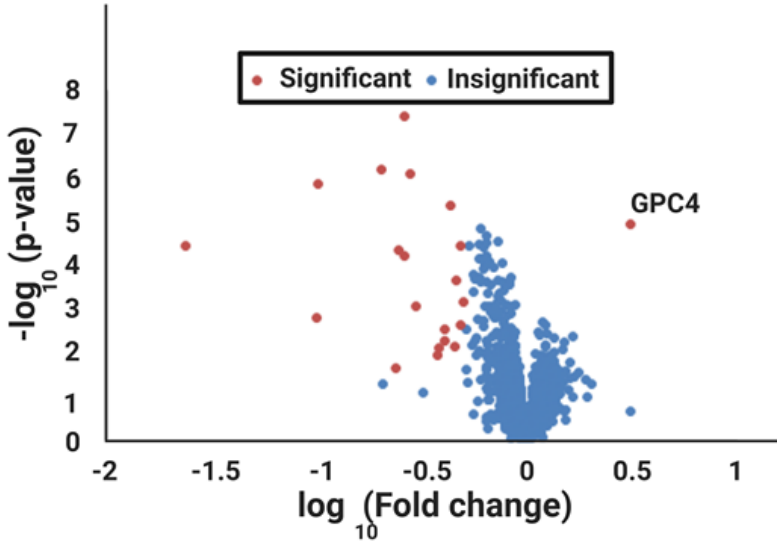

Figure 19: *The volcano plot shows the proteins that have a mitotic phase-dependent regulation pattern. The volcano plots highlight the mitotic significantly (red dots) and insignificantly (blue dots) regulated proteins.*

The quantitative comparison between the protein abundances of mitotic and exponentially growing cells showed 21 differently regulated proteins. A total of 20 proteins showed downregulation during the mitosis, whereas only one protein showed upregulation (Figure 19, table 20, and table 2 of the appendices).

Table 20: *The differentially regulated proteins between mitotic and spontaneously growing cells.*

Accession	Gene	Anova (p)	Max fold change	Highest mean condition	Lowest mean condition
O75487	GPC4	1.2E-05	3.11	(+)OA	(-)OA
O76080	ZFAND5	3.6E-05	43.09	(-)OA	(+)OA
Q9BYG3	NIFKO	1.6E-03	10.07	(-)OA	(+)OA
Q12972	PPP1R8	1.3E-06	10.01	(-)OA	(+)OA
P14635	CCNB1	6.7E-07	4.99	(-)OA	(+)OA
P29966	MARCKOS	2.3E-02	4.21	(-)OA	(+)OA
Q9H1E3	NUCKOS1	4.5E-05	4.13	(-)OA	(+)OA
Q5T1J5	CHCHD2P9	6.3E-05	3.89	(-)OA	(+)OA
P31350	RRM2	3.8E-08	3.88	(-)OA	(+)OA
Q14807	KOIF22	8.0E-07	3.62	(-)OA	(+)OA
Q15004	PCLAF	8.6E-04	3.38	(-)OA	(+)OA
O75940	SMNDC1	1.2E-02	2.67	(-)OA	(+)OA
Q86TG7	PEG10	7.9E-03	2.66	(-)OA	(+)OA
Q15904	ATP6AP1	5.3E-03	2.47	(-)OA	(+)OA
Q99459	CDC5L	2.9E-03	2.46	(-)OA	(+)OA
Q8NFH5	NUP35	4.4E-06	2.34	(-)OA	(+)OA
Q8IWS0	PHF6	7.4E-03	2.21	(-)OA	(+)OA
P16989	YBX3	2.3E-04	2.18	(-)OA	(+)OA
Q16186	ADRM1	2.4E-03	2.08	(-)OA	(+)OA
Q96GD4	AURKOB	3.7E-05	2.07	(-)OA	(+)OA
Q8IY81	FTSJ3	7.1E-04	2.00	(-)OA	(+)OA

5.2.3- Screening the differentially regulated proteins among the analyzed conditions

The panel was divided into four groups: wild type spontaneously growing cells (2 runs), wild type mitotic cells (3 runs), knockout spontaneously growing cells (3 runs), and knockout mitotic cells (3 runs). A total of 39 proteins had variable expression levels among the analyzed conditions (Table 21, figure 20, and table 3 of the appendices). Figure 20 shows three examples of these proteins.

Table 21: *Examples of differentially regulated proteins among the four analyzed conditions.*

Accession	Gene	Anova (p)	Max fold change	Highest mean condition	Lowest mean condition
P04083	ANXA1	0.00	3.26	WT+OA	KO+OA
Q16186	ADRM1	0.05	2.12	WT	WT+OA
Q9Y314	NOSIP	0.00	2.02	WT	WT+OA
Q96KB5	PBK	0.00	9.46	WT	KO
Q9UI26	IPO11	0.00	5.00	WT	KO
P51572	BCAP31	0.00	2.31	KO	WT
P08670	VIM	0.03	2.31	KO	WT
O76080	ZFAND5	0.00	77.41	KO	KO+OA
Q9H1E3	NUCKS1	0.00	4.70	KO	KO+OA
Q14692	BMS1	0.05	2.19	KO	KO+OA
Q9H0S4	DDX47	0.05	2.02	KO	KO+OA

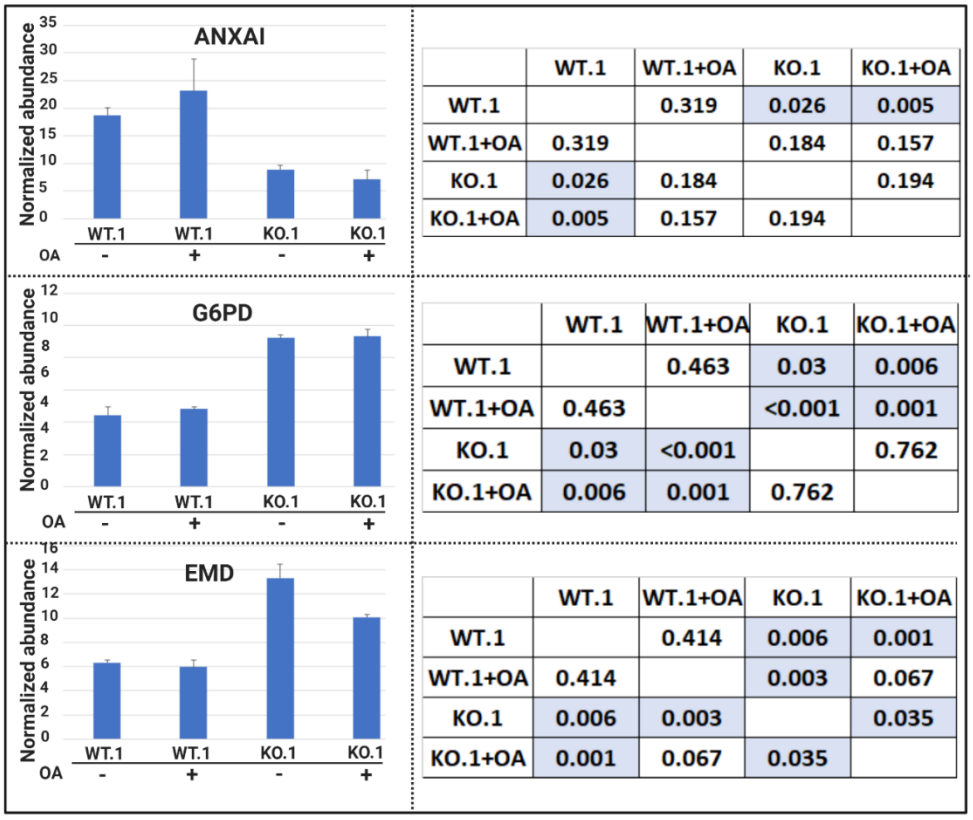

	WT.1	WT.1+OA	KO.1	KO.1+OA
WT.1		0.319	0.026	0.005
WT.1+OA	0.319		0.184	0.157
KO.1	0.026	0.184		0.194
KO.1+OA	0.005	0.157	0.194	

	WT.1	WT.1+OA	KO.1	KO.1+OA
WT.1		0.463	0.03	0.006
WT.1+OA	0.463		<0.001	0.001
KO.1	0.03	<0.001		0.762
KO.1+OA	0.006	0.001	0.762	

	WT.1	WT.1+OA	KO.1	KO.1+OA
WT.1		0.414	0.006	0.001
WT.1+OA	0.414		0.003	0.067
KO.1	0.006	0.003		0.035
KO.1+OA	0.001	0.067	0.035	

Figure 20: *Examples of the expression profile of some differently regulated proteins. (left side) The genotype and the treatment were plotted on the x-axis and the standardized, normalized abundance on the y axis. (right side) The tables show p-values (unpaired and two-sided T-test) of the compared intensities. The significant p-values (p<0.05) are highlighted in blue.*

5.2.4- Validation of differentially regulated proteins

Among the identified differentially regulated proteins, three proteins were selected to validate the mass spectrometric results by making use of western blotting. The selected proteins are Annexin I (ANXA1), Glucose-6-phosphate 1-dehydrogenase (G6PD), and Emerin (EMD). All three proteins were detected using monoclonal antibodies (Material and Methods 4.5).

Besides the previously used cell lines in proteome analysis, additional two cell lines were adjoined to the original panel. WT.2 is an additional wild type HAP1 cell line, and KO.2 is an additional PBK knockout cell line. Thus, four cell lines were analyzed by western blot with EtOH/OA-treatment. Western blot analysis was performed on three biological replicates of each condition to validate the differentially regulated proteins.

Annexin I (ANXA1): Western blot results were compatible with proteome analysis in WT.1 and KO.1 cell lines (Fig. 20 and Fig. 21). ANXA1 had higher expression levels in wild type than knockout cells, and this protein was slightly upregulated after OA-treatment in WT.1, but this increase was not significant. KO.2 and WT.2 showed a similar expression pattern, but the differences were not significant. ANXA1 had variable expression levels between two clones of the same genotype cells.

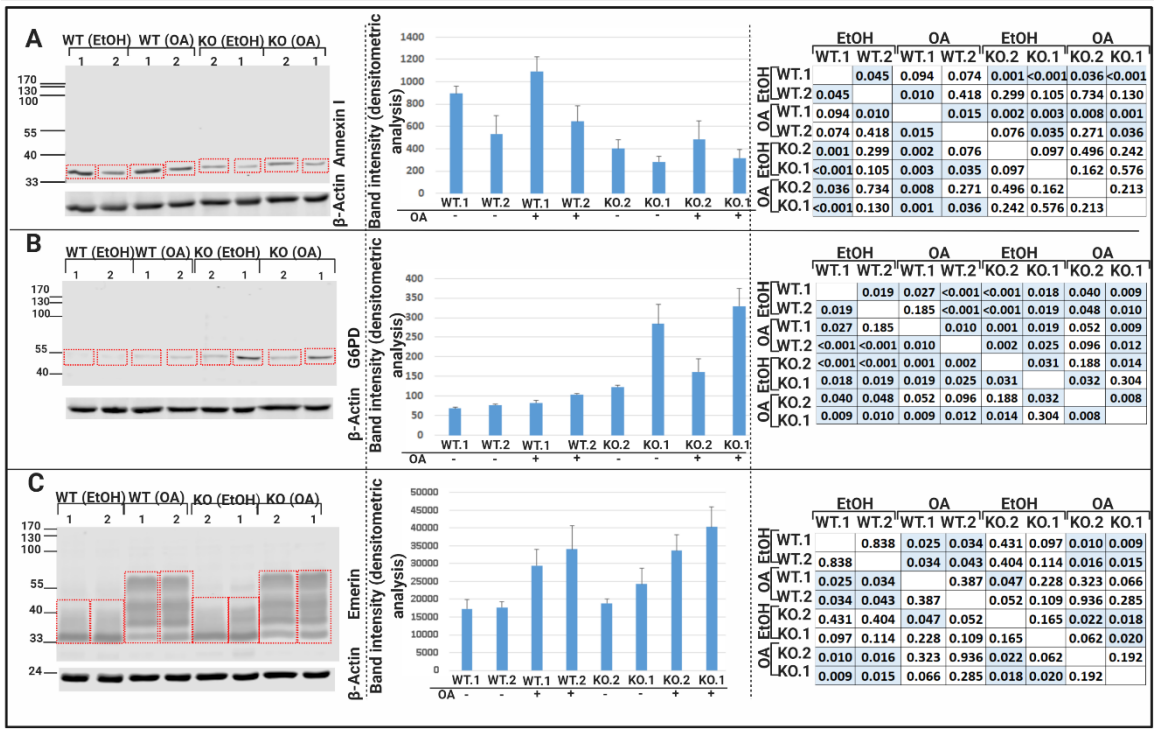

Figure 21: *Western blot validation of three differently regulated proteins. (A) ANXA, (B) G6PD, (C) EMD. Western blot images are on the left side, the quantification of the bands' intensities is in the middle, and p-values of unpaired two-sided t-test was given on the right side. The significant values (p<0.05) were highlighted in blue. Each experiment was conducted in three replicates. β-Actin was used as a loading control. The quantified bands are surrounded by dotted red lines. The means and standard deviations were used to generate these figures.*

Glucose-6-phosphate 1-dehydrogenase (G6PD): Comparing proteome and western blot analysis of WT.1 and KO.1 cell lines showed that G6PD had similar regulation patterns in both mass spectrometry and western blot. G6PD had much higher expression levels in knockout cell lines than the wild type, regardless of the treatment. Likewise, WT.2 and KO.2 also have a roughly similar expression pattern, but G6PD showed noticeably varying expression levels among the same genotypic cell clones.

Emerin (EMD): EMD western blot analysis did not show differences in protein expression levels between knockout cells and wild type cells in the same treatment status (OA or EtOH). The determining factor for EMD expression regulation was the treatment with OA, which was associated with an elevation in EMD expression levels (Fig. 21C). This result contrasts with the proteome analysis, which identified the highest expression

levels in the EtOH-treated knockout cells and did not detect a considerable difference between the OA-treated and EtOH-treated wild type cells.

5.3- Phosphoproteomic analysis of HAP1 cells

The mass spectrometer Synapt G2S renders the possibility to measure the samples in two acquisition modes: $HDMS^E$ and DDA. Although DDA is the most commonly used approach to identify PTM, it selects the top N most intense precursor ions recorded in MS for further fragmentation in MS/MS, which leads to missing values in low-abundance peptides (Riley and Coon, 2016; Matafora et al., 2017). In contrast to DDA, $HDMS^E$ fragments all the precursor ions, which ensure high coverage of the precursor ions, which requires precursors-products matching before interpreting the DIA data (Shliaha et al., 2013). The interruption of this sophisticated data is performed by a commercial algorithm (PLGS in this work) or in-house developed algorithms. The matching process generates some false identifications from the adducts or in-source fragmentation (Zhang et al., 2019). Therefore, the samples were measured by both acquisition modes ($HDMS^E$ and DDA) to take advantage of each approach.

The WT.1 and KO.1 HAP1 cells were treated with OA to arrest cells in mitosis or with the vehicle (EtOH) as control representing non-mitotic WT.1 and KO.1 HAP1 cellular states, leading to four different conditions. Three replicates were prepared for each condition. The phosphopeptides of these samples were enriched in three rounds of titanium immobilized chromatography, as explained in the methods section. The second and the third rounds were pooled before the measurement, whereas the first round was measured without pooling.

The measurements were performed using mass spectrometer Synapt G2S by $HDMS^E$ and DDA acquisition modes.

5.4- Comparing the identifiers with the unique phosphosites

The acquired phosphopeptides were exported as Excel tables. Each phosphopeptide was given as an amino acid sequence and a number that refers to the phosphorylated residues' position. The manual analysis of the exported phosphopeptides in this format is error prone. Thus, the identified phosphopeptides were converted into identifiers and unique phosphosites. The identifiers were made of UniProt accession, followed by the phosphorylated residue's position and the phosphorylated residue itself (S or T or Y). The unique phosphosites were 11-amino acid sequences, which have the phosphorylated residue (S or T or Y) in the middle and the adjacent 5 amino acids on both sides. The utility of both coding systems was determined to define the most appropriate approach to be applied.

A total of 4237 and 1171 phosphosites were identified by HDMS^E and DDA, respectively, using the identifiers. These numbers reduced to 4211 in HDMS^E and 1169 in DDA when unique phosphosites were used (appendices 4 and 5). The inequality in the acquired counts by these two methods (26 and 2 phosphosites in HDMS^E and DDA, respectively) is attributed to two factors:

- The first factor: one phosphopeptide may be assigned to more than one protein, which generates more than one identifier for a single phosphosite. IEDVGSDEEDD provides an example of this case. This phosphosite was assigned to heat shock protein HSP 90 with the identifier P08238*255*S and putative heat shock protein HSP 90 with the identifier Q58FF8*177*S.
- The second factor: one phosphopeptide may be attributed to more than one location in the protein itself when the sequence of this phosphosite is repeated within the protein sequence. An example of this observation is APAKESPRKGA. This phosphosite was repeated three times within the sequence of treacle protein. It was assigned to treacle protein with two identifiers: Q13428*381*S and Q13428*906*S.

Both observations led to the identification of additional 26 phosphosites counted in HDMS^E using the identifiers. In contrast, the second observation was only found in the DDA data set. The unique phosphosites were used to analyze the identified phosphosites to exclude counting one phosphosite twice or more.

5.5- Qualitative analysis of phosphopeptides

5.5.1- Description of the identified phosphopeptides

The HDMS^E method identified a much higher number of peptides, phosphopeptides, proteins, and phosphoproteins than the DDA method did. A total of 10151 unique peptides derived from 1672 unique proteins were identified by HDMS^E comparing with 1710 unique peptides from 717 unique proteins in DDA. Within the identified peptides, 4479 unique phosphopeptides from 1185 unique phosphoproteins and 1201 unique phosphopeptides from 575 unique phosphoproteins were identified in HDMS^E and DDA, respectively (Fig. 22A and F).

Since not each phosphopeptide refers to one unique phosphosite, we used the unique phosphosites (11-amino acid phosphopeptides) to count the identified phosphosites. A total of 4211 unique phosphosites were identified in HDMS^E, and less than half of this number (1169) was identified using DDA (Fig. 22A and F). Collectively, 783 phosphosites were identified in both acquisition modes, and 386 were identified solely by DDA (Table 4 and 5 of the appendices).

The 4479 phosphopeptides that HDMS^E identified include 3775 mono phosphorylated peptides, 673 doubly phosphorylated peptides, and 31 triply phosphorylated peptides (ratios of 84%, 15%, and 1%), respectively. The distribution was slightly different using the DDA method; 1067 mono phosphorylated peptides, 130 doubly phosphorylated peptides, and 4 triply phosphorylated peptides (ratios of 89%, 10.5%, and approximately 0%), respectively (Fig. 22B and G).

The phosphopeptides enrichment rate was 44% of the identified peptides in HDMS^E acquisition mode and 70% in DDA acquisition mode. The distribution of the

phosphorylated residues in HDMS^E identifications was as follows: 3161 phosphoserine (pS), 813 phosphothreonine (pT) and 237 phosphotyrosine (pY) with percentages of 75%, 19%, and 6%, respectively. This distribution was slightly different in DDA: 1012 pS, 153 pT, and 4 pY with percentages of 86.5%, 13%, and 0.5% (Fig. 23D and I).

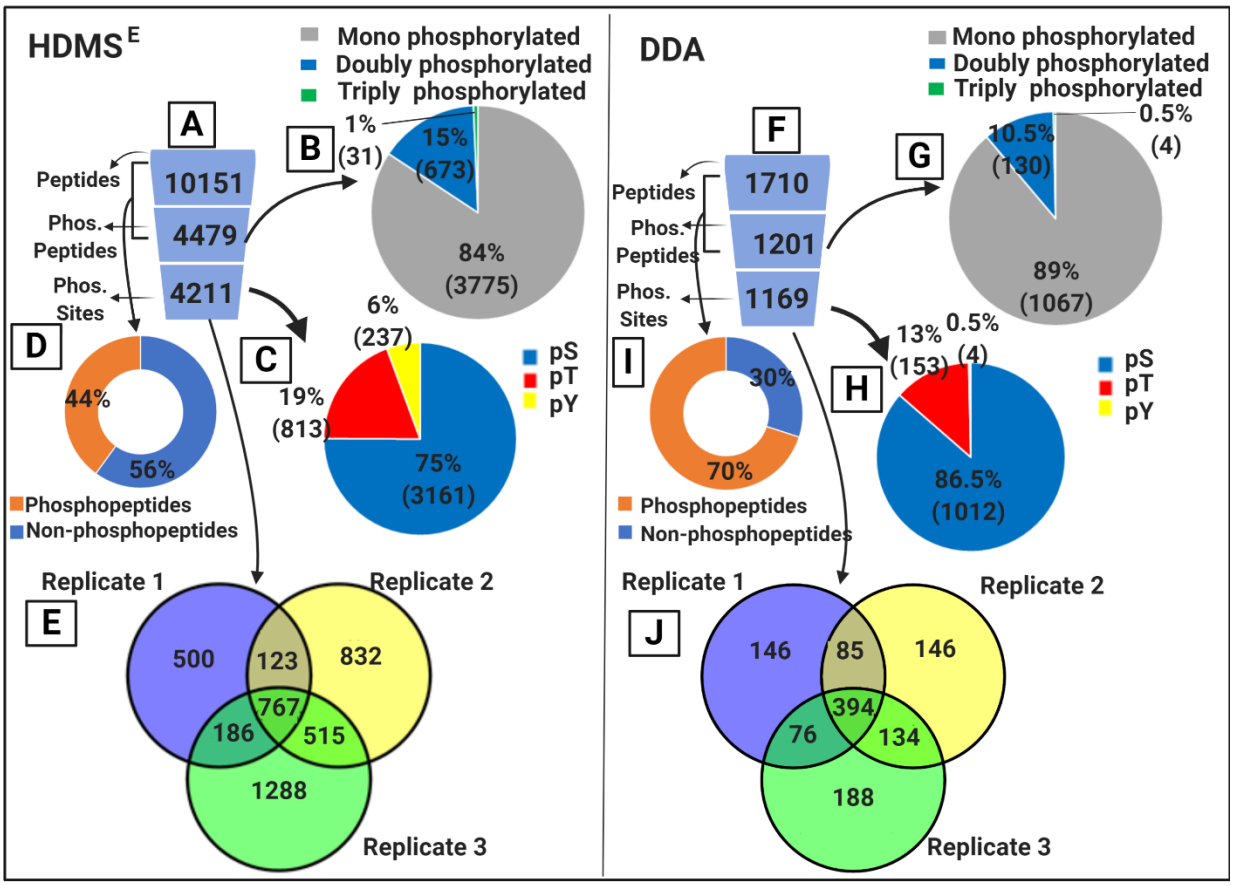

Figure 22: *An overview of HDMS^E and DDA identifications. A and F: The identified peptides, phosphopeptides, and phosphosites of the three replicates were combined and summarized in the figure. B and G: A pie chart shows the numbers and the percentages of mono and multi phosphorylated peptides. D and I: A pie chart shows the percentage of phosphopeptides. C and H: A pie chart shows the numbers and the percentages of the identified phosphorylated serine, threonine, and tyrosine residues. E and J: A Venn diagram represents the overlap between the biological replicates.*

The reproducibilities of HDMS^E and DDA acquisition modes were compared. Around 38% (1591 of 4211) of the acquired unique phosphosites by HDMS^E were identified at

least in two replicates. In contrast, this percentage was around 59% (689 of 1169) when the DDA acquisition mode was used (Fig. 22E and J).

5.5.2- The relation between the identified phospho- and non-phosphopeptides

The identified non-phosphopeptides may, in principle, arise from two sources: The co-eluted non-phosphopeptides and the phosphopeptides that lost their phosphoryl group during the enrichment process. The phosphosites' /non-phosphopeptides' sequences were compared in each acquisition mode to investigate the source of the identified non-phosphopeptides in this work. In total, 30.4% of the acquired phosphosite in the HDMS^{E} data set (1281 of 4211) were identified as non-phosphorylated form (Table 6 of the appendices), while the percentage was less than a tenth of this value in DDA, 2.3% (28 of 1169) (Table 7 of the appendices). Figure 23 presents these ratios and gives an example of a sequence that was identified in both forms. The substantial difference in the percentages of the sequences identified in phosphorylated and non-phosphorylated forms between HDMS^{E} and DDA data is ascribed to the used methods.

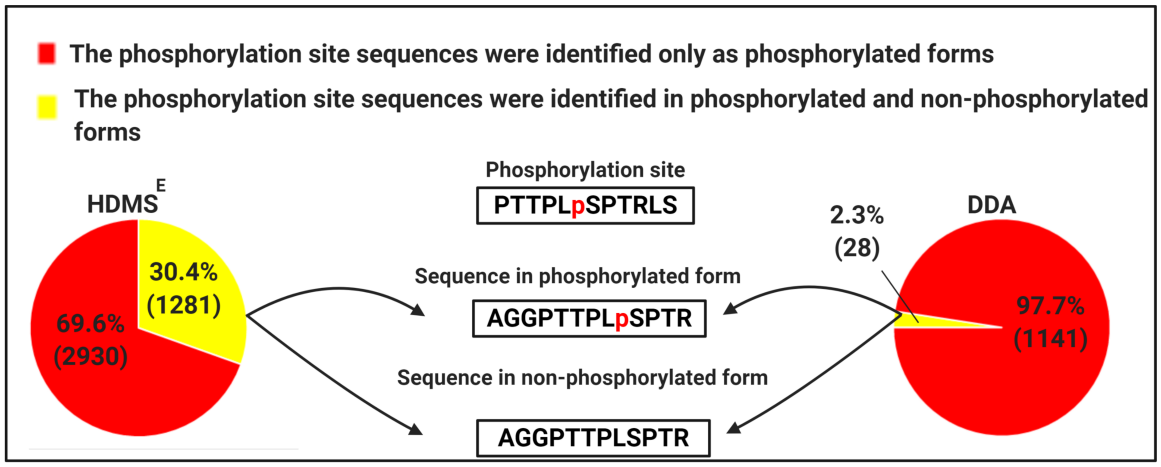

Figure 23: *The pie charts show the phosphosites ratios, which were identified in phosphorylated and non-phosphorylated forms, and an example of a sequence seen in both forms.*

DDA method acquires only the precursor ions with high abundances, whereas HDMS^E acquires all of them regardless of the abundances. This feature gives the impurities (non-phosphopeptides) a chance to be identified and overestimated. Therefore, the calculated percentage using the DDA data set (2.3%) represents the dephosphorylation events that happen during the enrichment step.

5.5.3- The relation between the identified phosphosites in both acquisition modes (HDMS^E and DDA)

A total of 783 phosphosites were identified in both acquisition modes, whereas 386 phosphosites were identified only in DDA. Some phosphosites that were identified solely in the DDA data set may be found in the HDMS^E data set as phosphopeptides but with different localization. The phosphopeptides of the HDMS^E approach were compared with the phosphosites identified solely by DDA. Overall, 135 of 386 phosphopeptides that were identified only in DDA acquisition mode were identified in HDMS^E acquisition mode but with other localization of phosphoryl group (Fig. 24 and Table.8 of the appendices).

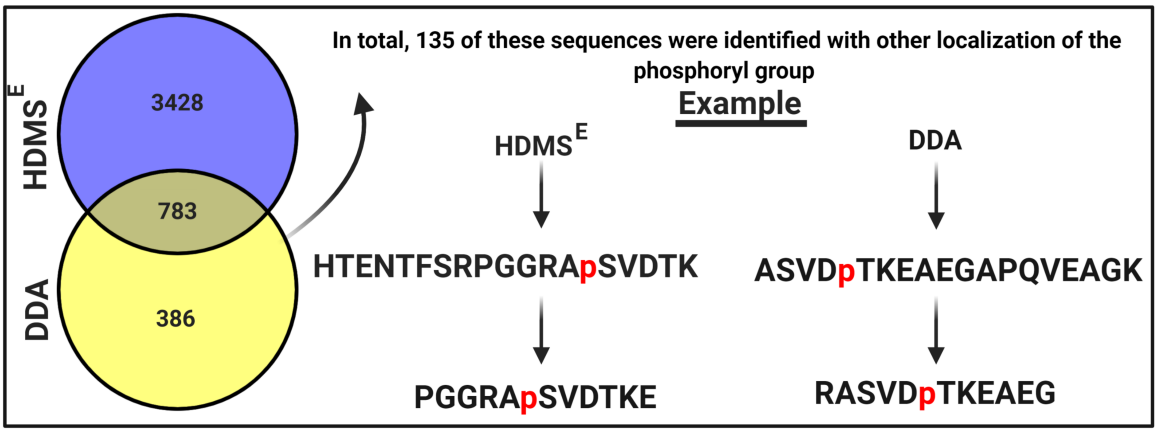

Figure 24: *Venn diagram shows the overlap between the phosphosites that were identified in HDMS^E and DDA acquisition modes (left side). An example of the phosphorylated sequences identified with different phosphoryl group localization (right side).*

5.5.4- Score distribution of identified phosphosites

The PLGS scoring system generates numbers (sores) that reflect the quality of the peptide-spectrum match. These scores' values depend on the number of the matched product-ions, product-ions' masses, total product-ions' intensities, and physicochemical properties. The PLGS scoring system does not have a cut-off value for the acceptable confidence of the identified phosphopeptides. Respectively in Mascot, the score is calculated based on the probability (p-value)—the random matches between theoretical and experimental spectra are excluded according to the applied p-value, which is adjusted to define the significant threshold.

The phosphosites were given the scores of the phosphopeptides, from which they are derived. The score-values of the phosphosites that were identified by HDMS^E and DDA were plotted against their percentage frequencies. The generated histograms were compared to find an appropriate cut-off value of the PLGS score. At this cut-off value, the number of the identified phosphosites obtained by both acquisition modes should increase significantly.

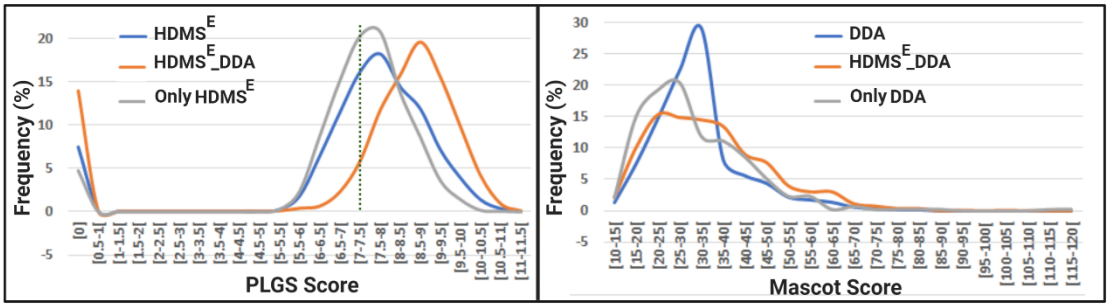

Figure 25: *PLGS (right side) and Mascot (left side) score distribution of the identified phosphosites. The blue histogram: the phosphosites were identified by HDMS^E. The orange histogram: the phosphosites were identified by both HDMS^E and DDA. The gray histogram: the phosphosites were identified only by HDMS^E. In the same way, the blue histogram: the phosphosites were identified by DDA. The orange histogram: the phosphosites were identified by both HDMS^E and DDA. The gray histogram: the phosphosites were identified only by DDA.*

PLGS scores values of all identified phosphosites by HDMS^E (HDMS^E), by both acquisition modes (HDMS^E-DDA), and exclusively by HDMS^E (only HDMS^E) were plotted against their percentage frequencies. Mascot scores of all identified phosphosites

by DDA (DDA), by both acquisition modes (DDA-HDMS^E), and exclusively by DDA exclusively (only-DDA) were plotted in the same way.

The three histograms of PLGS score percentage frequencies had a roughly normal distribution with outliers with a score of 0 (7.42%, 13.9%, and 4,75% for HDMS^E, HDMS^E-DDA, and only HDMS^E, respectively). Aside from these outliers, the rest of the identified phosphosites had scores higher than 5 (Fig. 25A). The percentage frequencies of HDMS^E and only HDMS^E increased dramatically at a score of 6. In contrast, the dramatic increase in the percentage frequencies of HDMS^E-DDA started from a score of 7. The phosphosites identified in HDMS^E and only HDMS^E have almost identical histograms, whose most score values (more than 90%) were higher than 6, and the peaks were in the range of [7.5-8[for both of them. However, the similarity between the distribution HDMS^E-DDA histogram and the other two histograms, HDMS^E-DDA histogram was shifted to the right side with score values ranging from 5.4 to 11 and reached the peak in the range of [8.5 -9[.

Similarly, Mascot scores distributions of DDA, HDMS^E-DDA, and only DDA had normal distributions with positive skewness (right-skewed), but they did not have outliers (Fig. 25B). More than 95% of the identified phosphosites had scores equal to or higher than 15. The histograms of DDA, HDMS^E-DDA, and only DDA reached their peaks at scores in ranges of [30-35[, [20-25[, and [25-30[, respectively. The percentage frequency of DDA histogram promptly declined after the peak, whereas the reduction was gradual in both DDA and HDMS^E-DDA.

Since the histogram of HDMS^E-DDA showed a dramatic increase at a PLGS score of 7, this score value was chosen as a cut-off value to filter the phosphosites of HDMS^E before doing the quantitative analysis.

5.6- Quantitative analysis of phosphopeptides

Since various cellular processes are mediated by rapid kinetic protein phosphorylation, it is worth studying the differently regulated phosphosites.

The quantitive analysis is composed of two comparisons. In the first one, the phosphoproteome of the mitotic cells (OA-treated wild type and knockout cells) and exponentially growing cells (EtOH-treated wild type and knockout cells) were compared to identify mitotic phosphorylation events. In the second one, the phosphoproteome of the mitotic wild type cells (OA-treated wild type cells) and mitotic knockout cells (OA-treated knockout cells) were compared to identify candidate PBK-dependent phosphorylation events.

Regarding $HDMS^E$ identifications, the phosphosites were filtered to remove the phosphosites with PLGS scores less than 7 before doing the quantitative analysis. In contrast, no score filtration was applied to DDA identifications since the Mascot search engine showed only the significant identifications according to the applied settings. Subsequently, stringent criteria were utilized to identify the differently regulated phosphosites. The phosphosites should be recognized at least in two of the three replicates, and the phosphopeptides that hold these phosphosites should show fold changes ≥ 20 with the t-test p-value of <0.05. Finally, the phosphosites that fulfilled these criteria and were derived from multiple phosphorylated peptides were manually checked one by one for their significance.

5.6.1- Identification of mitotic phosphosites

According to the regulation pattern of the phosphosites, two distinct populations were identified. One has an increased mitotic abundance (upregulated), and the other population has a decreased mitotic abundance (downregulated); see volcano plot in figure 26. The majority of the differently regulated phosphosites were upregulated in mitotic cells (treated with OA): 303 and 96 phosphosites in $HDMS^E$ and DDA, respectively showed mitotic regulation (Table.9 and 10 of the appendices).

Most of these phosphosites were identified on mono phosphorylated peptides. The phosphosites derived from multiply phosphorylated peptides were checked manually to be accepted as differently regulated or refused. Overall, 55 phosphosites were identified in both acquisition modes (Table 22).

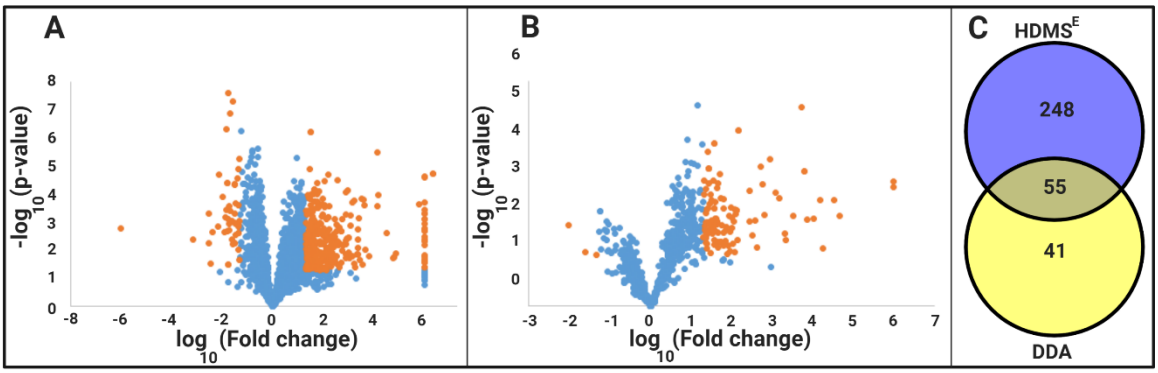

Figure 26: *The identified mitotic regulated phosphosites. The volcano plots highlight the mitotic significantly (red dots) and insignificantly (blue dots) regulated phosphosites. The measure of difference (log10 fold change) was plotted against their statistical significance (-log10 p-value). When the calculated fold change of infinity, it was replaced with 10^6. A: The volcano plot of HDMS^E identification. B: The volcano plot of DDA identification. C: Venn diagram shows the overlap between mitotic regulated phosphosites (up-and downregulated) that were identified by HDMS^E and DDA.*

Table 22: *A summary of up/downregulated phosphosites*

	HDMS^E		**DDA**		**HDMS^E and DDA**	
	Pho. Sites	Pho. Proteins	Pho. Sites	Pho. Proteins	Pho. Sites	Pho. Proteins
Upregulated	260	181	93	70	54	49
Downregulated	43	39	3	3	1	1

Pho. Sites: phosphosites, Pho. Proteins: phosphoproteins

Some of these sites (82 and 39 phosphosites in HDMS^E and DDA data sets, respectively) have been previously identified as mitotic phosphorylation (upregulated) or dephosphorylation events (downregulated) by Yamazaki et al., 2020, who studied the

phosphorylation in mitotic Hela cells. Here are two examples of identified mitotic regulated phosphosites whose impacts were studied in the literature:

The phosphorylation of Thr2106 on NUMA1 (Nuclear mitotic apparatus protein 1) was identified as an upregulated phosphosite during mitosis. A fold change of 45.66 and a p-value of 0.001 were determined in this work. Compton and Luo et al. 1995 observed this site as an essential mitotic phosphosite, and they confirmed their observation by mutating Thr2106 into serine, which abolished the mitotic spindle formation.

Tyr15 on CDK1 (Cyclin-dependent kinase 1) was pinpointed to be dephosphorylated during the mitotic phase in this analysis. Its fold change is close to 0.02 (downregulation), and it has a p-value of 0.001 in the mitotic phase. This result is consistent with the findings of Peng et al., 1998, who showed that the dephosphorylation Thr14 and Tyr15 are intrinsic modifications that lead to CDK1 activation.

The differentially regulated phosphosites were used to find potentially responsible kinases in the PhosphoSitePlus database (Hornbeck et al., 2012), to get an insight into the kinases that show increased activity during the mitotic phase. Overall, 39 substrates (36 upregulated and 3 downregulated) were found in the database. Table 23 shows examples of these findings, and table.11 of the appendices shows the 39 substrates.

Altogether, 26 protein kinases can phosphorylate these sites, including well-known mitotic kinases such as CDK1, AURKB, and PLK1. Besides the previously discussed sites (Thr2106 on NUMA1 and Tyr15 on CDK1), these substrate kinase associations might reveal roles of phosphorylation/dephosphorylation events during mitosis.

Table 23: *Examples of the mitotic regulated phosphosites that were found PhosphoSitePlus database and their upstream kinases.*

Kinase		Substrate						
Gene	ACC_ID	Gene	ACC_ID	11 amino acid sequence	Phosphorylated residue	Fold change	p-value	Identified in
Akt1	P31749	KHSRP	Q92945	PERSVSLTGAP	Ser193	778.66	0.01	HDMSE_DDA
		VIM	P08670	STRTYSLGSAL	Ser39	33.84	0.03	HDMSE
AurB	Q96GD4	DDX3X	O00571	KSSRFSGGFGA	Ser594	42.26	<0.001	HDMSE_DDA
		HMGN2	P05204	EPQRRSARLSA	Ser25	155.38	0.02	HDMSE
				RSARLSAKPAP	Ser29	155.38	0.02	HDMSE
		HMGN5	P82970	RSARLSAMLVP	Ser24	2156519,47	<0.001	HDMSE_DDA
				EPKRRSARLSA	Ser20	2156519,47	<0.001	HDMSE_DDA
		KIF4A	O95239	KLRRRTFSLTE	Thr799	58.73	<0.001	HDMSE
		PRRC2C	Q9Y520	RPVRRSGPIKK	Ser1013	29.55	<0.001	DDA
		RBM14	Q96PK6	DYARYSGSYND	Ser649	39.59	<0.001	HDMSE
CDK1	P06493	ANAPC1	Q9H1A4	LSRAHSPALGV	Ser355	44.13	<0.001	HDMSE_DDA
		HMGN5	P82970	MLVPVTPEVKP	Thr31	45.23	0.01	HDMSE_DDA
		HuR	Q15717	SQLYHSPARRF	Ser202	29.65	0.04	DDA
		NUMA1	Q14980	AAIGATPRAKG	Thr2106	45.66	<0.001	HDMSE
		VIM	P08670	RSLYASSPGGV	Ser55	270.89	0.02	HDMSE
CDK2	P24941	CALD1	Q05682	PTAAGTPNKET	Thr730	1088.80	0.02	HDMSE
		HMGN5	P82970	MLVPVTPEVKP	Thr31	45.23	0.01	HDMSE_DDA
		HuR	Q15717	SQLYHSPARRF	Ser202	29.65	0.04	DDA
		NCAPH	Q15003	LNIPGTPVLED	Thr49	134.78	0.05	HDMSE
		PAICS	P22234	YELLDSPGKVL	Ser27	29.84	<0.001	HDMSE
Chk1	O14757	HNRNPM	P52272	MDRVGSEIERM	Ser432	39.80	<0.001	HDMSE_DDA
		MATR3	P43243	DDRGPSLNPVL	Ser195	215.05	0.01	HDMSE
		TRIM28	Q13263	VKRSRSGEGEV	Ser473	84.45	<0.001	HDMSE_DDA
		HMGN1	P05114	PKRKVSSAEGA	Ser7	107.03	0.01	HDMSE
				KRKVSSAEGAA	Serer8	21.23	<0.001	DDA
ERK1	P27361	LIMA1	Q9UHB6	HPKPLSPDSRA	Ser362	0.02	<0.001	HDMSE
MAPKAPK2	P49137	HSPB1	P04792	LLRGPSWDPFR	Ser15	27.98	0.02	HDMSE_DDA
		TRIM28	Q13263	VKRSRSGEGEV	Ser473	84.45	<0.001	HDMSE_DDA
MOS	P00540	VIM	P08670	VINETSQHHDD	Ser459	90.52	0.01	HDMSE
Myt1	Q99640	CDK1	P06493	IGEGTYGVVYK	Tyr15	0.02	<0.001	HDMSE
p90RSK	Q15418	YBX1	P67809	RKYLRSVGDGE	Ser102	infinity	0.02	HDMSE
PLK1	P53350	ANAPC1	Q9H1A4	LSRAHSPALGV	Ser355	44.13	<0.001	HDMSE_DDA
		TP53BP1	Q12888	KAADISLDNLV	Ser1618	311.23	0.02	HDMSE
Src	P12931	CDK1	P06493	IGEGTYGVVYK	Tyr15	0.02	<0.001	HDMSE
Wee1	P30291	CDK1	P06493	IGEGTYGVVYK	Tyr15	0.02	<0.001	HDMSE
		CDK2	P24941	IGEGTYGVVYK	Tyr15	0.02	<0.001	HDMSE

5.6.2- Consensus motifs in the mitotic regulated phosphosites

In contrast to phosphopeptides enrichment using phospho-specific antibodies, IMAC/ TiO2 relies on phosphomonoester-metal interaction. Other than its tendency to capture peptides that contain acidic amino acid residues such as glutamic and aspartic acid, this method is independent of the residues surrounding the phosphosites in the target peptides. The differently regulated phosphosites were split into two groups: upregulated and downregulated phosphosites (Figure 27A and D). The unique phosphosites were analyzed to find consensus sequence motifs in each group separately. The overrepresented motifs were displayed as bar charts (Figure 27B and E), and the motifs that exceeded the occurrence threshold of 20 were visualized using plogo (O'Shea et al., 2013). Arginine (R) residues at position -3 (RXXpS), and leucine (L) residues at the position +1 (pSL), were enriched and had the highest trend in both $HDMS^E$ and DDA datasets (Figure 27C and F). Additional consensus sequence motifs that were upregulated in mitotic cells and were identified in $HDMS^E$: non-polar, aliphatic residues at position +1 proline (P), alanine (A), valine (V), or glycine (G) at position -1 to form the mitotic motifs pS/T, pSA, pSV, GpS (Figure 27E and F). Only the motif with valine at position +1 has been identified to be a novel mitotic motif, whereas all other motifs have been previously published as mitotic motifs (Gygi S, 2008; Yamazaki et al., 2020).

The analysis of the downregulated phosphosites did not reveal any significant consensus motif. The latter result could be attributed to the low number of significantly downregulated phosphosites.

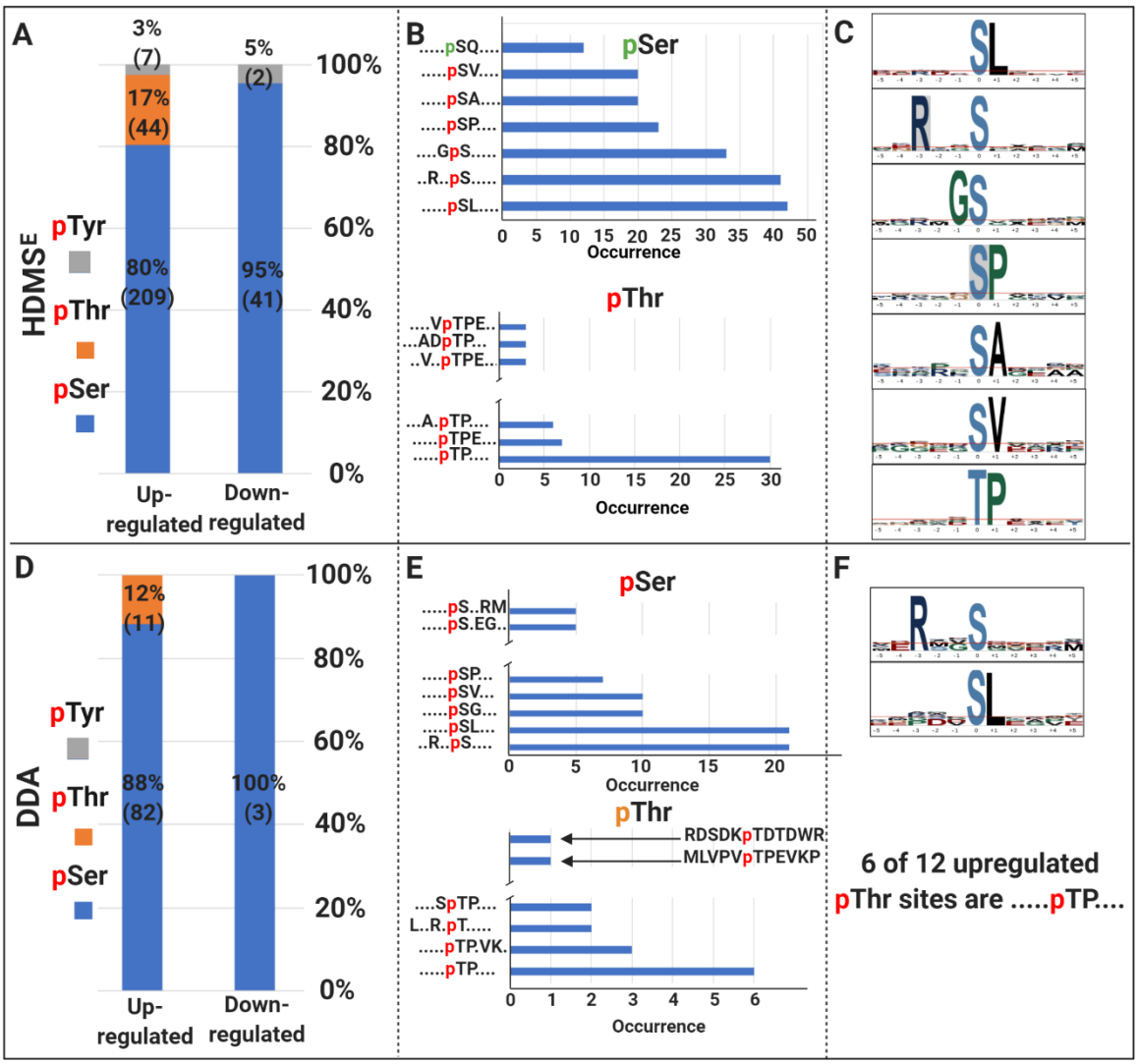

Figure 27: *Consensus mitotic phosphosite motifs. A and D: Bar charts show the distribution of the up/downregulated phosphosites during mitosis. B and E: Bar charts show the recurrence of the overrepresented motifs that were upregulated during mitosis. C and F: The sequence logos of the phosphosites were upregulated during mitosis. Regarding the downregulated phosphosites, no conserved motifs were identified as part of this analysis.*

5.6.3- Gene ontology analysis of the mitotically regulated phosphosites

The phosphoproteins that carry mitotic phosphorylation/dephosphosites were subjected to Gene ontology analysis to understand their roles on the molecular level (molecular

function), the locations of these activities (cellular component), and the major contexts of these activities (biological process).

FunRich version 3.1.3 was deployed to compute the GO terms (Table.11 and 12 of the appendices). The top five enriched molecular functions, cellular components, and biological processes functions that have p-value (Hypergeometric test) < 0.05 were visualized as pie charts (Fig. 28).

The top five enriched molecular functions include RNA binding, transcription regulator activity, cytoskeletal protein binding, ribonucleoprotein, and translation regulator activity. The cellular components in which these activities happen are distributed between the nucleus and the cytoplasm. The majority of the analyzed phosphoproteins have both nuclear and cytoplasmic localization. These post-translational modifications that occur during the cell cycle determine their cellular localization.

An example of these phosphoproteins is anaphase-promoting complex subunit 1 (ANAPC1). It was identified in $HDMS^E$ and DDA data set to be noticeably phosphorylated at Ser355. ANAPC1 has mainly a nuclear localization during the interphase. It is phosphorylated at Ser355 from prophase to the anaphase and translocates from the nucleus to the centrosomes (Kraft et al., 2003).

The enriched biological processes involved regulating the nucleobases, cell growth, cell cycle regulation, and chromosome organization.

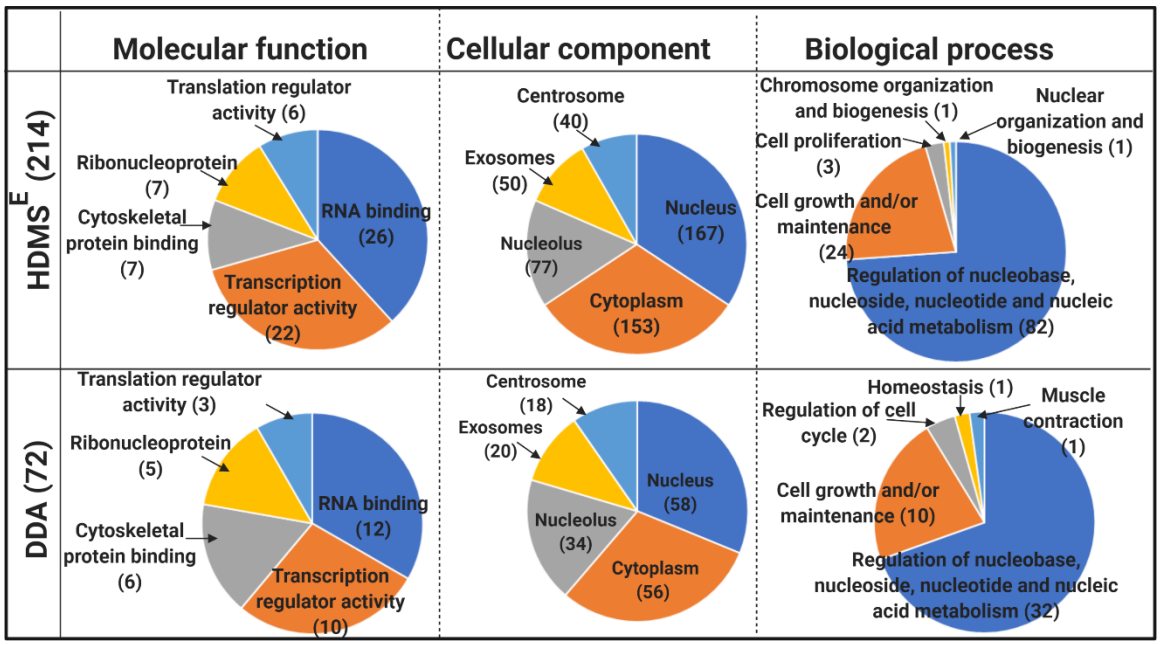

Figure 28: *Gene ontology analysis of the phosphoproteins, which showed mitotic phosphorylation/dephosphosites. These phosphoproteins include 214 in HDMS^E and 72 phosphoproteins in DDA. The molecular functions, the cellular component, and the biological processes were computed using FunRich version 3.1.3, and the top five most enriched gene ontology terms were visualized as pie charts.*

The top five enriched biological functions and the cellular components were identical in both HDMS^E and DDA results. In the same manner, the majority of the over-presented biological processes were similar in both acquisition modes, too.

Hence, the majority of the highly enriched phosphosites belong to proteins that have RNA-binding properties and are involved in transcription regulation. This observation suggests that these mitotic phosphorylation events play a role in controlling the functions of transcription regulator proteins during mitosis.

5.7- PBK phosphosites in HAP1 cells

PBK knockout cells were verified at the protein level using western blot that showed a PBK band only in the wild type cells (Fig. 29). The acquired PBK-derived

phosphopeptides were checked to compare this result with the phosphoproteome data. In HDMS^E acquisition mode, a PBK-derived doubly phosphorylated peptide (pSVLCSTPTINIPApSPFMQK) was identified in the third replicate of the wild type OA- treated cell line with a score value of 7.5. This peptide stretches of 19-37 residues and carries two phosphosites: Ser19 and Ser32. It was identified: by two fragments, b10 (pSVLCSTPTINI) and y8 (PApSPFMQK). The sequence of b10 compromises four residues that are able to carry the phosphoryl group (Ser19, Ser23, Thr24, and Thr 26). The phosphoryl group was localized at the first serine residue, which cannot be confirmed because of the three other possible localization sites. In contrast to b10, y8 has only on the phosphosite (Ser32), so the phosphoryl group is unambiguously localized to this residue (Fig. 29).

Similarly, one mono phosphorylated peptide (GLSHpSPWAVK) using DDA acquisition mode in the third replicate of the wild type OA- treated cell line with a Mascot score of 26.84. This mono phosphorylated peptide spans 10 amino acid residues (55 to 64). It contains two possible phosphosites (Ser57 and Ser59). The phosphoryl group was localized at Ser59. This localization is the significant best match, according to the Mascot probability-based searched algorithm.

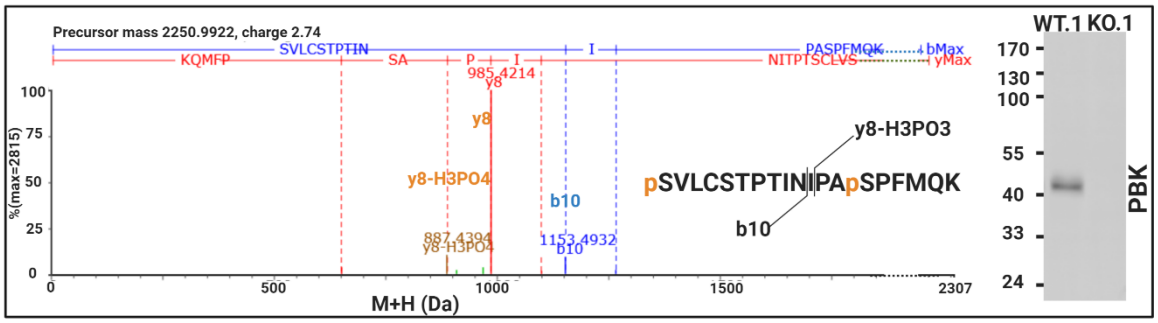

Figure 29: *The verification of HAP1 cell lines genotypes. (Right side) An example of PBK identified PBK phosphosites (Ser19 and Ser32). (Left side) Western blot detection of PBK in both wild type PBK knockout HAP1 cells.*

Proteome analysis ascertained these results. A total of 5 PBK-derived peptides were identified in the runs of the wild type cells (treated and non-treated). In each run of the wild type cells, at least 3 PBK-derived peptides were identified. In contrast, PBK knockout cells did not display any PBK-derived peptides.

5.8- Candidate PBK-dependent phosphorylation events

A comparison between the phosphoproteome of the mitotic wild type (OA-treated wild type cells) and PBK knockout cells (OA-treated knockout cells) was conducted to find candidate PBK-dependent phosphorylation events. The identified phosphosites were filtered according to the analysis criteria (identified at least in two replicates with fold changes ≥20 and the t-test p-value of <0.05) to find these candidates. This comparison revealed that five phosphosites had an upregulation pattern in the mitotic wild type cells. Four of them were acquired from $HDMS^E$ data analysis and one from DDA data analysis (Table. 24).

Among the identified candidates, four phosphosites were identified on mono phosphorylated peptides, and only one was identified on a doubly phosphorylated peptide (SFKLpSGFpSFKK). The phosphosite SFKLpSGFSFK was identified on mono and doubly phosphorylated phosphopeptides. Figure 30 shows examples of the identified PBK-dependent phosphosites.

These four candidates include two phosphosites that belong to transcription factors. The first transcription factor is activity-dependent neuroprotector homeobox protein (ADNP). The structure of ADNP contains nine C2H2-ZNF domains and a homeobox domain (DNA binding domain). ADNP plays a role in cellular growth, chromatin remodeling, microtubule, and autophagy regulation (Karagoz et al., 2019). The phosphorylation of Ser98 of ADNP was identified as a candidate PBK-dependent phosphorylation event. The other transcription factor is upstream element-binding protein 1 (FUBP1). It regulates the transcription of several oncogenes (*c-myc*) and cell cycle inhibitors (p21/CDKN1A) (Hoang et al., 2019). The phosphorylation of Thr229 of FUBP1 was upregulated in the mitotic wild type cells. Interestingly, this phosphosite Thr229 (FUBP1) has the sequence TGADKP, which shows an evident similarity to the PBK specific substrate TGEKP, with an alanine-aspartic acid residues substitution instead of the glutamic acid residue.

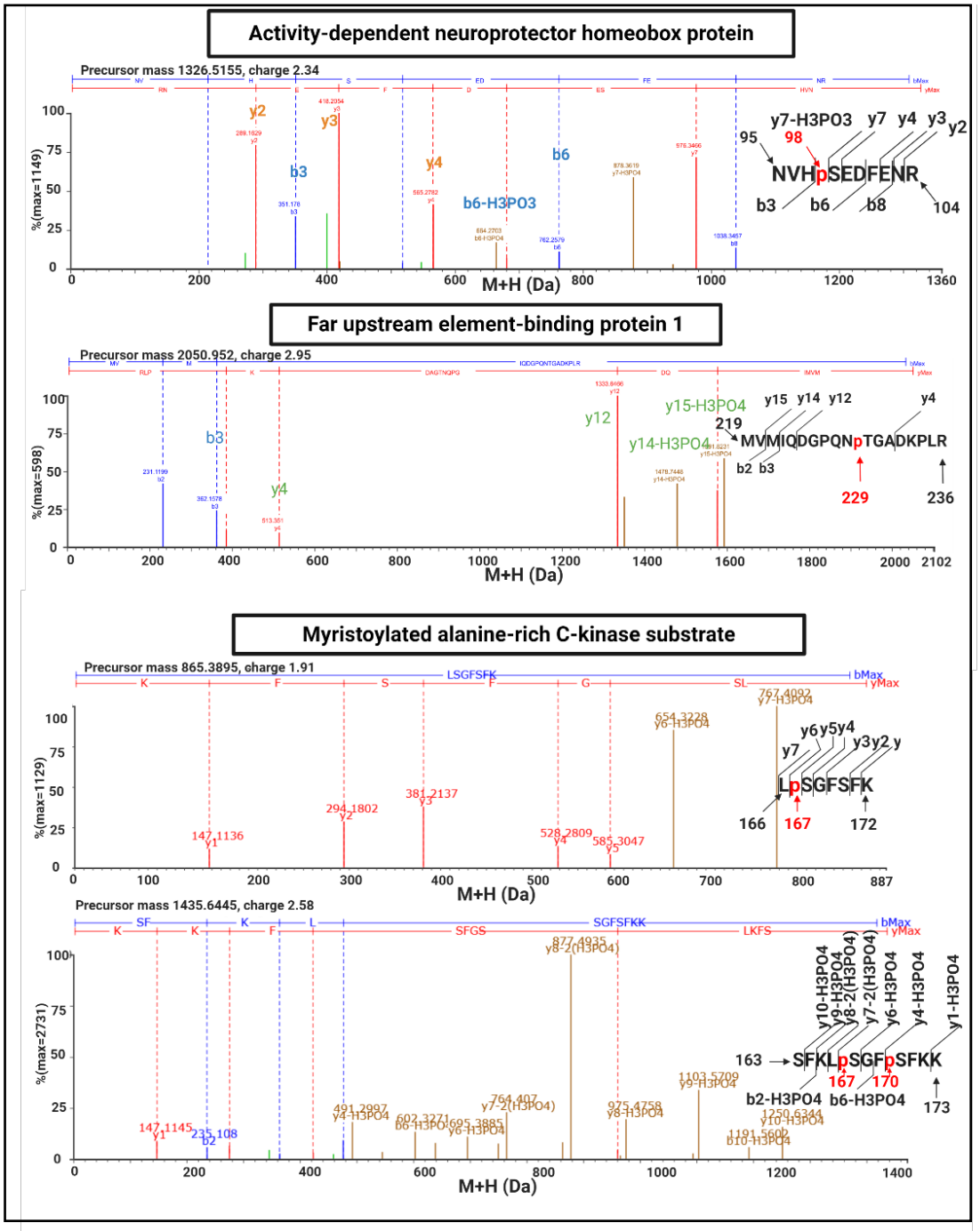

Figure 30: *Examples of the identification of candidate PBK-dependent phosphosites. The residues were numbered according to UniProtKB protein sequences.*

Table 24: The identified PBK dependent phosphoryalation events

Gene (ACC_ID)	Identified sequences [a]	11 amino acid sequence	Phos. Residue [b]	Fold change	p-value	Identified in
ADNP (Q9H2P0)	NVHpSEDFENR	FRNVHSEDFEN	S98	171.08	0.02	HDMS^{E}
FUBP1 (Q96AE4)	MVMIQDGPQNpTGADKPLR	DGPQNTGADKP	T229	104.60	0.00	HDMS^{E}
MARCKS (P29966)	SFKLpSGFSFK	KSFKLSGFSFK	S167	48.77	0.00	HDMS^{E}
	SFKLpSGFpSFKK	KLSGFSFKKNK	S170	21.05	0.00	HDMS^{E}
PGRMC1 (O00264)	LLKEGEEPTVYpSDEEEPKDESAR	EPTVYSDEEEP	S181	20.91	0.03	DDA

[a] The phosphoryl group was shown in red, whereas the amino acids were shown in black.

[b] The numbers of the phosphorylated residues were given according to UniProt protein sequences.

Myristoylated alanine-rich C-kinase substrate (MARCS) carries two candidates (Ser167 and Ser170). This protein has a role in regulating the motion of subcellular organelles (Brudvig and Weimer, 2015).

Membrane-associated progesterone receptor component 1 (PGRMC1) carries the fifth candidate (Ser181). PGRMC1 entails various molecular pathways, such as cell cycle regulation, tumorigenesis, and progression (Xu et al., 2011; Ryu et al., 2017).

Considering that PBK enhances the stability of MKP1 phosphatase (Li et al., 2011; Win et al., 2018), PBK activity may be accompanied by some dephosphorylation events. Nevertheless, neither $HDMS^E$ nor DDA data analysis revealed significantly downregulated phosphorylation events in mitotic WT.1 cells.

6- Discussion

6.1- HAP1 cell line and PBK activation in these cells

HAP1 cells are near-haploid cell line, derived from KBM-7, which is chronic myelogenous leukemia (CML) cell line. The failed attempt to make KBM-7 pluripotent by overexpression of five essential pluripotency transcription factors (POU5F1, SOX2, KLF4, and MYC) led to the generation of a new near-haploid cell line, called HAP1. This cell line has lost the expression of all myeloid marker proteins and grows adherently. HAP1 cells retain the partial disomy of a fragment of chromosome 15 of the parent cell line. However, HAP1 cells lost the second copy of chromosome 8, making them near-haploid (Essletzbichler et al., 2014). HAP1 cell line is a powerful tool to study loss-of-function mutations, which can be achieved by mutating the single allele, and then directly analyzing the resulted phenotype due to the lack of the second allele (Gerhards et al., 2018). During cell replication the diploid cells rapidly overtake the culture due to their better growth properties (Olbrich et al., 2017). However, knockout HAP1 cells will not restore their ability to express the knockout genes; they will stay entirely knockout.

HAP1 cells were adopted as a model to identify target sites that are going to be phosphorylated by PBK, a MAPK kinase involved in cell cycle progression and mitosis. The dysregulation of its expression and activity is associated with tumor aggressiveness, invasion, metastatic spread, and poor prognosis in many cancers. Various studies suggested PBK as a treatment target after highlighting its impact on tumor cell proliferation, growth, and survival (Herbert et al., 2018). Although several PBK-dependent phosphorylation events are described in the literature, so far, no systematic study has been done to determine PBK-specific target sites.

As PBK activity is restricted to the mitotic phase, appropriate treatment is required to activate this kinase. The HAP1 cell models were treated either with okadaic acid (OA) or double thymidine block and nocodazole (DTB-Noc) to compare the treatment efficiencies (Fig. 14). The genotypes of both HAP1 cell models (wild type: WT.1 and knockout: KO.1) were verified using western blot, mass spectrometry analysis (Fig. 29).

The phosphorylation of the conserved C2H2-ZNF proteins linker (TGEKP) was used as a marker for PBK activation and mitotic phase entry. Western blot analysis reveals that OA-treatment was noticeably superior DTB-Noc in terms of PBK activation and cell viability. TGEKP phosphorylation was utterly absent in both non-treated wild type cells and PBK knockout cells (OA-treated/non-treated) (Fig. 14 and 17B). The western blot affirms that no alternative kinase can phosphorylate the TGEKP sequence of C2H2-ZNF proteins in vivo, confirming the findings of Rizkallah et al., 2015, who presented PBK as the master regulator of C2H2-ZNF proteins through the phosphorylation of TGEKP.

Suzuki K et al., 2015 claimed that CDK1 could phosphorylate TGEKP. Their observation depends on an in vitro kinase assay and the inhibition of TGEKP phosphorylation in mitotic Xenopus egg upon the treatment with roscovitine (CDK1 inhibitor). These findings do not exclude the possibility that CDK1 is the indirect kinase of TGEKP. Indeed, CDK1 activates PBK through its phosphorylation at Thr9 in the mitotic phase (Matsumoto et al., 2004); consequently, the activation of CDK1 enhances PBK activity, which phosphorylates the C2H2-ZNF proteins linker (TGEKP).

Since OA-treatment induces mitosis (Holder et al., 2019), it is essential to calculate the mitotic index in analyzed cells to estimate the percentage of mitotic cells in the total cell population. Histone H3 (H3) phosphorylation occurs substantially at several residues such as Ser10 and Ser28. The phosphorylation of Ser28 occurs during prophase to metaphase (Sawicka and Seiser, 2012; Goto et al., 2002). Ser10 is a potential target residue of PBK (Park et al., 2006). So, Ser10 is not an appropriate mitotic marker in mitotic PBK knockout cells. Therefore, H3-phosphorylated Ser28 was used in this work as a mitotic marker to trace the mitotic cells. Hereto, flow cytometry was used to determine the wild type and PBK knockout HAP1 cellular mitotic index by detecting the mitotic marker pSer28 with anti-H3 pSer28 antibody (Fig. 16). OA-treatment induced a prominent mitotic arrest in both wild type and PBK knockout HAP1 cells. The arrested cells also showed good viability levels. Hence, OA-treatment for 6 h is enough to arrest the HAP1 cells in the mitotic phase

Thus, OA-treatment could be deployed to arrest both wild type and PBK knockout HAP1 cells in the mitotic phase. Both cell lines were treated with OA or just with the EtOH alone to create four conditions. Three replicates were prepared for each condition.

The cells were harvested. pSer28 and pTGEKP were screened. The total protein fraction was extracted, digested, and the acquired peptides were measured by $HDMS^E$ acquisition mode. The phosphopeptides were enriched, and measured in both $HDMS^E$ and DDA acquisition modes (Fig. 13).

6.2- The role of PBK in p38 activation

The impact of PBK on p38 phosphorylation is still debatable. PBK was initially identified as an upstream kinase of p38. It phosphorylates p38 at threonine 180 and activates it (Abe et al., 2000). PBK is also a negative indirect regulator of p38. It increases the stability of dual threonine-tyrosine dual-specificity phosphatase MKP1, which dephosphorylates and deactivates p38 (Li et al., 2011). The investigation of p38 phosphorylation of both wild type and PBK knockout cells showed that p38 phosphorylation is upregulated in the mitotic phase dramatically regardless of PBK genotype (Fig. 17A). This observation suggests that PBK is not the major kinase of p38, but instead, other mitotic kinases might be responsible for this phosphorylation event.

6.3- The proteome analysis

The temporal regulation of the identified proteins among the studied conditions was investigated. Concerning the proteome analysis, the identified proteins in the three biological replications showed a high degree of overlap (97%), and their abundances had a strong correlation ($r \geq 0.94$), which reflects a high reproducibility (Fig. 18B and C). The quantitative analysis of the identified proteins showed: 39 proteins with differently regulated pattern among the four studied conditions (figure 19, table 20, and table 3 of the appendices), three proteins had PBK-dependent regulation pattern (table 19), and 21 proteins had a mitotic dependent regulation pattern (figure 19 and table 2 of the

appendices). Most of the mitotic regulated proteins (n=20) were downregulated during mitosis, and GPC4 was upregulated. The reduction in protein abundance of various proteins during the mitotic phase matches the previous findings of Tanenbaum et al., 2015, who reported the reduction of protein syntheses during the mitotic phase. They attributed it to the inhibition in both transcriptional and translational efficiency.

Annexin A1 (ANXA1), Glucose-6-phosphate 1-dehydrogenase (G6PD), and Emerin (EMD) were selected for validation by western blot analysis. According to the proteome data, ANXA1 showed downregulation in PBK knockout cells, whereas G6PD and EMD showed upregulation. Regarding ANXA1 and G6PD, proteome and the western blot results of wild type (WT.1) and PBK knockout (KO.1) were consistent. Introducing the clones (WT.2 and KO.2) showed variable levels between the same genotype clones with the same treatment status. This finding reveals that HAP1 cells have a strong clonal effect, which has an apparent impact on protein levels among different clones. Thus, according to these results, the diversity among clones having the same genotype leads to variation in protein expression (Fig. 21). Consequently, studying protein regulation in HAP1 cells requires that measurements have to be confirmed in more than one cell clone representing each genotype to obtain robust and reliable results.

Western blot analysis of EMD revealed an OA-regulation-dependent pattern. The expression of EMD increased significantly upon OA-treatment (Fig. 21). Instead of one EMD band, mitotic cells show multiple bands leading to an intense smear. Comparable western blot patterns of EMD have not been reported in the literature. This smear might be due to post-translational modifications. Since OA is a phosphatase inhibitor, these mitotic modifications are most likely due to differential phosphorylation events. Protein degradation is excluded since the sizes of the detected proteins are higher than unmodified EMD.

The noticed inconsistency between proteome and western blot results of EMD could be attributed to the poor western blot quantitation of the actual protein abundance in ghost and smeared bands. According to Butler et al., 2019, quantification of smeared bands gives misleading western blot results. In future experiments, one might consider

dephosphorylating the total protein extract before loading it onto SDS-PAGE to get more comparable measurements.

6.4- The phosphoproteome analysis

Mass spectrometric data of phosphosites studied in HAP1 cell models were exported from Progenesis QI as excel tables containing peptide sequences combined with the location of the phosphorylated residue (appendices 4 and 5). The identified phosphosites were coded as identifiers or converted into unique phosphosites. The comparison of these two methods showed that the identifiers overestimate the number of identified phosphosites (Fig. 11). This disadvantage arises from the phosphopeptides that appear in the protein more than once and from shared phosphopeptides among different proteins. The unique phosphosites surpassed the identifiers since they represent the unique phosphosites themselves (two examples were presented in page 66). This strategy (unique phosphosites) can be used to analyze other PTMs, such as acetylation and glycosylation.

6.4.1- Qualitative analysis of phosphopeptides

DDA is the current state-of-the-art method for phosphopeptides identification. It depends on the selection of the highest abundant precursors, which are fragmented and identified. This selection step decreases the complexity of the spectra. The number of the identified phosphopeptides decreases as well, especially in proteins of low abundance. $HDMS^E$ overcomes this limitation through the fragmentation of all analyzed precursors regardless of their abundances. Although $HDMS^E$ provides higher identification rates, it generates multiplexed fragment ion spectra, which are processed and deconvoluted by sophisticated software (PLGS in this work). The correct identification of the phosphopeptides requires enough information regarding the phosphoryl group's localization, which should be included in the deconvoluted tandem mass spectra (Olsen and Mann, 2013). This complicated process may produce many false identifications owing to the inability of PLGS to find the real localization site using the deconvoluted tandem mass spectra.

As expected, HDMS^E increased the number of the identified phosphosites more than three and a half times as much as DDA. Overall, 67% of the phosphosites that were identified by DDA were also identified by HDMS^E (Fig. 22).

The reproducibility of HDMS^E was much lower than DDA. 38% of the phosphosites were identified at least in two replicates in HDMS^E (Fig. 22E and J). The percentage was much higher in DDA (59%) (Fig. 22E and J). Taking into account the low percentage of the identified phosphopeptides in HDMS^E (44%) comparing with DDA (70%) (Fig. 22D and I)., the low reproducibility of HDMS^E may be attributed to the high complexity of measured samples by HDMS^E, which consist of the enriched phosphopeptides and the low abundant co-eluted non-phosphopeptides. The later ones interfere during the measurement of the analytes of interest (the phosphopeptides). DDA selects high abundant precursors (mostly phosphopeptides) and removes low abundant precursors (mostly non-phosphopeptides). This feature reduces the complexity of the analyzed sample. Thus, DDA leads to more reproducible results.

- PLGS search engine is a protein-centric search program. It gives the identified phospho- and non-phosphopeptides scores representing the strength of the matches between theoretical masses in the database and the observed MS/MS peaks. PLGS score increases when matches between the theoretical and experimental masses increase, but it is not the only determinant factor. The physicochemical attributes such as the total y ion intensity ratio to the total b ion intensity, the loss of H2O and NH3 from peptides containing specific amino acids affect the value of the calculated score (Li et al., 2009). PLGS scoring system has no cutoff value that can differentiate between reliable and unreliable identifications.
- Mascot score calculation is inspired by the Mowse scoring system, which increases upon increasing the number of matches between the experimental masses and the theoretical masses in the database. It decreases when the database increases and when the theoretical fragments that have similar masses to the experimental one increase. Mascot score differentiates between significant and

insignificant identification using a specific significance threshold (p-value = 0.05 in this work).

The scores of the identified phosphosites were plotted against their percentage frequencies. Three histograms were generated for each acquisition mode, as described in the results (Fig. 25).

PLGS histograms named $HDMS^E$ (all identified phosphosites by $HDMS^E$), $HDMS^E$-DDA (identified by both acquisition modes), and only $HDMS^E$ (identified exclusively by $HDMS^E$). The three histograms were examined and compared to determine a cutoff value of the PLGS score. Despite the similar distribution of PLGS histograms, $HDMS^E$–DDA is shifted to the right side and has a noticeable increase in the number of identified phosphosites at a PLGS score reaching 7. Most phosphosites that were identified in both acquisition modes have a PLGS score equal to or higher than 7. Likewise, DDA, DDA-$HDMS^E$, and only DDA histograms had normal distributions. Thus, the identified phosphosites in both acquisition modes did not tend to have a different range of Mascot scores. The phosphosites with PLGS scores equal to or higher than 7 should have higher reliability, so only these phosphosites were subjected to the quantitative analysis.

6.4.2- Quantitative analysis of phosphopeptides

The identified phosphosites were assigned to the abundances of the phosphopeptides from which they are derived. The previously mentioned exclusion criteria were applied before doing the analysis. Briefly, the analyses were conducted to investigate: (i) the mitotic regulated phosphosites, the associated kinases, and the consensus phosphomotifs associated with the cell cycle phase regardless of the genotype (ii) candidate PBK-dependent phosphosites (Fig. 7 and Table 24)

The analysis identified numerous phosphosites that were upregulated or downregulated during mitosis. The vast majority of these sites were upregulated during the mitotic phase. Since these phosphosites are the outcomes of the activation of specific kinases, tracing these candidate kinases will provide more information regarding the mitotic kinase activity during the cell cycle. The identified mitotic phosphosites were searched in

the PhosphoSitePlus database (Hornbeck et al., 2012) to find the corresponding kinases. A total of 26 kinases are responsible for the phosphorylation of 39 sites (Table 23 and 6 of the appendices). Some of these phosphosites have been studied well in the literature so far. For example, non-histone chromosomal protein HMG-17 (HMGN2) is a nucleosome binding protein, which regulates the chromatin during the mitotic transition. Its phosphorylation status of HMGN2 controls its binding ability. During the interphase, Ser25 and Ser29 are not phosphorylated, and HMGN2 is bound to the nucleosome. In the mitotic phase, aurora B phosphorylates these two residues (Ser25; Ser29), and HMGN2 disassociates from the nucleosome (Hengeveld et al., 2012).

The investigation of the biological impact and upstream kinases of the other identified mitotic regulated phosphosites, which was not mentioned in the literature, will provide a deeper understanding of their roles in mitosis.

Motif Enrichment Analysis revealed that the mitotic upregulated phosphorylation motifs could be classified into seven mitotic kinase consensus phosphorylation motifs in the $HDMS^E$ data set (RXXpS, pSL, pS/T, pSA, pSV, and GpS). Two of them (RXXpS and pSL) were also identified in the DDA data set. All these mitotic phosphormotifs except pSV were identified previously in the literature as a mitotic phosphorylation motif (Gygi S, 2008; Yamazaki et al., 2020). The enriched motifs include CDK1 conserved motifs (pSP, pTP, and pSL) (Brown et al., 2015; Cesaro and Pinna, 2015) and the conserved basophilic motifs (RXXpS) of PKA (Limbutara et al., 2019). The other enriched motifs could not be matched to specific kinases (Fig. 27).

Candidate PBK-dependent phosphorylation events were investigated using the previously mentioned criteria to identify candidate direct or indirect PBK substrates. In $HDMS^E$ acquisition mode, four phosphosites showed significant upregulation in mitotic wild type cells comparing with mitotic PBK knockout HAP1 cells: Thr229 on far upstream element-binding protein 1 (FUBP1), Ser98 on activity-dependent neuroprotector homeobox protein (ADNP), Ser167, and Ser170 on myristoylated alanine-rich C-kinase substrate (MARCKS) were upregulated in the mitotic wild type cells (Table 24). Ser181 on membrane-associated progesterone receptor component 1 (PGRMC1) was identified as a PBK-dependent phosphorylation event in DDA acquisition mode

FUBP1 is a DNA binding protein. It regulates *c-Myc* gene transcription through its binding to the far upstream element in the promoter region. In cancer cells, FUBP1 upregulation is accompanied by high proliferation rates and prolonged cell survival (Hoang et al., 2019). The phosphorylated Thr229 was identified by Rusin et al., 2017 in the mitotic phosphoproteome of HEK293 cells, but neither its function nor its upstream kinase was identified. Thr229 is located within the KH2 domain, which is a DNA binding domain. Asn229 to Thr229 substitution was observed in acute lymphoblastic leukemia (Debaize and Troadec, 2019), which suggests a vital role of Thr229 in regulating the function of FUBP1. Additionally, Thr229 is located in the sequence (TGADKP) that shows a similarity to the specific substrate of PBK (TGEKP). Thus, PBK may be the direct upstream kinase of this site.

ADNP is a C2H2 ZNF protein. It comprises nine C2H2 ZNF domains and a homeobox domain. ADNP binds to heterochromatin protein 1 (HP1), chromodomain-helicase-DNA-binding protein 4 (CHD4), and DNA specific sequences. These interactions mediate the regulation of the transcripts of the target genes (Gozes, 2018). Ser98 locates between the first and the second zinc finger domains and might have a role in regulating these interactions.

MARCKS is one of the dynamics molecules regulators. It has an effector domain (ED), which is rich with positively charged lysine residues interspersed by serine residues, Ser167, Ser170 are some of these residues. ED allows MARCKS to attach to the plasma membrane. The phosphorylation of Ser167 and the neighboring serine residues neutralize the positive charge and reduce the ability of ED to bind the membrane. Thus, MARCKS will be able to translocate to other cell compartments. Although PKC was reported as a kinase of these neighboring serine residues, other kinases may share PKC in this activity or be an upstream kinase of PKC and consequently promote this phosphorylation event (El Amri et al., 2018).

PGRMC1 is involved in many biological processes, such as heme-binding, regulation of cytochrome P450 enzymes, and cell cycle regulation. The overexpression of PGRMC1 and the increased phosphorylation of Ser181 were reported in breast cancer (Neubauer et al., 2008). This phosphorylation event is associated with increased tumorigenesis in the

MCF7 breast cancer cell line treated with norethisterone. Casein Kinase 2 (CK2) is a direct kinase of Ser181. It activates PGRMC1 to forward the intracellular progestin signals (Willibald et al., 2017).

Apart from MARCKS and PGRMC1 that have known published direct kinases, no direct kinases have been mentioned in the literature to be responsible for PBK-candidate phosphorylation events in the other targets (FUBP1 and ADNP).

6.5- Potential therapeutic targets in respect to PBK-dependent phosphosites and murine knockout model

The question to be answered is how to relate results obtained using cell culture to PBK knockout mice. Western blot analysis revealed strong phosphorylation signals due to PBK kinase activity in HAP1 mitotic cells (treated with OA). In HAP1 PBK knockout cells, the phosphorylation signal is not present anymore (Fig. 14). Since the HAP1 cells still proliferate, it seems that the phosphorylation of C2H2 linker (TGEKP) is not essential for the functionality of C2H2 zinc finger proteins. Thus, it can be stated that the phosphorylation of the C2H2 linker by PBK is not an exclusive mechanism for dissociating zinc finger proteins from their DNA binding sites. As reviewed by (Herbert et al., 2018). PBK is a nonessential mitotic kinase since the PBK knockout/knockdown cells are viable and able to proliferate.

The upregulated activity of PBK is associated with cell growth and tumorigenesis in many tumor cells. Thus, PBK was suggested to play a supportive role in cell proliferation Targeting PBK by selective inhibitors is expected to reduce tumor growth with minimal toxicity to the non-tumor cells. PBK knockout mice have not yet been studied in depth; however, these mice have a higher sensitivity to UV radiation than the wild type mice. This observation was attributed to the phosphorylation of DUSP1 by PBK. The phosphorylated active DUSP1 deactivates the tumor suppressor kinase p38 (Li et al., 2011b). One might speculate that mice depleted of PBK should be less prone to developing tumors and metastasis, highlighting the importance of PBK inhibitors. The research advance of selective PBK inhibitors has just been reviewed by Han et al., 2021.

Although PBK knockout mice hardly show any phenotype, PBK might have essential roles in human pathological conditions. One cannot exclude that inhibition of PBK functions might have therapeutic relevance. Consequently, the experimentally identified PBK-candidates phosphorylation events on ADNP, FUBP1, MARKS, and PGRMC1 in this work might be prospective therapeutic targets.

7- Conclusion and outlook

In this study, HAP1 cells (wild type and PBK knockout) were used as a model to investigate mitotic specific phosphorylation events and PBK-dependent phosphosites. Proteomic and phosphoproteomic shotgun strategies were used. A new strategy was applied to convert the identified phosphopeptides to unique phosphosites, which is essential to perform the qualitative and quantitative analysis. This strategy can be applied not only to analyze the phosphopeptides but also other modifications. Proteome and phosphoproteome analysis showed:

- A total of 20 proteins were downregulated during the mitotic phase.
- Around 350 mitotic regulated phosphosites were identified; some of them are known mitotic phosphorylation events.
- Motif analysis of the identified phosphosites generated a few consensus motifs that are widely phosphorylated during the mitotic phase.
- All the acquired phosphomotifs except one motif (pSV) were previously mentioned in the literature as conserved phosphorylation motifs.
- Five candidate PBK-dependent phosphosites. These sites belong to chromatin regulating proteins (ADNP and FUBP1) as well as dynamic regulatory proteins (MARCKS and PGRMC1).
- One of the candidate PBK-dependent phosphosites (TGADKP) has a similarity to PBK specific substrate (TGEKP).
- HAP1 cell line has been demonstrated to be an appropriate system to study the loss of function of a specific kinase.

The impact of these phosphorylation events on protein functions should be investigated further to understand the biological processes in which PBK is involved. Regarding proteome analysis in HAP1, at least two clones of each cell genotype should be analyzed since HAP1 cells manifested variable values of protein abundances among different clones of the same genotype. PBK knockout mice indicate that other kinases, which display pleiotropic functions, might have replaced PBK functions, thus replacing PBK's function on the cellular level.

8- Abbreviations

Abbreviation	Definition
ABC	ammonium bicarbonate
AC	alternating current
ADNP	activity-dependent neuroprotector homeobox protein
ANAPC1	anaphase-promoting complex subunit 1
APC/C	anaphase-promoting complex/cyclosome
ATP	adenosine triphosphate
AURKA/B	Aurora kinase A/B
BAD	Bcl2-associated agonist of cell death
BCL2L1	Bcl-2-like protein 1
BSA	bovine serum albumin
CDK1	Cyclin-dependent kinase 1
CEM	chain ejection model
CHFR	Checkpoint with forkhead-associated and RING finger domains
c-Jun	Jun Proto-Oncogene
c-MYC	Myc proto-oncogene protein
CRM	charge residue model
DC	direct current
DDA	dependent acquisition
DIA	data independent acquisition
DTT	dithiothreitol
DUSP1	Dual specificity protein phosphatase 1
Ensa	α-endosulfine
ERK2	Signal-related protein kinase 2 (ERK2)
ESI	electrospray ionization
FCS	fetal calf serum
FoxM1	Forkhead box protein M1
GO	Ggene ontology
Gwl	Greatwall kinase
hDlg	drosophila Discs-large tumor suppressor protein
HDMSE	data independent acquisition using ion mobility separation
HMGN2	non-histone chromosomal protein HMG-17
IAA	Iodoacetamide
IEM	ion emission model
IMAC	immobilized metal affinity chromatography
IMDM	Iscove's Modified Dulbecco's Medium
IMS	Ion mobility separation
IκBα	Nuclear factor of kappa light polypeptide gene enhancer in B-cells inhibitor, alpha
JNK	C-Jun N-Terminal Kinase
LC	liquid chromatography unite

LGN/GPSM2	Leu-Gly-Asn repeat-enriched protein/G Protein Signaling Modulator 2
m/z	mass-to-charge ratio
MAPK	mitogen-activated protein kinase
MAPKK	Mitogen-activated protein kinase kinase
MARCS	myristoylated alanine-rich C-kinase substrate
MOAC	metal oxide affinity chromatography
MYT1	myelin transcription factor 1
NUMA1	Nuclear mitotic apparatus protein 1
OA	okadaic acid
PBK	PDZ-binding kinase
PGRMC1	membrane-associated progesterone receptor component 1
Plk1	Serine/threonine-protein kinase PLK1
PP1	protein phosphatase 1
PP2A	protein phosphatase 2A
PRPK/TP53RK	p53-related protein kinase/ TP53 Regulating Kinase
PRX	Periaxin
PTEN	Phosphatase and tensin homologue deleted on chromosome ten
PTM	post-translational modifications
RF	radio frequency
SDC	Sodium deoxycholate
SDS-PAGE	sodium dodecyl sulfate polyacrylamide gel electrophoresis
SRIG	stacked rings ion guide
TMA	tissue microarrays
TOF	time of flight analyzer
TOPK	T-lymphokine-activated killer cell-originated protein kinase
VCP/p97	Valosin Containing Protein
Wee1	wee1-like protein kinase

9- References

Abe, Y., Matsumoto, S., Kito, K., Ueda, N., 2000. Cloning and expression of a novel MAPKK-like protein kinase, lymphokine-activated killer T-cell-originated protein kinase, specifically expressed in the testis and activated lymphoid cells. J. Biol. Chem. 275, 21525–21531. https://doi.org/10.1074/jbc.M909629199

Andersson, L., Porath, J., 1986. Isolation of phosphoproteins by immobilized metal (Fe3+) affinity chromatography. Analytical Biochemistry 154, 250–254. https://doi.org/10.1016/0003-2697(86)90523-3

Ayllón and O'Connor - 2007 - PBKTOPK promotes tumour cell proliferation throug.pdf, n.d.

Booher, R.N., Holman, P.S., Fattaey, A., 1997. Human Myt1 is a cell cycle-regulated kinase that inhibits Cdc2 but not Cdk2 activity. J. Biol. Chem. 272, 22300–22306. https://doi.org/10.1074/jbc.272.35.22300

Brown, N.R., Korolchuk, S., Martin, M.P., Stanley, W.A., Moukhametzianov, R., Noble, M.E.M., Endicott, J.A., 2015. CDK1 structures reveal conserved and unique features of the essential cell cycle CDK. Nat Commun 6. https://doi.org/10.1038/ncomms7769

Brudvig, J.J., Weimer, J.M., 2015. X MARCKS the spot: myristoylated alanine-rich C kinase substrate in neuronal function and disease. Front. Cell. Neurosci. 9. https://doi.org/10.3389/fncel.2015.00407

Bruno, M., Mahgoub, M., Macfarlan, T.S., 2019. The Arms Race Between KRAB–Zinc Finger Proteins and Endogenous Retroelements and Its Impact on Mammals. Annu. Rev. Genet. 53, 393–416. https://doi.org/10.1146/annurev-genet-112618-043717

Butler, T.A.J., Paul, J.W., Chan, E.-C., Smith, R., Tolosa, J.M., 2019. Misleading Westerns: Common Quantification Mistakes in Western Blot Densitometry and Proposed Corrective Measures [WWW Document]. BioMed Research International. https://doi.org/10.1155/2019/5214821

Cembella, A.D., 1989. Occurrence of okadaic acid, a major diarrheic shellfish toxin, in natural populations ofDinophysis spp. from the eastern coast of North America. J Appl Phycol 1, 307. https://doi.org/10.1007/BF00003466

Cesaro, L., Pinna, L.A., 2015. The generation of phosphoserine stretches in phosphoproteins: mechanism and significance. Mol. BioSyst. 11, 2666–2679. https://doi.org/10.1039/C5MB00337G

Chen, J.-G., Horwitz, S.B., 2002. Differential Mitotic Responses to Microtubule-stabilizing and -destabilizing Drugs 5.

Chen, J.-H., Liang, Y.-X., He, H.-C., Chen, J.-Y., Lu, J.-M., Chen, G., Lin, Z.-Y., Fu, X., Ling, X.-H., Han, Z.-D., Jiang, F.-N., Zhong, W.-D., 2015. Overexpression of PDZ-binding kinase confers malignant phenotype in prostate cancer via the regulation of E2F1. International Journal of Biological Macromolecules 81, 615–623. https://doi.org/10.1016/j.ijbiomac.2015.08.048

Compton, D.A., Luo, C., n.d. Mutation of the predicted p34cdc2 phosphorylation sites in NuMA impair the assembly of the mitotic spindle and block mitosis 14.

Debaize, L., Troadec, M.-B., 2019. The master regulator FUBP1: its emerging role in normal cell function and malignant development. Cell. Mol. Life Sci. 76, 259–281. https://doi.org/10.1007/s00018-018-2933-6

Dephoure, N., Zhou, C., Villen, J., Beausoleil, S.A., Bakalarski, C.E., Elledge, S.J., Gygi, S.P., 2008. A quantitative atlas of mitotic phosphorylation. Proceedings of the National Academy of Sciences 105, 10762–10767. https://doi.org/10.1073/pnas.0805139105

Dickey, R.W., Bobzin, S.C., Faulkner, D.J., Bencsath, F.A., Andrzejewski, D., 1990. Identification of okadaic acid from a Caribbean dinoflagellate, Prorocentrum concavum. Toxicon 28, 371–377. https://doi.org/10.1016/0041-0101(90)90074-H

Differential Mitotic Responses to Microtubule-stabilizing and -destabilizing Drugs | Cancer Research [WWW Document], n.d. URL https://cancerres.aacrjournals.org/content/62/7/1935.short (accessed 1.13.21).

Dohadwala, M., da Cruz e Silva, E.F., Hall, F.L., Williams, R.T., Carbonaro-Hall, D.A., Nairn, A.C., Greengard, P., Berndt, N., 1994. Phosphorylation and inactivation of protein phosphatase 1 by cyclin-dependent kinases. Proc. Natl. Acad. Sci. U.S.A. 91, 6408–6412. https://doi.org/10.1073/pnas.91.14.6408

Dong, C., Tang, X., Xie, Y., Zou, Q., Yang, X., Zhou, H., 2016. The crystal structure of an inactive dimer of PDZ-binding kinase. Biochemical and Biophysical Research Communications 476, 586–593. https://doi.org/10.1016/j.bbrc.2016.05.166

Dovat, S., 2002. A common mechanism for mitotic inactivation of C2H2 zinc finger DNA-binding domains. Genes & Development 16, 2985–2990. https://doi.org/10.1101/gad.1040502

Draetta, G., 1993. cdc2 activation: the interplay of cyclin binding and Thr161 phosphorylation. Trends in Cell Biology 3, 287–289. https://doi.org/10.1016/0962-8924(93)90001-H

El Amri, M., Fitzgerald, U., Schlosser, G., 2018. MARCKS and MARCKS-like proteins in development and regeneration. J Biomed Sci 25, 43. https://doi.org/10.1186/s12929-018-0445-1

Essletzbichler, P., Konopka, T., Santoro, F., Chen, D., Gapp, B.V., Kralovics, R., Brummelkamp, T.R., Nijman, S.M.B., Bürckstümmer, T., 2014. Megabase-scale deletion using CRISPR/Cas9 to generate a fully haploid human cell line. Genome Res. 24, 2059–2065. https://doi.org/10.1101/gr.177220.114

Fenaille, F., Barbier Saint-Hilaire, P., Rousseau, K., Junot, C., 2017. Data acquisition workflows in liquid chromatography coupled to high resolution mass spectrometry-based metabolomics: Where do we stand? Journal of Chromatography A 1526, 1–12. https://doi.org/10.1016/j.chroma.2017.10.043

Fujibuchi, T., Abe, Y., Takeuchi, T., Ueda, N., Shigemoto, K., Yamamoto, H., Kito, K., 2005. Expression and phosphorylation of TOPK during spermatogenesis. Dev Growth Differ 47, 637–644. https://doi.org/10.1111/j.1440-169X.2005.00834.x

Fukukawa, C., Ueda, K., Nishidate, T., Katagiri, T., Nakamura, Y., 2010. Critical roles of LGN/GPSM2 phosphorylation by PBK/TOPK in cell division of breast cancer cells. Genes Chromosom. Cancer 49, 861–872. https://doi.org/10.1002/gcc.20795

Fulda, S., Mikkat, S., Huang, F., Huckauf, J., Marin, K., Norling, B., Hagemann, M., 2006. Proteome analysis of salt stress response in the cyanobacterium Synechocystis sp. strain PCC 6803. PROTEOMICS 6, 2733–2745. https://doi.org/10.1002/pmic.200500538

García-Gutiérrez, L., Delgado, M.D., León, J., 2019. MYC Oncogene Contributions to Release of Cell Cycle Brakes. Genes (Basel) 10. https://doi.org/10.3390/genes10030244

Gerhards, N.M., Blomen, V.A., Mutlu, M., Nieuwenhuis, J., Howald, D., Guyader, C., Jonkers, J., Brummelkamp, T.R., Rottenberg, S., 2018. Haploid genetic screens identify genetic vulnerabilities to microtubule-targeting agents. Molecular Oncology 12, 953–971. https://doi.org/10.1002/1878-0261.12307

Giles, K., Pringle, S.D., Worthington, K.R., Little, D., Wildgoose, J.L., Bateman, R.H., 2004. Applications of a travelling wave-based radio-frequency-only stacked ring ion guide. Rapid Communications in Mass Spectrometry 18, 2401–2414. https://doi.org/10.1002/rcm.1641

Giles, K., Williams, J.P., Campuzano, I., 2011. Enhancements in travelling wave ion mobility resolution: Enhancements in travelling wave ion mobility resolution. Rapid Commun. Mass Spectrom. 25, 1559–1566. https://doi.org/10.1002/rcm.5013

Goto, H., Tomono, Y., Ajiro, K., Kosako, H., Fujita, M., Sakurai, M., Okawa, K., Iwamatsu, A., Okigaki, T., Takahashi, T., Inagaki, M., 1999. Identification of a Novel Phosphorylation Site on Histone H3 Coupled with Mitotic Chromosome Condensation. J. Biol. Chem. 274, 25543–25549. https://doi.org/10.1074/jbc.274.36.25543

Goto, H., Yasui, Y., Nigg, E.A., Inagaki, M., 2002. Aurora-B phosphorylates Histone H3 at serine28 with regard to the mitotic chromosome condensation. Genes to Cells 7, 11–17. https://doi.org/10.1046/j.1356-9597.2001.00498.x

Gould, K.L., Nurse, P., 1989. Tyrosine phosphorylation of the fission yeast cdc2 + protein kinase regulates entry into mitosis. Nature 342, 39–45. https://doi.org/10.1038/342039a0

Gowdy, P.M., Anderson, H.J., Roberge, M., 1998. Entry into mitosis without Cdc2 kinase activation. Journal of Cell Science 111, 3401–3410.

Gozes, I., 2018. ADNP Regulates Cognition: A Multitasking Protein. Front Neurosci 12. https://doi.org/10.3389/fnins.2018.00873

Graves, P.R., Thoma, S., Iii, B., Wu, Z., Stephenson, M.T., n.d. Serine 216 and Promotes 14-3-3 Protein Binding. Cell Growth 12.

Gray, K.A., Seal, R.L., Tweedie, S., Wright, M.W., Bruford, E.A., 2016. A review of the new HGNC gene family resource. Hum Genomics 10. https://doi.org/10.1186/s40246-016-0062-6

Haag, A.M., 2016. Mass Analyzers and Mass Spectrometers, in: Mirzaei, H., Carrasco, M. (Eds.), Modern Proteomics – Sample Preparation, Analysis and Practical Applications, Advances in Experimental Medicine and Biology. Springer International Publishing, Cham, pp. 157–169. https://doi.org/10.1007/978-3-319-41448-5_7

Han, Z., Li, L., Huang, Y., Zhao, H., Luo, Y., 2021. PBK/TOPK: A Therapeutic Target Worthy of Attention. Cells 10. https://doi.org/10.3390/cells10020371

He, F., Yan, Q., Fan, L., Liu, Y., Cui, J., Wang, J., Wang, L., Wang, Y., Wang, Z., Guo, Y., Huang, G., 2010. PBK/TOPK in the differential diagnosis of cholangiocarcinoma from hepatocellular carcinoma and its involvement in prognosis of human cholangiocarcinoma. Human Pathology 41, 415–424. https://doi.org/10.1016/j.humpath.2009.05.016

Hengeveld, R.C.C., Hertz, N.T., Vromans, M.J.M., Zhang, C., Burlingame, A.L., Shokat, K.M., Lens, S.M.A., n.d. Development of a Chemical Genetic Approach for Human Aurora B Kinase Identifies Novel Substrates of the Chromosomal Passenger Complex*□S 13.

Herbert, K.J., Ashton, T.M., Prevo, R., Pirovano, G., Higgins, G.S., 2018. T-LAK cell-originated protein kinase (TOPK): an emerging target for cancer-specific therapeutics. Cell Death Dis 9, 1089. https://doi.org/10.1038/s41419-018-1131-7

Hershko, A., 1999. Mechanisms and regulation of the degradation of cyclin B. Philos. Trans. R. Soc. Lond., B, Biol. Sci. 354, 1571–1575; discussion 1575-1576. https://doi.org/10.1098/rstb.1999.0500

Ho, C., Lam, C., Chan, M., Cheung, R., Law, L., Lit, L., Ng, K., Suen, M., Tai, H., n.d. Electrospray Ionisation Mass Spectrometry: Principles and Clinical Applications 10.

Hoaglund-Hyzer, C.S., Li, J., Clemmer, D.E., 2000. Mobility Labeling for Parallel CID of Ion Mixtures. Anal. Chem. 72, 2737–2740. https://doi.org/10.1021/ac0000170

Hoang, V.T., Verma, D., Godavarthy, P.S., Llavona, P., Steiner, M., Gerlach, K., Michels, B.E., Bohnenberger, H., Wachter, A., Oellerich, T., Müller-Kuller, U., Weissenberger, E., Voutsinas, J.M., Oehler, V.G., Farin, H.F., Zörnig, M., Krause, D.S., 2019. The transcriptional regulator FUBP1 influences disease outcome in murine and human myeloid leukemia. Leukemia 33, 1700–1712. https://doi.org/10.1038/s41375-018-0358-8

Hogan, C.J., Carroll, J.A., Rohrs, H.W., Biswas, P., Gross, M.L., 2009. Combined charged residue-field emission model of macromolecular electrospray ionization. Anal. Chem. 81, 369–377. https://doi.org/10.1021/ac8016532

Holder, J., Poser, E., Barr, F.A., 2019. Getting out of mitosis: spatial and temporal control of mitotic exit and cytokinesis by PP 1 and PP 2A. FEBS Lett 593, 2908–2924. https://doi.org/10.1002/1873-3468.13595

Hornbeck, P.V., Kornhauser, J.M., Tkachev, S., Zhang, B., Skrzypek, E., Murray, B., Latham, V., Sullivan, M., 2012. PhosphoSitePlus: a comprehensive resource for investigating the structure

and function of experimentally determined post-translational modifications in man and mouse. Nucleic Acids Research 40, D261–D270. https://doi.org/10.1093/nar/gkr1122

Hunter, T., n.d. Isolation of a Human Cyclin cDNA: Evidence for Cyclin mRNA and Protein Regulation in the Cell Cycle and for Interaction with ~34~~~ 14.

IAPs: from caspase inhibitors to modulators of NF-κB, inflammation and cancer | Nature Reviews Cancer [WWW Document], n.d. URL https://www.nature.com/articles/nrc2889 (accessed 8.21.20).

Ishidate, T., Matsumine, A., Toyoshima, K., Akiyama, T., 2000. The APC-hDLG complex negatively regulates cell cycle progression from the G0/G1 to S phase. Oncogene 19, 365–372. https://doi.org/10.1038/sj.onc.1203309

Ishikawa, C., Senba, M., Mori, N., 2018. Mitotic kinase PBK/TOPK as a therapeutic target for adult T-cell leukemia/lymphoma. Int. J. Oncol. 53, 801–814. https://doi.org/10.3892/ijo.2018.4427

Jantz, D., Berg, J.M., 2004. Reduction in DNA-binding affinity of Cys2His2 zinc finger proteins by linker phosphorylation. Proc Natl Acad Sci U S A 101, 7589–7593. https://doi.org/10.1073/pnas.0402191101

Jensen, S.S., Larsen, M.R., 2007. Evaluation of the impact of some experimental procedures on different phosphopeptide enrichment techniques. Rapid Commun. Mass Spectrom. 21, 3635–3645. https://doi.org/10.1002/rcm.3254

Jurneczko, E., Barran, P.E., 2011. How useful is ion mobility mass spectrometry for structural biology? The relationship between protein crystal structures and their collision cross sections in the gas phase. Analyst 136, 20–28. https://doi.org/10.1039/c0an00373e

Karagoz, K., Mehta, G.A., Khella, C.A., Khanna, P., Gatza, M.L., 2019. Integrative proteogenomic analyses of human tumours identifies ADNP as a novel oncogenic mediator of cell cycle progression in high-grade serous ovarian cancer with poor prognosis. EBioMedicine 50, 191–202. https://doi.org/10.1016/j.ebiom.2019.11.009

Kiyono, T., Hiraiwa, A., Fujita, M., Hayashi, Y., Akiyama, T., Ishibashi, M., 1997. Binding of high-risk human papillomavirus E6 oncoproteins to the human homologue of the Drosophila discs large tumor suppressor protein. Proceedings of the National Academy of Sciences 94, 11612–11616. https://doi.org/10.1073/pnas.94.21.11612

Konermann, L., Ahadi, E., Rodriguez, A.D., Vahidi, S., 2013. Unraveling the Mechanism of Electrospray Ionization. Anal. Chem. 85, 2–9. https://doi.org/10.1021/ac302789c

Kraft, C., 2003. Mitotic regulation of the human anaphase-promoting complex by phosphorylation. The EMBO Journal 22, 6598–6609. https://doi.org/10.1093/emboj/cdg627

Kurylo, I., Hamdi, A., Addad, A., Boukherroub, R., Coffinier, Y., 2017. Comparison of Ti-Based Coatings on Silicon Nanowires for Phosphopeptide Enrichment and Their Laser Assisted Desorption/Ionization Mass Spectrometry Detection. Nanomaterials 7, 272. https://doi.org/10.3390/nano7090272

Kyhse-Andersen, J., 1984. Electroblotting of multiple gels: a simple apparatus without buffer tank for rapid transfer of proteins from polyacrylamide to nitrocellulose. J. Biochem. Biophys. Methods 10, 203–209. https://doi.org/10.1016/0165-022x(84)90040-x

Lei, B., Qi, W., Zhao, Y., Li, Y., Liu, S., Xu, X., Zhi, C., Wan, L., Shen, H., 2015. PBK/TOPK expression correlates with mutant p53 and affects patients' prognosis and cell proliferation and viability in lung adenocarcinoma. Human Pathology 46, 217–224. https://doi.org/10.1016/j.humpath.2014.07.026

Levy, E.D., Michnick, S.W., Landry, C.R., 2012. Protein abundance is key to distinguish promiscuous from functional phosphorylation based on evolutionary information. Phil. Trans. R. Soc. B 367, 2594–2606. https://doi.org/10.1098/rstb.2012.0078

Li, G.-Z., Vissers, J.P.C., Silva, J.C., Golick, D., Gorenstein, M.V., Geromanos, S.J., 2009. Database searching and accounting of multiplexed precursor and product ion spectra from the data independent analysis of simple and complex peptide mixtures. PROTEOMICS 9, 1696–1719. https://doi.org/10.1002/pmic.200800564

Li, S., Zhu, F., Zykova, T., Kim, M.O., Cho, Y.Y., Bode, A.M., Peng, C., Ma, W., Carper, A., Langfald, A., Dong, Z., 2011. T-LAK cell-originated protein kinase (TOPK) phosphorylation of MKP1 protein prevents solar ultraviolet light-induced inflammation through inhibition of the p38 protein signaling pathway. J. Biol. Chem. 286, 29601–29609. https://doi.org/10.1074/jbc.M111.225813

Li, Y., Yang, Z., Li, W., Xu, S., Wang, Tao, Wang, Ting, Niu, M., Zhang, S., Jia, L., Li, S., 2016. TOPK promotes lung cancer resistance to EGFR tyrosine kinase inhibitors by phosphorylating and activating c-Jun. Oncotarget 7, 6748–6764. https://doi.org/10.18632/oncotarget.6826

Limbutara, K., Kelleher, A., Yang, C.-R., Raghuram, V., Knepper, M.A., 2019. Phosphorylation Changes in Response to Kinase Inhibitor H89 in PKA-Null Cells. Scientific Reports 9, 2814. https://doi.org/10.1038/s41598-019-39116-2

Lu, H., Xiao, J., Ke, C., Ni, X., Xiu, R., Tian, Q., Pan, H., Zou, L., Wang, F., Ma, T., Ji, X., Yuan, P., Liu, L., Zhang, J., Jia, W., Duan, Q., Zhu, F., 2019. TOPK inhibits autophagy by phosphorylating ULK1 and promotes glioma resistance to TMZ. Cell Death Dis 10, 583. https://doi.org/10.1038/s41419-019-1805-9

Luo, Q., Lei, B., Liu, S., Chen, Y., Sheng, W., Lin, P., Li, W., Shen, H., n.d. Expression of PBK/TOPK in cervical cancer and cervical intraepithelial neoplasia 6.

Manning, G., Plowman, G.D., Hunter, T., Sudarsanam, S., 2002. Evolution of protein kinase signaling from yeast to man. Trends Biochem. Sci. 27, 514–520. https://doi.org/10.1016/s0968-0004(02)02179-5

Masuda, T., Tomita, M., Ishihama, Y., 2008. Phase Transfer Surfactant-Aided Trypsin Digestion for Membrane Proteome Analysis. J. Proteome Res. 7, 731–740. https://doi.org/10.1021/pr700658q

Matafora, V., Corno, A., Ciliberto, A., Bachi, A., 2017. Missing Value Monitoring Enhances the Robustness in Proteomics Quantitation. J. Proteome Res. 16, 1719–1727. https://doi.org/10.1021/acs.jproteome.6b01056

Matsumoto, S., Abe, Y., Fujibuchi, T., Takeuchi, T., Kito, K., Ueda, N., Shigemoto, K., Gyo, K., 2004. Characterization of a MAPKK-like protein kinase TOPK. Biochemical and Biophysical Research Communications 325, 997–1004. https://doi.org/10.1016/j.bbrc.2004.10.133

Meraldi, P., Nigg, E.A., 2001. Centrosome cohesion is regulated by a balance of kinase and phosphatase activities. Journal of Cell Science 114, 3749–3757.

Miller, C.J., Turk, B.E., 2018. Homing in: Mechanisms of Substrate Targeting by Protein Kinases. Trends Biochem. Sci. 43, 380–394. https://doi.org/10.1016/j.tibs.2018.02.009

Neubauer, H., Clare, S.E., Wozny, W., Schwall, G.P., Poznanović, S., Stegmann, W., Vogel, U., Sotlar, K., Wallwiener, D., Kurek, R., Fehm, T., Cahill, M.A., 2008. Breast cancer proteomics reveals correlation between estrogen receptor status and differential phosphorylation of PGRMC1. Breast Cancer Research 10, R85. https://doi.org/10.1186/bcr2155

Oh, S.-M., Zhu, F., Cho, Y.-Y., Lee, K.W., Kang, B.S., Kim, H.-G., Zykova, T., Bode, A.M., Dong, Z., 2007. T-lymphokine-activated killer cell-originated protein kinase functions as a positive regulator of c-Jun-NH2-kinase 1 signaling and H-Ras-induced cell transformation. Cancer Res. 67, 5186–5194. https://doi.org/10.1158/0008-5472.CAN-06-4506

Oh, Y.M., Kwon, Y.E., Kim, J.M., Bae, S.J., Lee, B.K., Yoo, S.J., Chung, C.H., Deshaies, R.J., Seol, J.H., 2009. Chfr is linked to tumour metastasis through the downregulation of HDAC1. Nat Cell Biol 11, 295–302. https://doi.org/10.1038/ncb1837

Okumura, E., Morita, A., Wakai, M., Mochida, S., Hara, M., Kishimoto, T., 2014. Cyclin B-Cdk1 inhibits protein phosphatase PP2A-B55 via a Greatwall kinase-independent mechanism. J. Cell Biol. 204, 881–889. https://doi.org/10.1083/jcb.201307160

Olbrich, T., Mayor-Ruiz, C., Vega-Sendino, M., Gomez, C., Ortega, S., Ruiz, S., Fernandez-Capetillo, O., 2017. A p53-dependent response limits the viability of mammalian haploid cells. PNAS. https://doi.org/10.1073/pnas.1705133114

Olsen, J.V., Mann, M., 2013. Status of Large-scale Analysis of Post-translational Modifications by Mass Spectrometry. Mol Cell Proteomics 12, 3444–3452. https://doi.org/10.1074/mcp.O113.034181

O'Shea, J.P., Chou, M.F., Quader, S.A., Ryan, J.K., Church, G.M., Schwartz, D., 2013. pLogo: a probabilistic approach to visualizing sequence motifs. Nat Methods 10, 1211–1212. https://doi.org/10.1038/nmeth.2646

Park, J.-H., Lin, M.-L., Nishidate, T., Nakamura, Y., Katagiri, T., 2006. PDZ-binding kinase/T-LAK cell-originated protein kinase, a putative cancer/testis antigen with an oncogenic activity in breast cancer. Cancer Res. 66, 9186–9195. https://doi.org/10.1158/0008-5472.CAN-06-1601

Park, J.-H., Nishidate, T., Nakamura, Y., Katagiri, T., 2010. Critical roles of T-LAK cell-originated protein kinase in cytokinesis. Cancer Science 101, 403–411. https://doi.org/10.1111/j.1349-7006.2009.01400.x

Park, J.-H., Yoon, D.-S., Choi, H.-J., Hahm, D.-H., Oh, S.-M., 2013. Phosphorylation of IκBα at serine 32 by T-lymphokine-activated killer cell-originated protein kinase is essential for chemoresistance against doxorubicin in cervical cancer cells. J. Biol. Chem. 288, 3585–3593. https://doi.org/10.1074/jbc.M112.422170

Parker, L.L., Atherton-Fessler, S., Piwnica-Worms, H., 1992. p107wee1 is a dual-specificity kinase that phosphorylates p34cdc2 on tyrosine 15. Proc. Natl. Acad. Sci. U.S.A. 89, 2917–2921. https://doi.org/10.1073/pnas.89.7.2917

Pathan, M., Keerthikumar, S., Ang, C.-S., Gangoda, L., Quek, C.Y.J., Williamson, N.A., Mouradov, D., Sieber, O.M., Simpson, R.J., Salim, A., Bacic, A., Hill, A.F., Stroud, D.A., Ryan, M.T., Agbinya, J.I., Mariadason, J.M., Burgess, A.W., Mathivanan, S., 2015. FunRich: An open access standalone functional enrichment and interaction network analysis tool. Proteomics 15, 2597–2601. https://doi.org/10.1002/pmic.201400515

Pearlman, S.M., Serber, Z., Ferrell, J.E., 2011. A Mechanism for the Evolution of Phosphorylation Sites. Cell 147, 934–946. https://doi.org/10.1016/j.cell.2011.08.052

Pirovano, G., Ashton, T.M., Herbert, K.J., Bryant, R.J., Verrill, C.L., Cerundolo, L., Buffa, F.M., Prevo, R., Harrap, I., Ryan, A.J., Macaulay, V., McKenna, W.G., Higgins, G.S., 2017. TOPK modulates tumour-specific radiosensitivity and correlates with recurrence after prostate radiotherapy. Br J Cancer 117, 503–512. https://doi.org/10.1038/bjc.2017.197

Pringle, S.D., Giles, K., Wildgoose, J.L., Williams, J.P., Slade, S.E., Thalassinos, K., Bateman, R.H., Bowers, M.T., Scrivens, J.H., 2007. An investigation of the mobility separation of some peptide and protein ions using a new hybrid quadrupole/travelling wave IMS/oa-ToF instrument. International Journal of Mass Spectrometry 261, 1–12. https://doi.org/10.1016/j.ijms.2006.07.021

Rappsilber, J., Mann, M., Ishihama, Y., 2007. Protocol for micro-purification, enrichment, pre-fractionation and storage of peptides for proteomics using StageTips. Nat Protoc 2, 1896–1906. https://doi.org/10.1038/nprot.2007.261

Riley, N.M., Coon, J.J., 2016. Phosphoproteomics in the Age of Rapid and Deep Proteome Profiling. Anal Chem 88, 74–94. https://doi.org/10.1021/acs.analchem.5b04123

Rizkallah, R., Alexander, K.E., Hurt, M.M., 2011. Global mitotic phosphorylation of C2H2 zinc finger protein linker peptides. Cell Cycle 10, 3327–3336. https://doi.org/10.4161/cc.10.19.17619

Rizkallah, R., Batsomboon, P., Dudley, G.B., Hurt, M.M., 2015. Identification of the oncogenic kinase TOPK/PBK as a master mitotic regulator of C2H2 zinc finger proteins. Oncotarget 6, 1446–1461. https://doi.org/10.18632/oncotarget.2735

Ruotolo, B.T., Verbeck, Thomson, L.M., Woods, A.S., Gillig, K.J., Russell, D.H., 2002. Distinguishing between Phosphorylated and Nonphosphorylated Peptides with Ion Mobility−Mass Spectrometry. J. Proteome Res. 1, 303–306. https://doi.org/10.1021/pr025516r

Rusin, S.F., Adamo, M.E., Kettenbach, A.N., 2017. Identification of Candidate Casein Kinase 2 Substrates in Mitosis by Quantitative Phosphoproteomics. Front. Cell Dev. Biol. 5, 97. https://doi.org/10.3389/fcell.2017.00097

Ryu, C.S., Klein, K., Zanger, U.M., 2017. Membrane Associated Progesterone Receptors: Promiscuous Proteins with Pleiotropic Functions – Focus on Interactions with Cytochromes P450. Front. Pharmacol. 8. https://doi.org/10.3389/fphar.2017.00159

Sa, L., A, J., Lf, C., Pk, D., Y, Y., M, A., X, C., J, T., Tr, H., Mt, W., 2018. The Human Transcription Factors. Cell 172, 650–665. https://doi.org/10.1016/j.cell.2018.01.029

Sacco, F., Perfetto, L., Castagnoli, L., Cesareni, G., 2012. The human phosphatase interactome: An intricate family portrait. FEBS Lett. 586, 2732–2739. https://doi.org/10.1016/j.febslet.2012.05.008

Salaun, P., Rannou, Y., Claude, P., 2008. Cdk1, Plks, Auroras, and Neks: The Mitotic Bodyguards, in: Li, J.J., Li, S.A., Mohla, S., Rochefort, H., Maudelonde, T. (Eds.), Hormonal Carcinogenesis V, Advances in Experimental Medicine and Biology. Springer New York, New York, NY, pp. 41–56. https://doi.org/10.1007/978-0-387-69080-3_4

Sanbhnani, S., Yeong, F.M., 2012. CHFR: a key checkpoint component implicated in a wide range of cancers. Cell. Mol. Life Sci. 69, 1669–1687. https://doi.org/10.1007/s00018-011-0892-2

Sawicka, A., Seiser, C., 2012. Histone H3 phosphorylation – A versatile chromatin modification for different occasions. Biochimie, Special Section on Epigenetics 94, 2193–2201. https://doi.org/10.1016/j.biochi.2012.04.018

Sekiya, T., Murano, K., Kato, K., Kawaguchi, A., Nagata, K., 2017. Mitotic phosphorylation of CCCTC-binding factor (CTCF) reduces its DNA binding activity. FEBS Open Bio 7, 397–404. https://doi.org/10.1002/2211-5463.12189

Shinde, S.R., Gangula, N.R., Kavela, S., Pandey, V., Maddika, S., 2013. TOPK and PTEN participate in CHFR mediated mitotic checkpoint. Cell. Signal. 25, 2511–2517. https://doi.org/10.1016/j.cellsig.2013.08.013

Shliaha, P.V., Bond, N.J., Gatto, L., Lilley, K.S., 2013. Effects of Traveling Wave Ion Mobility Separation on Data Independent Acquisition in Proteomics Studies. J. Proteome Res. 12, 2323–2339. https://doi.org/10.1021/pr300775k

Simons-Evelyn, M., Bailey-Dell, K., Toretsky, J.A., Ross, D.D., Fenton, R., Kalvakolanu, D., Rapoport, A.P., 2001. PBK/TOPK Is a Novel Mitotic Kinase Which Is Upregulated in Burkitt's Lymphoma and Other Highly Proliferative Malignant Cells. Blood Cells, Molecules, and Diseases 27, 825–829. https://doi.org/10.1006/bcmd.2001.0452

Spellman, P.T., Sherlock, G., Zhang, M.Q., Iyer, V.R., Anders, K., Eisen, M.B., Brown, P.O., Botstein, D., Futcher, B., 1998. Comprehensive identification of cell cycle-regulated genes of the yeast Saccharomyces cerevisiae by microarray hybridization. Mol. Biol. Cell 9, 3273–3297. https://doi.org/10.1091/mbc.9.12.3273

Stahl, D.C., Swiderek, K.M., Davis, M.T., Lee, T.D., 1996. Data-controlled automation of liquid chromatography/tandem mass spectrometry analysis of peptide mixtures. J Am Soc Mass Spectrom 7, 532–540. https://doi.org/10.1016/1044-0305(96)00057-8

Steen, H., Jebanathirajah, J.A., Rush, J., Morrice, N., Kirschner, M.W., 2006. Phosphorylation Analysis by Mass Spectrometry: Myths, Facts, and the Consequences for Qualitative and Quantitative Measurements. Mol Cell Proteomics 5, 172–181. https://doi.org/10.1074/mcp.M500135-MCP200

Suzuki, K., Sako, K., Akiyama, K., Isoda, M., Senoo, C., Nakajo, N., Sagata, N., 2015. Identification of non-Ser/Thr-Pro consensus motifs for Cdk1 and their roles in mitotic regulation of C2H2 zinc finger proteins and Ect2. Sci Rep 5, 7929. https://doi.org/10.1038/srep07929

Swingle, M., Ni, L., Honkanen, R.E., 2007. Small-molecule inhibitors of ser/thr protein phosphatases: specificity, use and common forms of abuse. Methods Mol. Biol. 365, 23–38. https://doi.org/10.1385/1-59745-267-X:23

Tanenbaum, M.E., Stern-Ginossar, N., Weissman, J.S., Vale, R.D., 2015. Regulation of mRNA translation during mitosis. Elife 4. https://doi.org/10.7554/eLife.07957

Tape, C.J., Worboys, J.D., Sinclair, J., Gourlay, R., Vogt, J., McMahon, K.M., Trost, M., Lauffenburger, D.A., Lamont, D.J., Jørgensen, C., 2014. Reproducible Automated Phosphopeptide Enrichment Using Magnetic TiO 2 and Ti-IMAC. Anal. Chem. 86, 10296–10302. https://doi.org/10.1021/ac5025842

Thiesen, H.-J., Bach, C., 1990. Target Detection Assay (TDA): a versatile procedure to determine DNA binding sites as demonstrated on SP1 protein 7.

Vandre, D.D., Wills, V.L., 1992. Inhibition of mitosis by okadaic acid: possible involvement of a protein phosphatase 2A in the transition from metaphase to anaphase. Journal of Cell Science 101, 79–91.

Vaquerizas, J.M., Kummerfeld, S.K., Teichmann, S.A., Luscombe, N.M., 2009. A census of human transcription factors: function, expression and evolution. Nature Reviews Genetics 10, 252–263. https://doi.org/10.1038/nrg2538

Vilas, C.K., Emery, L.E., Denchi, E.L., Miller, K.M., 2018. Caught with One's Zinc Fingers in the Genome Integrity Cookie Jar. Trends in Genetics 34, 313–325. https://doi.org/10.1016/j.tig.2017.12.011

Wang, X., Kiyokawa, H., Dennewitz, M.B., Costa, R.H., 2002. The Forkhead Box m1b transcription factor is essential for hepatocyte DNA replication and mitosis during mouse liver regeneration. Proc. Natl. Acad. Sci. U.S.A. 99, 16881–16886. https://doi.org/10.1073/pnas.252570299

Williams, B.C., Filter, J.J., Blake-Hodek, K.A., Wadzinski, B.E., Fuda, N.J., Shalloway, D., Goldberg, M.L., 2014. Greatwall-phosphorylated Endosulfine is both an inhibitor and a substrate of PP2A-B55 heterotrimers. Elife 3, e01695. https://doi.org/10.7554/eLife.01695

Willibald, M., Bayer, G., Stahlhut, V., Poschmann, G., Stühler, K., Gierke, B., Pawlak, M., Seeger, H., Mueck, A.O., Niederacher, D., Fehm, T., Neubauer, H., 2017. Progesterone receptor membrane component 1 is phosphorylated upon progestin treatment in breast cancer cells. Oncotarget 8, 72480–72493. https://doi.org/10.18632/oncotarget.19819

Wilm, M., 2011. Principles of electrospray ionization. Mol. Cell Proteomics 10, M111.009407. https://doi.org/10.1074/mcp.M111.009407

Win, S., Than, T., Kaplowitz, N., 2018. The Regulation of JNK Signaling Pathways in Cell Death through the Interplay with Mitochondrial SAB and Upstream Post-Translational Effects. IJMS 19, 3657. https://doi.org/10.3390/ijms19113657

Wolfe et al. - 2000 - DNA Recognition by Cys sub2sub His sub2su.pdf, n.d.

Wolfe, S.A., Nekludova, L., Pabo, C.O., 2000. DNA Recognition by Cys 2 His 2 Zinc Finger Proteins. Annu. Rev. Biophys. Biomol. Struct. 29, 183–212. https://doi.org/10.1146/annurev.biophys.29.1.183

Wu, C.H., 2003. The Protein Information Resource. Nucleic Acids Research 31, 345–347. https://doi.org/10.1093/nar/gkg040

Wu, J.Q., Guo, J.Y., Tang, W., Yang, C.-S., Freel, C.D., Chen, C., Nairn, A.C., Kornbluth, S., 2009. PP1-mediated dephosphorylation of phosphoproteins at mitotic exit is controlled by inhibitor-1 and PP1 phosphorylation. Nat. Cell Biol. 11, 644–651. https://doi.org/10.1038/ncb1871

Xiao, J., Duan, Q., Wang, Z., Yan, W., Sun, H., Fan, X., Zeng, X., Chen, J., Shao, C., Zhu, F., n.d. Phosphorylation of TOPK at Y74, Y272 by Src increases the stability of TOPK and promotes tumorigenesis of colon cancer 12.

Xu, J., Zeng, C., Chu, W., Pan, F., Rothfuss, J.M., Zhang, F., Tu, Z., Zhou, D., Zeng, D., Vangveravong, S., Johnston, F., Spitzer, D., Chang, K.C., Hotchkiss, R.S., Hawkins, W.G., Wheeler, K.T., Mach, R.H., 2011. Identification of the PGRMC1 protein complex as the putative sigma-2 receptor binding site. Nat Commun 2, 380. https://doi.org/10.1038/ncomms1386

Yamazaki, H., Kosako, H., Yoshimura, S.H., 2020. Quantitative proteomics indicate a strong correlation of mitotic phospho-/dephosphorylation with non-structured regions of substrates. Biochimica et Biophysica Acta (BBA) - Proteins and Proteomics 1868, 140295. https://doi.org/10.1016/j.bbapap.2019.140295

Yang, Y.-F., Pan, Y.-H., Cao, Y., Fu, J., Yang, X., Zhang, M.-F., Tian, Q.-H., 2017. PDZ binding kinase, regulated by FoxM1, enhances malignant phenotype via activation of β-Catenin signaling in hepatocellular carcinoma. Oncotarget 8, 47195–47205. https://doi.org/10.18632/oncotarget.17587

Zhang, C., Zuo, T., Wang, X., Wang, H., Hu, Y., Li, Z., Li, W., Jia, L., Qian, Y., Yang, W., Yu, H., 2019. Integration of Data-Dependent Acquisition (DDA) and Data-Independent High-Definition MSE (HDMSE) for the Comprehensive Profiling and Characterization of Multicomponents from Panax japonicus by UHPLC/IM-QTOF-MS. Molecules 24. https://doi.org/10.3390/molecules24152708

Zhang, Y., Chen, L., Yang, S., Fang, D., 2012. E2F1: a potential negative regulator of hTERT transcription in normal cells upon activation of oncogenic c-Myc. Med. Sci. Monit. 18, RA12-15. https://doi.org/10.12659/msm.882192

Zhou, B., Zhang, Z.-Y., 2002. The activity of the extracellular signal-regulated kinase 2 is regulated by differential phosphorylation in the activation loop. J. Biol. Chem. 277, 13889–13899. https://doi.org/10.1074/jbc.M200377200

Zhou, H., Ye, M., Dong, J., Han, G., Jiang, X., Wu, R., Zou, H., 2008. Specific Phosphopeptide Enrichment with Immobilized Titanium Ion Affinity Chromatography Adsorbent for Phosphoproteome Analysis. J. Proteome Res. 7, 3957–3967. https://doi.org/10.1021/pr800223m

Zhou, X.M., Liu, Y., Payne, G., Lutz, R.J., Chittenden, T., 2000. Growth factors inactivate the cell death promoter BAD by phosphorylation of its BH3 domain on Ser155. J. Biol. Chem. 275, 25046–25051. https://doi.org/10.1074/jbc.M002526200

Zhu, F., Zykova, T.A., Kang, B.S., Wang, Z., Ebeling, M.C., Abe, Y., Ma, W.-Y., Bode, A.M., Dong, Z., 2007. Bidirectional signals transduced by TOPK-ERK interaction increase tumorigenesis of HCT116 colorectal cancer cells. Gastroenterology 133, 219–231. https://doi.org/10.1053/j.gastro.2007.04.048

Zlobec, I., Molinari, F., Kovac, M., Bihl, M.P., Altermatt, H.J., Diebold, J., Frick, H., Germer, M., Horcic, M., Montani, M., Singer, G., Yurtsever, H., Zettl, A., Terracciano, L., Mazzucchelli, L., Saletti, P., Frattini, M., Heinimann, K., Lugli, A., 2010. Prognostic and predictive value of TOPK stratified by KRAS and BRAF gene alterations in sporadic, hereditary and metastatic colorectal cancer patients. Br J Cancer 102, 151–161. https://doi.org/10.1038/sj.bjc.6605452

Zykova, T., Zhu, F., Wang, L., Li, H., Lim, D.Y., Yao, K., Roh, E., Yoon, S.-P., Kim, H.-G., Bae, K.B., Wen, W., Shin, S.H., Nadas, J., Li, Y., Ma, W., Bode, A.M., Dong, Z., 2018. Targeting PRPK Function Blocks Colon Cancer Metastasis. Mol Cancer Ther 17, 1101–1113. https://doi.org/10.1158/1535-7163.MCT-17-0628

Zykova, T.A., Zhu, F., Lu, C., Higgins, L., Tatsumi, Y., Abe, Y., Bode, A.M., Dong, Z., 2006. Lymphokine-activated killer T-cell-originated protein kinase phosphorylation of histone H2AX prevents arsenite-induced apoptosis in RPMI7951 melanoma cells. Clin. Cancer Res. 12, 6884–6893. https://doi.org/10.1158/1078-0432.CCR-06-0410

Zykova, T.A., Zhu, F., Vakorina, T.I., Zhang, J., Higgins, L.A., Urusova, D.V., Bode, A.M., Dong, Z., 2010. T-LAK Cell-originated Protein Kinase (TOPK) Phosphorylation of Prx1 at Ser-

32 Prevents UVB-induced Apoptosis in RPMI7951 Melanoma Cells through the Regulation of Prx1 Peroxidase Activity. J. Biol. Chem. 285, 29138–29146. https://doi.org/10.1074/jbc.M110.135905

10- Supplements

Supplement S1A: Quantitative Western blot analysis of the phosphorylated p38

	bands' intensity_first replication	bands' intensity_second replication	bands' intensity_third replication	mean	Standard deviation
WT.1	435	255	323	337.6667	90.89188
WT.1+OA	7530	7090	5170	6596.667	1254.963
KO.1	223	290	71.1	194.7	112.1605
KO.1+OA	8230	6960	7910	7700	660.5301

Supplement S1B: unpaired two-tailed T-test of repression factors of bands' intensities

p-value	WT.1	WT.1+OA	KO.1	KO.1+OA
WT.1		0.012791	0.164506	0.002289
WT.1+OA	0.012791		0.012059	0.26974
KO.1	0.164506	0.012059		0.00203
KO.1+OA	0.002289	0.26974	0.00203	

S1A and S1B relate to Fig. 18 on page 57

Supplement S2A: Quantitative Western blot analysis of the phosphorylated TGEKP

	bands' intensity_first replication	bands' intensity_second replication	bands' intensity_third replication	mean	Standard deviation
WT.1	1970	1070	561	1200.333	713.4846
WT.1+OA	18000	30600	22200	23600	6415.606
KO.1	267	438	244	316.3333	105.9921
KO.1+OA	466	523	128	372.3333	213.5096

Supplement S2B: unpaired two-tailed T-test of repression factors of bands' intensities

p-value	WT	WT+OA	KO	KO+OA
WT		0.025081	0.162377	0.174443
WT+OA	0.025081		0.02436	0.024393
KO	0.162377	0.02436		0.711976
KO+OA	0.174443	0.024393	0.711976	

S2A and S2B relate to Fig. 18 on page 57

Supplement S3A: Quantitative analysis of Annexin in proteomic data

	WT.1	WT.1+OA	KO.1	KO.1+OA
Abundance_first replication	19.69257	29.82382	9.449411	5.155222
Abundance_second replication	17.7586	20.08069	7.943781	8.187765
Abundance_third replication		19.48165	9.327794	7.92707

Supplement S3B: unpaired two-tailed T-test of repression factors of the abundancies

p-value	WT.1	WT.1+OA	KO.1	KO.1+OA
WT.1		0.319	0.026	0.005
WT.1+OA	0.319		0.184	0.157
KO.1	0.026	0.184		0.194
KO.1+OA	0.005	0.157	0.194	

Supplement 4A: Quantitative analysis of G6PD in proteomic data

	WT.1	WT.1+OA	KO.1	KO.1+OA
Abundance_first replication	4.786588	4.848468	9.060687	9.683864
Abundance_second replication	4.09749	4.704566	9.173096	9.446361
Abundance_third replication		4.919635	9.424504	8.811213

Supplement 4B: unpaired two-tailed T-test of repression factors of the abundancies

p-value	WT.1	WT.1+OA	KO.1	KO.1+OA
WT.1		0.463	0.03	0.006
WT.1+OA	0.463		<0.001	0.001
KO.1	0.03	<0.001		0.762
KO.1+OA	0.006	0.001	0.762	

Supplement 5A: Quantitative analysis of Emerin in proteomic data

	WT.1	WT.1+OA	KO.1	KO.1+OA
Abundance_first replication	6.471736	6.61968	14.52191	10.11614
Abundance_second replication	6.167542	5.570053	12.20927	10.30265
Abundance_third replication		5.731552	13.23182	9.83261

Supplement 5B: unpaired two-tailed T-test of repression factors of the abundancies

p-value	WT.1	WT.1+OA	KO.1	KO.1+OA
WT.1		0.414	0.006	0.001
WT.1+OA	0.414		0.003	0.067
KO.1	0.006	0.003		0.035
KO.1+OA	0.001	0.067	0.035	

S3A, S3B, S4A, S4B, S5A, and S5B relate to Fig. 21 on page 62

Supplement 6A: Quantitative Western blot analysis of Annexin

	bands' intensity_first replication	bands' intensity_second replication	bands' intensity_third replication	mean	Standard deviation
WT.1	817	924	939	893.333333	66.5306947
WT.2	495	393	710	532.666667	161.821919
WT.1+OA	1010	1030	1240	1093.33333	127.410099
WT.2+OA	598	533	803	644.666667	140.919599
KO.1	388	333	485	402	76.9610291
KO.2	282	235	331	282.666667	48.0034721
KO.1+OA	527	301	624	484	165.737745
KO.2+OA	336	229	381	315.333333	78.0790198

Supplement 6B: unpaired two-tailed T-test of repression factors of bands' intensities

p-value	WT.1	WT.2	WT.1+OA	WT.2+OA	KO.1	KO.2	KO.1+OA	KO.2+OA
WT.1		0.04555875	0.09457764	0.07409799	0.00122158	0.00036183	0.03631439	0.00069741
WT.2	0.04555875		0.010481	0.4179966	0.29971245	0.10585283	0.73435957	0.13082163
WT.1+OA	0.09457764	0.010481		0.01527643	0.00284933	0.0037723	0.00856079	0.00191314
WT.2+OA	0.07409799	0.4179966	0.01527643		0.07663312	0.03586444	0.27165398	0.03596917
KO.1	0.00122158	0.29971245	0.00284933	0.07663312		0.09777587	0.49688412	0.2427891
KO.2	0.00036183	0.10585283	0.0037723	0.03586444	0.09777587		0.16215904	0.57677167
KO.1+OA	0.03631439	0.73435957	0.00856079	0.27165398	0.49688412	0.16215904		0.21390837
KO.2+OA	0.00069741	0.13082163	0.00191314	0.03596917	0.2427891	0.57677167	0.21390837	

Supplement 7A: Quantitative Western blot analysis of G6PD

	bands' intensity_first replication	bands' intensity_second replication	bands' intensity_third replication	mean	Standard deviation
WT.1	65.4	67.7	71.2	68.1	2.920616
WT.2	76.5	79	74.3	76.6	2.351595
WT.1+OA	81.1	78.3	89.1	82.83333	5.60476
WT.2+OA	107	104	101	104	3
KO.1	124	127	120	123.6667	3.511885
KO.2	336	235	281	284	50.56679
KO.1+OA	145	140	201	162	33.86739
KO.2+OA	315	295	379	329.6667	43.87862

Supplement 7B: unpaired two-tailed T-test of repression factors of bands' intensities

p-value	WT.1	WT.2	WT.1+OA	WT.2+OA	KO.1	KO.2	KO.1+OA	KO.2+OA
WT.1		0.018682	0.02713	0.00012	<0.001	0.017532	0.039844	0.009016
WT.2	0.018682		0.184503	0.000329	0.000113	0.019064	0.048012	0.009714
WT.1+OA	0.02713	0.184503		0.00982	0.001037	0.019387	0.052467	0.009478
WT.2+OA	0.00012	0.000329	0.00982		0.001979	0.024971	0.096206	0.012071
KO.1	<0.001	0.000113	0.001037	0.001979		0.031074	0.187796	0.014335
KO.2	0.017532	0.019064	0.019387	0.024971	0.031074		0.031702	0.304077
KO.1+OA	0.039844	0.048012	0.052467	0.096206	0.187796	0.031702		0.00752
KO.2+OA	0.009016	0.009714	0.009478	0.012071	0.014335	0.304077	0.00752	

Supplement 8A: Quantitative Western blot analysis of Emerin

	bands' intensity_first replication	bands' intensity_second replication	bands' intensity_third replication	mean	Standard deviation
WT.1	19800	17500	14500	17266.67	2657.693
WT.2	19600	16600	16800	17666.67	1677.299
WT.1+OA	33500	30500	24500	29500	4582.576
WT.2+OA	35100	40100	27000	34066.67	6610.85
KO.1	19000	17400	20100	18833.33	1357.694
KO.2	22100	21200	29400	24233.33	4497.036
KO.1+OA	36000	28500	36500	33666.67	4481.443
KO.2+OA	41800	45100	34000	40300	5700

Supplement 8B: unpaired two-tailed T-test of repression factors of bands' intensities

p-value	WT.1	WT.2	WT.1+OA	WT.2+OA	KO.1	KO.2	KO.1+OA	KO.2+OA
WT.1		0.838194	0.024695	0.033944	0.43072	0.09739	0.009794	0.009413
WT.2	0.838194		0.034281	0.042957	0.40421	0.113958	0.015802	0.014597
WT.1+OA	0.024695	0.034281		0.387438	0.046799	0.228445	0.3232	0.065608
WT.2+OA	0.033944	0.042957	0.387438		0.052241	0.109459	0.935581	0.285146
KO.1	0.43072	0.40421	0.046799	0.052241		0.164844	0.021589	0.01825
KO.2	0.09739	0.113958	0.228445	0.109459	0.164844		0.061746	0.020475
KO.1+OA	0.009794	0.015802	0.3232	0.935581	0.021589	0.061746		0.192161
KO.2+OA	0.009413	0.014597	0.065608	0.285146	0.01825	0.020475	0.192161	

S6A, S6B, S7A, S7B, S8A, and S8B relate to Fig. 22 on page 64

11- Appendices

The original data were processed, archived in Zenodo, and assigned to the digital object identifier (DOI): https://doi.org/10.5281/zenodo.4662900. The appendices are listed as follows:

Appendix_Table.1: The identified peptides

Appendix_Table.2: Proteins that have a mitotic phase-dependent regulation pattern.

Appendix_Table.3: The differently regulated proteins among four conditions.

Appendix_Table.4: The identified peptides and phosphopeptides using HDMS^E acquisition mode.

Appendix_Table.5: The identified peptides and phosphopeptides using DDA acquisition mode.

Appendix_Table.6: The relation between the identified phospho- and non-phosphopeptides that were identified using HDMS^{E}aquisition mode.

Appendix_Table.7: The relation between the identified phospho- and non-phosphopeptides that were identified using DDA acquisition mode.

Appendix_Table.8: The relation between the identified phosphosites in HDMS^E and DDA acquisition modes.

Appendix_Table.9: The identified mitotically regulated phosphosites using HDMS^E acquisition mode.

Appendix_Table.10: The identified mitotically regulated phosphosites using DDA acquisition mode.

Appendix_Table.11: The identified mitotic phosphosites that were found in the Phosphositeplus database.

Appendix_Table.12: Gene ontology analysis of the mitotically regulated phosphosites that were identified using HDMS^E acquisition mode.

Appendix_Table.13: Gene ontology analysis of the mitotically regulated phosphosites that were identified using DDA acquisition mode.

12- Acknowledgment

It is my pleasure to introduce people who have provided me the help and support during my Ph.D. First of all, I would like to thank my supervisor **Prof. Dr. Hans-Jürgen Thiesen,** for his constant encouragement, guidance, and inputs that helped me to improve and accomplish my project. His faith helped me handle the research challenges, and his supervision taught me how to be an independent researcher. I am very grateful to **Dr. Peter Lorenz,** who provided me an intensive training and enriched my work with his constructive comments and suggestions. I really appreciate his support.

I would like to express my deep appreciation to **Dr. Robby Engelmann** for the fruitful cooperation during flow cytometry experiments. He helped me to improve my methods and to run my experiments smoothly.

My profound thanks go to **Prof. Dr. Michael O. Glocker,** who gave me the opportunity to do a part of the lab work in Proteome Center Rostock. He has been an invaluable source of advice that helped me to pursue the research.

I am grateful for working with **Dr. Stefan Mikkat** from Core Facility Proteomics. He provided professional proteomics training. The discussion with him was inspiring. It enabled me to bring many insights into this dissertation. I could not finalize this project without his advice and training.

Further, I would like to thank **Ms. Manuela Ruß** for the technical support during the sample preparation.

I would like to express my gratitude to **the German academic exchange service (DAAD)** for the financial support, enjoyable courses, workshops, and events. I feel privileged to be selected for the scholarship program "Research Grants – Doctoral Programmes in Germany."

Finally, I would like to thank my family and friends. Above all, my mum for her love, belief, patience, unceasing support, and encouragement.

13- Declaration of Originality

I hereby declare that this Ph.D. Thesis entitled "**Phosphoproteome analysis of the near-haploid cell line HAP1 reveals phosphorylation events originating from PDZ-binding kinase/T-LAK cell-originated protein kinase (PBK/TOPK)**" is the result of my original work and was carried out under the supervision of Prof. Dr. H-J Thiesen, Institute of Immunology, University Medicine Rostock, University of Rostock.

All sources used in this work are clearly referenced, and the assistance I received in this work is fully acknowledged.

Furthermore, I confirm that no degree has been granted to me for this Ph.D. thesis or any part of it before, either at the University of Rostock or any other university or scientific institution.

Hasan Albony Rostock, 29.04.2021

14- Curriculum vitae

Personal data

Name: Hasan Albony
Place and date of birth: Syria. Damas Suburb 27.12.1981
Nationality: Syrian

Education

04.2014- now: Ph.D. candidate at Institute for Immunology, Rostock University, Germany.
2007– 2012: Master of clinical diagnostics (Microbiology and Biochemistry), Faculty of Pharmacy, Damascus University, Damascus, Syria.
2000 – 2005: Bachelor in pharmaceutical sciences, Faculty of Pharmacy, Damascus University, Damascus Syria.
1996 – 2000: High School, Damascus, Syria.
1993 – 1996: Secondary School, Damas Suburb, Syria.
1987 – 1993: Elementary School, Damas Suburb, Syria.

Experience

2009 – 2013: An assistant instructor in biochemistry lab in International University for Science and Technology (IUST) in Syria, Daraa, Syria.
2007 – 2011: An assistant instructor in microbiology and biochemistry labs in Damascus University, Damascus, Syria.
2008-2009: Training at Al Assad University Hospital, Damascus, Syria.

Academic and Professional Affiliation

Member, Graduate Academy, University of Rostock; Germany
Member, Structured curriculum for MD/Ph.D. students, University Medicine Rostock, University of Rostock, Germany.

Grants

2015 - 2019: DAAD Research Grants – Doctoral Programmes in Germany.

Languages

Arabic: Mother language.
German: C1.
English: Good (reading and writing).

Conferences and workshops

Poster presentation at the 52nd Annual German Society for Mass Spectrometry (DGMS) Conference. 10th -13th March 2019. Rostock, Germany.

Leadership for Syria Programme. April 2017-July 2018. University of Konstanz-Germany.

Workshop at Sumaya University for Technology, in collaboration with the Arab Federation of Clinical Biology 12th-14th November 2009. Amman, Jordan

Oral presentations

H. Albony, H.-J. Thiesen. *Phosphoproteome analysis of the near-haploid cell line HAP1 to reveal phosphorylation events originating from PDZ-binding kinase/T-LAK cell-originated protein kinase (PBK/TOPK)*. Proteome Center Rostock/Institute of Immunology Group meeting, 27th of January 2020.

H. Albony, H.-J. Thiesen. *Comparison of Data-Dependent and -Independent Mass Spectrometric acquisition to investigate PDZ-binding kinase/T-LAK cell-originated protein kinase (PBK/TOPK) dependent phospho-proteome*. Proteome Center Rostock/Institute of Immunology Group meeting, 28th of January 2019.

H. Albony, H.-J. Thiesen. *Analysis of PDZ-binding kinase/T-LAK cell-originated protein kinase (PBK/TOPK) dependent phosphoproteome*. Participants' Camp Winter Semester 2018/2019. 6th of December 2018.

H. Albony, H.-J. Thiesen. *Mass spectrometric analysis of PBK deficient HAP1 cells*. Participants' Camp Summer Semester 2018. 5th of July 2018.

H. Albony, H.-J. Thiesen. *Mitotic phospho-proteome analysis of wild type and PBK knockout HAP1 cells.* Proteome Center Rostock/Institute of Immunology Group meeting, 5th of February 2018.

H. Albony, H.-J. Thiesen. *Generation of PDZ-binding kinase (PBK) stable cell line for protein-protein interaction studies*. Participants' Camp Semester Summer Semester 2017. 28th of June 2017.

H. Albony, H.-J. Thiesen. *Synchronization of HAP1 cells to study PDZ-binding kinase/T-LAK cell-originated protein kinase (PBK/TOPK) activity.* Participants' Camp. Winter Semester 2016/2017. 14th of December 2016.

H. Albony, H.-J. Thiesen. *Synchronization of HAP1 Cells to Study PDZ-binding Kinase/T-LAK Cell-originated Protein Kinase (PBK/TOPK) Activity.* Proteome Center Rostock/Institute of Immunology Group meeting, 19th of December 2016.

H. Albony, H.-J. Thiesen. *Mass spectrometric analysis of PBK deficient HAP1 cells*. Participants' Camp. Summer Semester 2016. 30th of June 2016.

H. Albony, H.-J. Thiesen. *Mass spectrometric analysis of PBK deficient HAP1 cells.* Proteome Center Rostock/Institute of Immunology Group meeting, 1st of February 2016.

H. Albony, H.-J. Thiesen. *NeutrAvidin ELISA troubleshooting – how to reliably determine serum antibodies against frameshift peptides?* Participants' Camp. Winter Semester 2015/2016. 3th of December 2015.

H. Albony, H.-J. Thiesen. *Frame-shift mutations in renal cancer.* Proteome Center Rostock/Institute of Immunology Group meeting, 12th of January 2015.

H. Albony, H.-J. Thiesen. *Analysis of humoral immune responses to frame shift proteins in renal cancer.* Participants' Camp. Winter Semester 2014/2015. 4th of December 2014.

H. Albony, H.-J. Thiesen. *Experiences in ELISA assays with respect to state-of-the-art publications.* Proteome Center Rostock/Institute of Immunology Group meeting, 23rd of June 2014.

Publications

Albony H, Al-Koubyli F, Emel S. "*Studying serum ST2 levels at heart failure patients*". J Lab diag. 9; 2013.